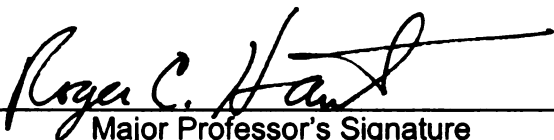This is to certify that the
thesis entitled

ROTATIONAL TRACTION AT THE AMERICAN FOOTBALL SHOE-
SURFACE INTERFACE AND ITS APPLICATION TO ANKLE
INJURY

presented by

MARK R. VILLWOCK

has been accepted towards fulfillment
of the requirements for the

_____M.S._____ degree in ____Engineering Mechanics____

_____
Major Professor's Signature

_____03/25/09_____
Date

PLACE IN RETURN BOX to remove this checkout from your record.
TO AVOID FINES return on or before date due.
MAY BE RECALLED with earlier due date if requested.

DATE DUE	DATE DUE	DATE DUE
SEP 0 3 2012		

ROTATIONAL TRACTION AT THE AMERICAN FOOTBALL SHOE-SURFACE
INTERFACE AND ITS APPLICATION TO ANKLE INJURY

By

Mark R. Villwock

A THESIS

Submitted to
Michigan State University
in partial fulfillment of the requirements
for the degree of

MASTER OF SCIENCE

Engineering Mechanics

2009

ABSTRACT

ROTATIONAL TRACTION AT THE AMERICAN FOOTBALL SHOE-SURFACE
INTERFACE AND ITS APPLICATION TO ANKLE INJURY

By

Mark R. Villwock

While linear traction is necessary during an athletic contest, it is generally accepted that excessive rotational traction results in high forces being transmitted to vulnerable anatomic structures which may then precipitate ankle and knee injuries. Our laboratory has combined mechanical testing of the football shoe-surface interface with human cadaver experiments to investigate rotational traction and its application to ankle injury. Chapter 1 provides an overview of artificial surfaces and documents injuries that may be related to the shoe-surface interface. In Chapter 2, rotational traction measurements are documented for ten football shoes across four surfaces. The artificial surfaces were found to exhibit higher peak torque and rotational stiffness in comparison to natural grass. Chapter 3 further investigates rotational traction on third-generation, artificial surfaces. Infill material and fiber type were found to significantly affect peak torque. Chapter 4 presents the results of a cadaver study on ankle injuries generated by excessive external rotation of the foot/ankle complex. The method of foot constraint affected the mode of failure and the amount of foot rotation at failure. Chapter 5 documents the development of a biofidelic ankle that may be used to assess the risk of ankle injury for various shoe-surface interfaces. Finally, Chapter 6 provides a synopsis of this thesis and offers recommendations for future areas of research. The data presented in this thesis may be applicable to injury prediction and be helpful in the development of future strategies for injury prevention.

ACKNOWLEDGMENTS

TABLE OF CONTENTS

LIST OF TABLES

LIST OF FIGURES

LIST OF PUBLICATIONS

Peer-Reviewed Manuscripts

Villwock MR, Meyer EG, Powell JP, Fouty AJ, Haut RC. (2009) Football playing surface and shoe design affect rotational traction. Am J Sports Med. 37(3):518-525.

Villwock MR, Meyer EG, Powell JP, Fouty AJ, Haut RC. (2009) The effects of various infills, fiber structures, and shoe designs on generating rotational traction on an artificial surface. J Sports Eng Tech. 223(1):11-19.

Villwock MR, Meyer EG, Powell JP, Haut RC. A biomechanical investigation of ankle injury under external foot/ankle complex rotation using the human cadaver model. J Appl Biomech. In Review.

Villwock MR, Meyer EG, Powell JP, Haut RC. Development and evaluation of a surrogate ankle for use with a rotational traction apparatus. J Sports Eng Tech. In Review.

Meyer EG, Villwock MR, Haut RC. Osteochondral microdamage from valgus bending of the knee. Clin Biomech. In Review.

Déjardin LM, Cabassu JB, Villwock MR, Malinowski R, Haut RC. *In vivo* evaluation of a novel angle stable interlocking nail for the stabilization of tibial fractures in dogs. In Preparation.

Peer-Reviewed Abstracts

Villwock MR, Meyer EG, Powell JP, Fouty AJ, Haut RC. (2008) Football playing surface components may affect lower extremity injury risk. North American Congress on Biomechanics; Ann Arbor, MI: American and Canadian Society of Biomechanics.

Villwock MR, Meyer EG, Powell JP, Fouty AJ, Haut RC. (2008) Football shoe designs may affect lower extremity injury risk. North American Congress on Biomechanics; Ann Arbor, MI: American and Canadian Society of Biomechanics.

Villwock MR, Meyer EG, Powell JP, Haut RC. (2009) External rotation ankle injuries: Investigating ligamentous rupture. Summer Bioengineering Conference; Lake Tahoe, CA: American Society of Mechanical Engineering.

Cabassu JB, Villwock MR, Malinowski R, Haut RC, Déjardin LM. (2009). *In vivo* biomechanical evaluation of a novel angle-stable interlocking nail for diaphyseal fracture stabilization in dogs. ACVS Symposium; Washington, DC: American College of Veterinary Surgeons.

Powell JP, Villwock MR, Fouty AJ, Haut RC. Impact accelerations on different types of football playing surfaces. 2009 National Athletic Trainers' Association Annual Meeting and Clinical Symposia. San Antonio, TX: National Athletic Trainers' Association.

Chapter 1: Artificial Surfaces and Injury Risk

A study of high school football in Pennsylvania noted that 21% of the reported injuries were classified as either definitely or possibly field related (Harper et al., 1984). Two important interactions between the player and the surface are: the amount of energy absorbed by the surface during an impact (hardness), and the type of footing a surface provides (traction) (Rogers and Waddington, 1992). If the surface is excessively hard, high impact forces may result in compression fractures and the increased risk of injury during a fall (Adrian and Xu, 1990; Henderson et al., 1990). If the surface is too soft, player fatigue and performance may be affected (Henderson et al., 1990). The extremes of traction also pose similar tradeoffs between player performance and player safety. A certain level of traction is necessary for speed and agility, but too much traction can excessively stress joints and lead to lower extremity injury (McNitt et al., 1996).

Lower extremity injuries represent over half of the time loss injuries in football (Fernandez et al., 2007). Among the many factors that are associated with these injuries are the tractional characteristics of the shoe-surface interface. Frequently, the mechanism of injury involves a foot planted, or "fixated", on the ground while the upper body is excessively rotated. This can occur in noncontact situations, for example, when a player twists after a jump landing, and as a result of contact with another player. The resulting injuries range from mild lateral ankle sprains to ACL rupture (Boytim et al., 1991; Guise et al., 1976).

Historically, sporting events such as American football have occurred on natural grass fields. A natural grass field in a stadium may withstand 50 to 100 hours per year of

1

hard usage and, even then, requires constant maintenance to retain its quality (Gorham and Orofino, 1996). With the growing popularity of sports, stadium fields are receiving a rising demand to accommodate multiple teams and sports, dramatically increasing usage. This results in difficult and costly maintenance in order to ensure the field provides adequate aesthetic, performance and safety characteristics. The maintenance can also prove to be difficult, if not impossible, in harsh climates that involve cold weather and excessive rain. Indoor natural grass fields are possible, but the costs are not practical for most venues. These limitations of natural grass led to the creation of synthetic surfaces with the intention of providing superior performance characteristics while reducing maintenance costs.

The first artificial surface was invented in the 1960s (U.S. patent #3332828) under the name "Chemgrass". The product emerged into national attention with its installation in the Houston Astrodome in 1966, and was subsequently renamed "AstroTurf". The original product was more like a carpet surface intended to resemble grass, rather than a surface intended to mimic the performance of natural grass. AstroTurf was later installed in an outdoor stadium at Indiana State University in 1967, further solidifying its role as a natural grass alternative. Many competitors entered the market with similar products including TartanTurf, Omniturf, SuperTurf, ClubTurf, PolyTurf, and InstantTurf.

Since its introduction, numerous research projects have been conducted that examine the epidemiology of injury on this first-generation, artificial surface. Bramwell et al. (1972) and Powell and Schootman (1992; 1993) published studies that document significantly higher injury rates during sporting events played on artificial surfaces in comparison to natural grass. Other researchers constructed devices to measure the

rotational traction of artificial surfaces in comparison to natural grass. Bonstingl et al. (1975), Cawley et al. (2003), and Livesay et al. (2006) conclude that AstroTurf (The Monsanto Company, St. Louis, MO) yields higher torque than natural grass. Similar studies have examined the influence of cleated footwear on rotational traction and injury rates. Torg et al. (1974) and Lambson et al. (1996) conducted epidemiology studies of high school football and noted the shoe worn during an injury. The authors also measured the rotational traction of the various shoe models being worn by the high school teams in the respective year of their epidemiology study. Both studies conclude that the shoe design with the highest rotational traction yielded significantly higher injury rates. The results of the shoe and surface testing has led to the belief that higher rotational traction is an indicator of elevated injury risk.

In the late 1980s, a second-generation of artificial surface was introduced with an infill layer of sand. These surfaces were unsuccessful in American football due to their inherent hardness, erratic traction and abrasiveness. The 1990s resulted in the launch of yet another artificial surface, this time with a soft absorbent infill material (often crushed rubber or a combination of crushed rubber and sand) and longer, more durable pile fibers. This surface is often called the third-generation, artificial surface and is claimed to better simulate a natural grass field. Since its introduction, there is paucity of research regarding the effects of playing on this generation of artificial playing surface, yet they continue to grow in popularity and represent an increasing number of surfaces in football.

To date, there has not been a published epidemiology study that compares injury rates between the third-generation, artificial surface and natural grass. The rotational traction of FieldTurf and AstroPlay, the two most popular third-generation surfaces, has

only been documented in one published study conducted with a limited testing methodology (Livesay et al., 2006). The impact that variable components, such as infill material and fiber structure, have on rotational traction is unknown.

In the field of sports medicine there is not a well established injury risk criterion by which to judge shoe and surface designs. Torg et al. (1974) assigned football shoe designs a "safety" ranking. The level of "safety" was determined from an epidemiology study of Philadelphia high school football that noted the frequency of knee injuries associated with particular cleat designs. The shoe designs were then subjected to rotational traction testing and the magnitude of the shoe-surface interface release coefficient was related to a particular safety ranking. This was intended to identify future dangerous football shoes based solely on mechanical traction measurements. This analysis is more than thirty years old and is not considered applicable to the current state of American football and modern shoe-surface interactions. The best way to determine injury risk in sports may be through the development of biofidelic surrogates that can simulate physiological loading conditions. Similar devices, such as crash test dummies, are often used by the automobile industry to assess injury risk during a vehicular collision (Forman et al., 2006; McDonald et al., 2003; Tornvall et al., 2007). Crash test dummies are instrumented to record data about their dynamic behavior during an impact. The loads and displacements are then related to cadaveric studies in order to predict the relative risk of a particular injury. The development of a traction measurement apparatus that mimics the response of the human lower extremity under torsion may allow assessment of the risk of ankle or knee injury given certain shoe-surface interface combinations (Villwock et al., 2009).

A portion of this thesis focuses on the risk of ankle injury. Specifically, the risk of ankle injury due to an external rotation mechanism. This mechanism has been noted to induce injury often requiring a relatively long recovery time (Boytim et al., 1991; Ebraheim et al., 2003; Miller et al., 1995; Williams et al., 2007). In contrast to the soft tissue injuries reported in many clinical studies on the ankle (Boytim et al., 1991; Edwards and DeLee, 1984; Hopkinson et al., 1990), cadaveric experimental studies have typically generated a high frequency of bone fractures when the foot is externally rotated (Lauge-Hansen, 1950; Markolf et al., 1989; Schaffer and Manoli, 1987; Stiehl et al., 1992). In a majority of manuscripts that describe external rotation injuries of the ankle joint, the age and gender of the cadaveric test specimens have not been reported (Hirsch and Lewis, 1965; Markolf et al., 1989; Schaffer and Manoli, 1987). These variables may substantially affect both the failure load and the mode of failure to the joint. Most ankle sprains occur in persons under the age of 35 years (Nilsson, 1983). A younger specimen population may result in a high frequency of ligamentous injuries, prior to bone fracture, during excessive levels of external rotation of the foot/ankle complex. Measurement of the rotational moments and angular rotations required to induce soft tissue injury may then be used to develop a biofidelic ankle surrogate that can be used for the evaluation of athletic shoe-surface interfaces and their risk of ankle injury.

The research in this thesis includes the mechanical evaluation of surface and shoe designs as well as the biomechanical analyses of ankle injury risk from cadaveric tests. Chapter Two describes the rotational traction measurements performed across ten football shoes and four current football playing surfaces. Chapter Three details rotational traction on third-generation, artificial surfaces by examining nine playing surfaces

composed of various infill and fiber structures. Chapter Four examines the external rotation mechanism of ankle injury. The influence of foot constraint on injury location is examined, and the torque and rotation required to produce ankle injury is presented. These data were then used to establish a more biofidelic ankle used in the rotational traction apparatus. Chapter Five discusses the design of the surrogate ankle. This chapter outlines the biofidelic attributes of the ankle and how it may ultimately have relevance in establishing an ankle injury risk criterion for new football cleat and surface designs. Lastly, Chapter Six provides conclusions of this study and outlines recommendations for future work.

The data from the proposed research will make a significant contribution to the understanding of rotational traction created by the football shoe-surface interface. In conjunction with epidemiological studies, this research will aide in developing future lower leg injury risk criteria. The cadaver ankle experiments in combination with the biofidelic ankle may also be used to assess the risk of ankle injury from future shoe-surface interface designs.

REFERENCES

Adrian M and Xu D. (1990) Matching the playing field to the player. *In* Natural and Artificial Playing Fields: Characteristics and Safety Features. ASTM STP 1073. Schmidt RC, Hoerner EF, Milner EM, Morehouse CA, Eds. American Society for Testing and Materials. pp. 10-19.

Bonstingl RW, Morehouse CA, Niebel BW. (1975) Torques developed by different types of shoes on various playing surfaces. Med Sci Sports. 7(2):127-131.

Boytim MJ, Fischer DA, Neumann L. (1991) Syndesmotic ankle sprains. Am J Sports Med. 19(3):294-298.

Bramwell ST, Requa RK, Garrick JE. (1972) High school football injuries: a pilot comparison of playing surfaces. Med Sci Sports. 4(3):166-169.

Cawley PW, Heidt RS Jr., Scranton PE Jr., Losse GM, Howard ME. (2003) Physiologic axial load, frictional resistance, and the football shoe-surface interface. Foot Ankle Int. 24(7):551-556.

Ebraheim NA, Elgafy H, Padanilam T. (2003) Syndesmotic disruption in low fibular fractures associated with deltoid ligament injury. Clin Orthop Relat Res. 409:260-267.

Edwards GS, DeLee JC. (1984) Ankle diastasis without fracture. Foot Ankle. 4(6):305-312.

Fernandez WG, Yard EE, Comstock RD. (2007) Epidemiology of lower extremity injuries among U.S. high school athletes. Acad Emerg Med. 14(7):641-645.

Forman J, Lessley D, Shaw CG, Evans J, Kent R, Rouhana SW, Prasad P. (2006) Thoracic response of belted PMHS, the Hybrid III, and the THOR-NT mid-sized male surrogates in low speed, frontal crashes. Stapp Car Crash J. 50:191-215.

Gorham PM, Orofino TA. (1996) Actual field performance of synthetic turf as measured over a thirty year period. *In* Safety in American Football. ASTM STP 1305. Hoerner EF, Ed. American Society for Testing and Materials. pp. 123-131.

Guise ER. (1976) Rotational ligamentous injuries to the ankle in football. Am J Sports Med. 4(1):1-6.

Harper JC II, Morehouse CA, Waddington DV, Buckley WE. (1984) Turf management, athletic-field conditions, and injuries in high school football. Agric Exp Stn. Prog Rep 384. The Pennsylvania State University, University Park, PA.

Henderson RL, Waddington DV, Morehouse CA. (1990) Laboratory measurements of impact absorption on turfgrass and soil surfaces. *In* Natural and Artificial Playing Fields:

Characteristics and Safety Features. ASTM STP 1073. Schmidt RC, Hoerner EF, Milner EM, Morehouse CA, Eds. American Society for Testing and Materials. pp. 127-135.

Hirsch C, Lewis J. (1965) Experimental ankle joint fractures. Acta Orthop Scand. 36:408-417.

Hopkinson WJ, St. Pierre P, Ryan JB, Wheeler JH. (1990) Syndesmosis sprains of the ankle. Foot Ankle. 10(6):325-330.

Lauge-Hansen N. (1950) Fractures of the Ankle II. Combined Experimental-Surgical and Experimental-Roentgenologic Investigations. Arch Surg. 60:957-985.

Livesay GA, Reda DR, Nauman EA. (2006) Peak torque and rotational stiffness developed at the shoe-surface interface. Am J Sports Med. 34(3):415-422.

Markolf KL, Schmalzried TP, Ferkel RD. (1989) Torsional strength of the ankle in vitro. The supination-external-rotation injury. Clin Orthop Relat Res. 246:266-272.

McDonald JP, Shams T, Rangarajan N, Beach D, Huang T, Freemire J, Artis M, Wang Y, Haffner M. (2003) Design and development of a THOR based female crash test dummy. Stapp Car Crash J. 47:551-570.

McNitt AS, Waddington DV, Middour RO. (1996) Traction measurement on natural turf. *In* Safety in American Football. ASTM STP 1305. Hoerner EF, Ed. American Society for Testing and Materials. pp. 145-155.

Miller CD, Shelton WR, Barrett GR, Savoie FH, Dukes AD. (1995) Deltoid and syndesmosis ligament injury of the ankle without fracture. Am J Sports Med. 23(6):746-750.

Nilsson S. (1983) Sprains of the lateral ankle ligaments, part II: epidemiological and clinical study with special reference to different forms of conservative treatment. J Oslo City Hosp. 33(2-3):13-36.

Powell JW, Schootman M. (1992) A multivariate risk analysis of selected playing surfaces in the National Football League: 1980-1989. An epidemiological study of knee injuries. Am J Sports Med. 20(6):686-694.

Powell JW, Schootman M. (1993) A multivariate risk analysis of natural grass and AstroTurf playing surfaces in the National Football League 1980-1989. Int Turfgrass Soc Res J. 23:201-211.

Rogers JN, Waddington DV. (1992) Impact absorption characteristics on turf and soil surfaces. Agron J. 84:203-209.

Schaffer JJ, Manoli A. (1987) The Antiglide Plate for Distal Fibular Fixation. J Bone Joint Surg Am. 69-A(4):596-604.

Stiehl JB, Skrade DA, Johnson RP. (Dec, 1992) Experimentally produced ankle fractures in autopsy specimens. Clin Orthop Relat Res. 285:244-249.

Torg JS, Quedenfeld TC, Landau S. (1974) The shoe-surface interface and its relationship to football knee injuries. J Sports Med. 2(5):261-269.

Tornvall FV, Holmqvist K, Davidsson J, Svensson MY, Haland Y, Ohrn H. (2007) A new THOR shoulder design: a comparison with volunteers, the Hybrid III, and THOR NT. Traffic Inj Prev. 8(2):205-215.

Villwock MR, Meyer EG, Powell JP, Fouty AJ, Haut RC. (2009) Football playing surface and shoe design affect rotational traction. Am J Sports Med. 37(3):518-525.

Williams GN, Jones MH, Amendola A. (2007) Syndesmotic ankle sprains in athletes. Am J Sports Med. 35(7):1197-1207.

Chapter 2: Football Playing Surface and Shoe Design Affect Rotational Traction

ABSTRACT:

High rotational traction between football shoes and the playing surface may be a potential mechanism of injury for the lower extremity. A mobile testing apparatus with a compliant ankle was used to apply rotations and measure the torque at the shoe-surface interface. The mechanical surrogate was used to compare five football cleat patterns (total of ten shoe models) and four football surfaces (FieldTurf, AstroPlay, and 2 natural grass systems) on site at actual surface installations. Both artificial surfaces yielded significantly higher peak torque and rotational stiffness than the natural grass surfaces. The only cleat pattern that produced a peak torque significantly different than all others was the turf-style cleat, and it yielded the lowest torque. The model of shoe had a significant effect on rotational stiffness. A potential shoe design factor that may influence rotational stiffness is the material(s) used to construct the shoe's upper. As football shoes and surfaces continue to update their designs, new evaluations of their performance must be assessed under simulated loading conditions to ensure that player performance needs are met while minimizing injury risk.

INTRODUCTION:

Injuries to the lower extremity are among the most frequent injuries for all levels of sports and often account for more than 50% of reported injuries (Fernandez et al., 2007). In the National Football League (NFL), ankle and knee sprains combine to account for about 20% of all reported injuries (Powell and Schootman, 1992;1993). These injuries can occur during contact between players or in noncontact situations, such as a rapid change in direction or with a combination of high compressive load and twist during a jump landing (Arnold et al., 1979; Fauno and Wulff, 2004). Frequently the mechanism of injury involves a foot planted on the playing surface with an excessive internal rotation of the upper body (Guise, 1976).

Traction is defined by the ASTM committee on Sports Equipment and Facilities to be the resistance to relative motion between a shoe outsole and a sports surface, which does not necessarily obey classical (Coulomb) laws of friction (ASTM F2333, 2006). While linear traction is necessary for high-level performance during any athletic contest (Shorten et al., 2003), it is generally accepted that excessive rotational traction may precipitate ankle and knee injuries (Bonstingl et al., 1975; Lambson et al., 1996; Nigg and Yeadon, 1987; Torg et al., 1974). A previous study of ACL injuries in high school football players documented a significant relationship between cleat design, the amount of rotational traction and the risk of ACL injury on grass (Lambson et al., 1996). The "edge" cleat design produced significantly higher rotational traction and was associated with an ACL injury rate 3.4 times higher than that of all other designs combined.

Other studies have noted differences of injury rate in the presence or absence of specific risk factors, such as whether the surface was natural grass or AstroTurf. These

differences in injury rate may be due to variations in the structure and materials of the turfs (Hammer, 1981), the running speed of the players (Stanitski et al., 1974), or the coefficient of friction between the surface and shoe (Andreasson et al., 1986). The injury risk factor may also depend on the player's position and the type of play at the time of injury, both of which would influence loading mechanisms on the lower extremity (Powell and Schootman, 1992).

Although rotational traction has been documented in previous studies (usually as the peak torque magnitude recorded during dynamic testing) for numerous shoe-surface interfaces, most testing devices are not portable and therefore cannot be used to test the actual playing surfaces (Bonstingl et al., 1975; Cawley et al., 2003; Lambson et al., 1996; Torg et al., 1974). The aforementioned studies also have not evaluated the types of synthetic surfaces currently used in professional, college and high school football. The modern synthetic surface is a sharp contrast to the dense and abrasive turfs that were introduced in the 1960s. Artificial surfaces now consist of longer, more grass-like fibers that are surrounded and stabilized by infill materials, such as rubber and sand. A more recent study measured the peak torque and rotational stiffness developed at the shoe-surface interface of three infill systems with a portable testing device (Livesay et al., 2006). The limitations of that study were the small compressive normal force and the use of only the forefoot cleats rigidly mounted on a plate. Rotational stiffness (defined as the slope of the torque versus rotation data in a predefined angular range) was identified as a more sensitive indicator of the mechanical interaction between different shoe-surface combinations than the peak torque (Livesay et al., 2006).

There are limited data with regards to the rotational traction of cleated football shoes on modern third-generation, artificial surfaces. The purpose of the present study was to investigate the rotational shoe-surface interactions using a variety of shoes and surfaces currently employed in football by means of a mobile testing apparatus constructed with a surrogate lower leg. The first hypothesis of the study was that shoe designs with numerous and or large cleats around the peripheral margin of the sole would exhibit higher rotational traction than shoes with fewer or smaller cleats on the peripheral margins. The second hypothesis was that manufacturer and material variation between shoe models would result in rotational traction differences among shoe models within cleat pattern groups. The third hypothesis was that an artificial surface that allows greater infill contact with the cleat will produce higher rotational traction than natural grass and similar artificial surfaces which limit infill contact with the cleat. A better understanding of the interaction between current shoe-surface interfaces will provide athletic teams with information on the rotational traction of various shoe-surface combinations. These data may ultimately have relevance to the risk potential for rotational lower leg injuries on various shoe-surface interface combinations.

MATERIALS AND METHODS:

Four different surfaces were evaluated in this study: 1) an artificial surface with an infill composed of a sand/rubber blend (FieldTurf, FieldTurf Tarkett, Montreal, Quebec, Canada), 2) an artificial surface with a 100% rubber infill (AstroPlay, Southwest Recreational Industries, Inc., Leander, Texas), 3) natural grass composed of Kentucky bluegrass and a small percentage of ryegrass in combination with a native Michigan soil,

4) natural grass composed of Kentucky bluegrass and a small percentage of ryegrass in combination with a custom soil engineered for strength and drainage that consisted of 90% sand and 10% silt and clay. The FieldTurf system was the playing surface used in an indoor sports complex, and it was installed seven years prior to testing. The AstroPlay system was also the playing surface used in an indoor sports complex, and it was installed five years prior to testing. Both natural grass plots were part of outdoor football fields with full-time maintenance staff.

The FieldTurf was composed of parallel slit polyethylene fibers with an approximate 50/50 combination of layered silica sand and cryogenically processed crumb styrene-butadiene rubber (SBR) infill (FieldTurf.com, 2008), with a primary top layer of cryogenic rubber. The fiber layout of FieldTurf is constructed with a gauge length of 3/4". This measurement refers to the distance between rows of fiber tufts. The AstroPlay was composed of parallel slit polyethylene fibers constructed with a 3/8" gauge length and with an all cryogenically processed SBR crumb infill (SRISports.com, 2008).

Each surface was tested using ten different shoes (Table 2.1), yielding 40 different shoe-surface combinations. The shoes were grouped into five categories based on design properties: 1) cleated shoes with seven removable cleats, five covering the forefoot of the sole and two covering the heel region (7 Studded), 2) molded cleat shoes with twelve cleats around the perimeter of the sole, eight around the forefoot and four around the heel region (12 Studded), 3) molded cleat shoes with four cleats around the heel region and at least fifteen cleats distributed across the forefoot region (Hybrid), 4) cleat designs characterized by blade style cleats (Edge), 5) shoes which had a dense pattern of short elastomeric cleats distributed over the entire sole (Turf).

Table 2.1: Description of tested football shoes

Category	Mfr.	Model	Height	Cleat material	Number of cleats	Max cleat length (mm)	Image
12 Studded	Nike	Bladell TD	Mid-cut	Elastomeric	14	16.3	
	Adidas	Scorch 7 Fly	Low-cut	TPU	13	12.5	
Edge	Nike	Vapor Jet TD	Low-cut	TPU	12	12.0	
	Adidas	Scorch TRX	Low-cut	TPU	15	13.0	
	Adidas	Corner Blitz 7 MD	Mid-cut	Elastomeric	15	11.0	
Hybrid	Nike	Air Zoom Superbad FT	Mid-cut	Elastomeric	21	11.0	
	Adidas	Grid Iron	Mid-cut	Elastomeric	20	12.0	
7 Studded	Nike	Air Zoom Blade D	Mid-cut	TPU (Steel Tip)	7	12.5	
	Adidas	Quickslant D .	Mid-cut	TPU (Steel Tip)	7	12.5	
Turf	Adidas	Turf Hog LE	Mid-cut	Elastomeric	88	6.5	

Due to the mechanical interpenetration of the cleats and playing surface, as well as properties of the materials themselves, rotational traction is dependent on many factors which require that the measurements be made at loads and rates of loading that are expected to occur *in vivo* (ASTM F2333, 2006). A testing apparatus was developed to

simulate the anthropomorphic data of a 95th percentile male (Robbins, 1985). This included matching the compressive load to 1 x body weight (1000 N) and fabricating the surrogate lower leg with a tibia length of 44 cm (Robbins, 1985). In addition to reproducing key mass and length measurements for the surrogate leg, the ankle was designed to be compliant with regards to internal/external rotation by means of a deformable elastomeric washer at this location.

The testing apparatus (Figure 2.1) was designed to apply a dynamic rotation and measure the torque produced at the shoe/surface interface. The apparatus was fabricated to conform to an international standard method for measuring rotational traction characteristics of an athletic shoe-surface interface (ASTM F2333, 2006). The device consisted of an aluminum frame that could be raised and lowered to the ground with wheels to allow for easy mobility. The frame supported the surrogate lower limb, a suspended 425 N weight and a 0.25 m radius gear that were used to produce a torque on the shoe. The weights were released by means of a manual lever arm located on the side of the testing device. The drop height of the weight hanger was adjusted so that the input rotation angle of the shaft was 90 degrees. The rate of rotation was approximately 180 degrees per second, which exceeds the minimum of 45 degrees per second required by the ASTM testing standard (ASTM F2333, 2006). The frame was stabilized on the test surfaces by two operators standing on outboard platforms.
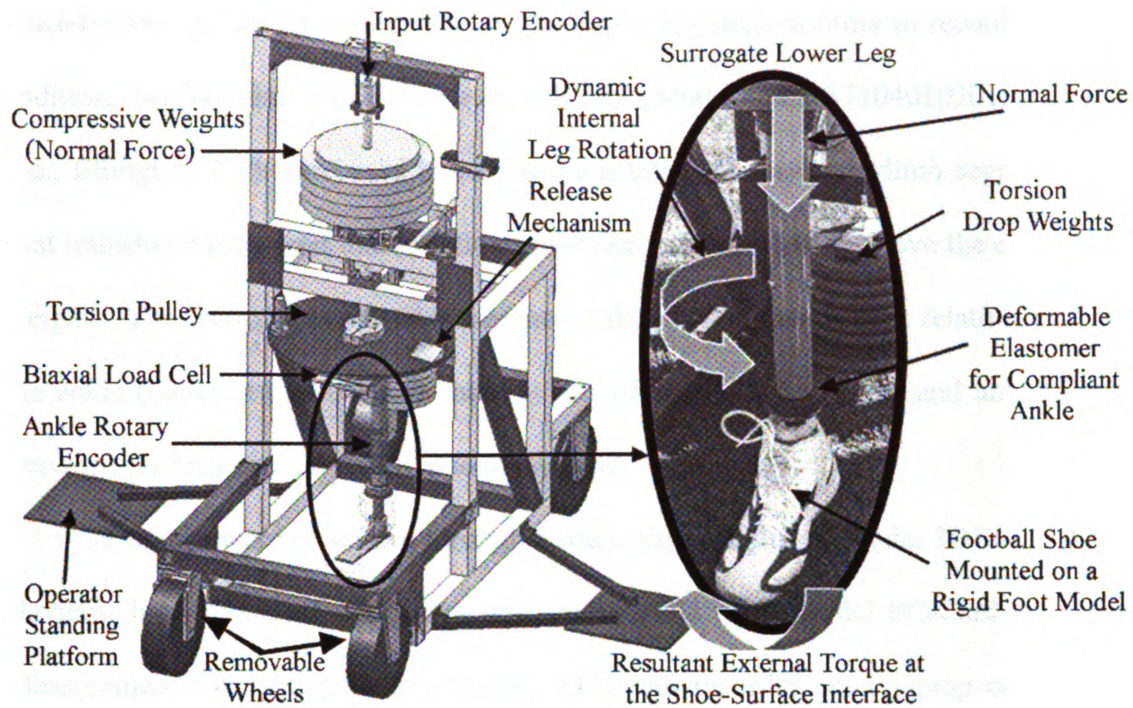
Figure 2.1: Description of rotational traction testing apparatus

To better represent a worst-case injury situation, the current study replicated a loading condition having full cleat contact with the ground. The peak torque measured in tests with full cleat contact has been shown to be typically 70% higher than tests with only forefoot cleats (Bonstingl et al., 1975). A rigid model of the right foot was fabricated and attached below the ankle position on the testing device. The foot represented a U.S. size 13 shoe and the center of rotation (COR) on the test device was adjustable. For all tests documented in this report, the COR was set at the midfoot, a distance of 14 cm from the heel.

The device generated a dynamic internal rotation of the leg, resulting in an externally directed ground reactionary torque on the foot. A torsional load cell (Model 1216CEW-2K, Interface, Scottsdale, AZ) calibrated for 170 Nm full-scale capacity was

placed below the gear and connected to the lower leg shaft in order to record torque. In addition, two angular displacement transducers (Model 0605-S7104010201, Trans-Tek Inc., Ellington, CT) were used to record the rotation of the lower limb segments. The first transducer measured total rotation of the leg and was located above the compressive weights. The second was placed inside the artificial leg to measure the relative rotation at the ankle (between the foot and shaft). The difference between leg and ankle rotation provided the shoe rotation relative to the ground.

The data were processed through a strain gage amplifier (Model 3B18-00, Analog Devices, Inc., Norwood, MA) connected to an A2D card (Model PC-Card-DAS16/16, Measurement Computing Corp., Norton, MA) and recorded on a laptop computer (N Series Lifebook, Fujitsu, Japan). A custom program was written in LabView (Version 7.0, National Instruments, Austin, TX) for data collection. Data were collected for 5 seconds at 1000 Hz and the recorded data from each trial consisted of 100 ms before and 900 ms after a torque threshold of 3 Nm was reached in the test. Five trials were performed for each shoe-surface combination. The testing apparatus was repositioned between trials to a new adjacent section of turf. The air temperature was also recorded for each day of testing.

Data from all trials were analyzed to determine the peak torque. Plots were created to document the change in torque relative to the degree of shoe rotation allowing for the calculation of rotational stiffness. In the current study, we found that the shoe upper could flex under the applied torque and rotate about the mid foot axis as the edge of the shoe plowed through the surface. Therefore, a calculation of rotational stiffness between fixed angles, as used by Livesay et al. (2006), was not advisable. It was

necessary to compute the stiffness between two predetermined levels of torque for all shoe-surface interfaces. The chosen interval was from the start of the test, identified by 3 Nm of torque, to 75% of the peak torque generated for each particular test.

The average peak torque and rotational stiffness of the five trials was used for subsequent statistical analyses. A two way ANOVA, surface (n=4) by shoe model (n=10), was conducted in SigmaStat (Version 2.03, SPSS Inc., Chicago, IL) to assess the effect of surface and shoe on the peak torque and rotational stiffness. Tukey post-hoc tests were performed when indicated. The effect of cleat pattern (n=5) was assessed by a one way ANOVA with Tukey post-hoc tests, when appropriate. Statistical significance was set at $p < 0.05$ in all analyses.

RESULTS:

Torque and rotational data were collected on each of the 40 shoe-surface combinations. The shoe was tested with full cleat contact on the ground and a compressive load of 1000N. The plots of torque versus relative rotation of the shoe were analyzed (Figure 2.2) and several distinct regions were noted: 1) the initial breakaway region, typified by the buildup of torque to begin rotation, 2) a period of increasing torque as the shoe continued to rotate, 3) a period of relatively constant torque which was attributed to slippage between the shoe and surface and 4) a period of unloading at the end of the test. The typical plot consisted of all four regions (Figure 2.2A). If the leading edge of a shoe was twisted and appeared to plow into the surface, as was the case of shoes with relatively pliable uppers (7Fly, Superbad, TRX, and Vapor), often only three regions were noted by the omission of a distinct slippage region (Figure 2.2B).
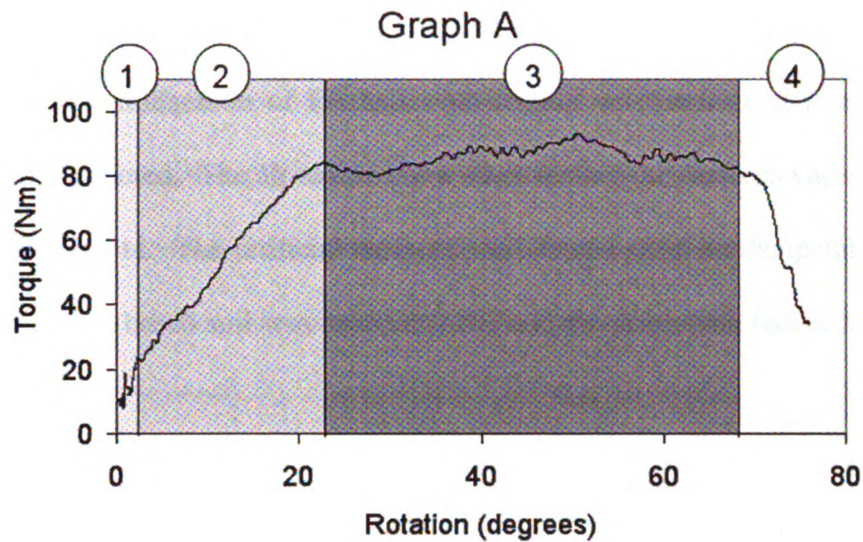
Figure 2.2A: The representative shape of the torque vs. shoe rotation plot that consisted of four regions (initial breakaway, build-up, slippage, unloading). The percent of rotation that occurred in each region was dependent on the shoe-surface combination and varied between shoes and surfaces.
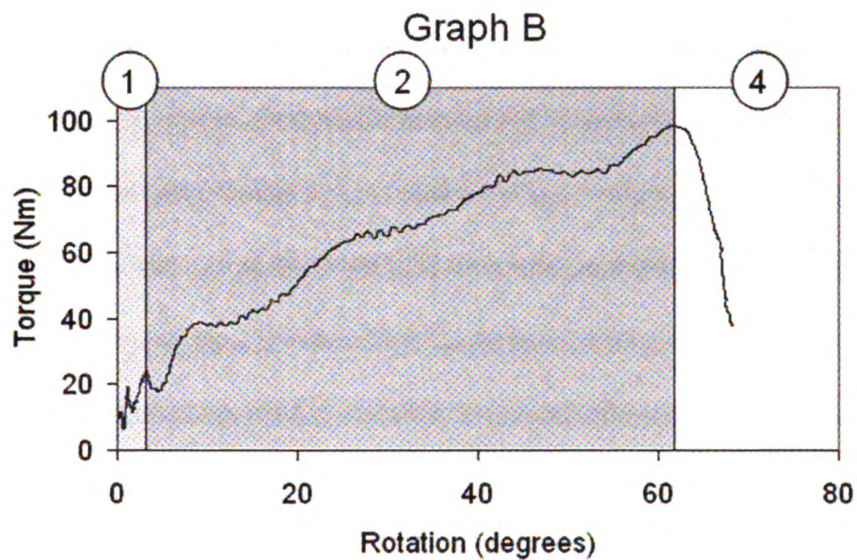
Figure 2.2B: The representative shape of the torque vs. shoe rotation plot that consisted of three regions (omission of slippage).

All natural grass testing was conducted in Michigan in early autumn at approximately the midseason of football. No testing was performed if moisture or a previous rain was noted. The air temperature when testing the surfaces varied during this series of experiments. The artificial surfaces were tested at an air temperature of 21°C, the grass with sand based soil was tested at 11°C and the grass with native Michigan soil was tested at 32°C.

Cleat Pattern

The classification of shoe groups did not yield any relationships between cleat pattern and rotational stiffness (Table 2.2). Significant differences in peak torque were only noted with comparison to the Turf cleat (Table 2.3). The Turf cleat produced significantly lower torque than all other groups ($p < 0.001$). There were no significant differences between the 12 Studded, Edge, Hybrid, and 7 Studded cleat pattern groups.

Table 2.2: Rotational stiffness - Nm/deg, mean of five trials (SD)

\# indicates significant difference from natural grass surfaces (p < 0.001)

Surface	Cleated Shoe										
	12 Studded		Edge		Blitz	Hybrid		7 Studded		Turf	MEAN
	Bladell	7Fly	Vapor	TRX		Superbad	Gridiron	BladeD	Qslant	TurfHog	
FieldTurf	4.0 (0.3)	3.7 (0.2)	4.0 (0.4)	3.0 (0.0)	5.1 (0.5)	2.5 (0.3)	4.2 (0.5)	3.1 (0.4)	3.4 (0.2)	3.1 (0.2)	3.6 # (1.5)
AstroPlay	3.2 (0.5)	3.8 (0.5)	3.6 (0.3)	3.2 (0.2)	4.3 (0.3)	2.4 (0.1)	4.3 (0.4)	3.4 (0.7)	3.3 (0.5)	3.4 (0.1)	3.5 # (1.3)
Grass Sand Based	2.2 (0.2)	2.0 (0.4)	2.3 (0.4)	2.0 (0.2)	2.5 (0.2)	1.7 (0.2)	2.5 (0.5)	2.9 (0.4)	2.7 (0.5)	1.6 (0.3)	2.2 (0.8)
Grass Native Soil	1.7 (0.2)	2.0 (0.3)	2.0 (0.3)	2.3 (0.3)	3.2 (0.7)	1.4 (0.2)	2.4 (0.5)	2.3 (0.7)	2.5 (0.7)	2.2 (0.7)	2.2 (0.9)
MEAN	2.8 (1.0)	2.9 (0.9)	3.0 (0.9)	2.6 (0.5)	3.8 (1.1)	2.0 (0.5)	3.3 (1.0)	2.9 (0.6)	3.0 (0.6)	2.6 (0.8)	

Table 2.3: Peak torque – Nm; mean of five trials (SD)

* indicates significant difference from all other surfaces (p = 0.008)

# indicates significant difference from natural grass surfaces (p < 0.001)

+ indicates significant difference from all other shoe models (p < 0.001)

Surface	Cleated Shoe										
	12 Studded		Edge		Blitz	Hybrid		7 Studded		Turf	MEAN
	BladeII	7Fly	Vapor	TRX	Blitz	Superbad	GridIron	BladeD	Qslant	TurfHog	MEAN
FieldTurf	135.8	120.4	131.6	129.0	121.8	117.4	112.4	119.6	113.4	81.4	118.3 #
	(8.2)	(2.2)	(2.3)	(7.4)	(2.7)	(6.1)	(5.4)	(4.9)	(4.8)	(4.0)	(15.2)
AstroPlay	121.6	107.8	118.4	117.0	109.2	119.8	109.6	130.8	105.8	78.4	111.8 #
	(8.3)	(4.9)	(7.3)	(7.0)	(3.8)	(3.8)	(5.6)	(6.4)	(6.7)	(4.4)	(14.5)
Grass Sand Based	115.6	107.4	100.4	98.6	74.2	101.4	84.8	112.4	104.6	59.6	95.9 *
	(5.9)	(9.4)	(6.1)	(4.7)	(3.8)	(4.8)	(5.7)	(12.3)	(2.8)	(3.8)	(18.0)
Grass Native Soil	87.6	95.0	98.6	79.8	77.8	73.6	81.4	83.0	94.4	60	83.1 *
	(8.4)	(6.8)	(6.0)	(6.8)	(5.7)	(4.7)	(6.1)	(2.0)	(8.0)	(3.1)	(12.3)
MEAN	115.2	107.7	112.3	106.1	95.8	103.1	97.1	111.5	104.6	69.9	
	(19.3)	(10.9)	(14.9)	(20.1)	(21.2)	(19.4)	(15.3)	(19.4)	(8.8)	(11.0)+	

Shoe Model

With the exception of the Adidas TurfHog, the model of shoe was not found to have a significant effect on the peak torque (Table 2.3). The model of shoe did significantly affect rotational stiffness (Tables 2.2 and 2.4). The Adidas Blitz produced significantly higher rotational stiffness than six other models. This was likely attributable to its large rubber cleats, and perhaps more importantly, relatively rigid upper and sole. By comparison, the shoe that produced a rotational stiffness significantly lower than five other models, the Nike Superbad, had a relatively pliable upper and sole, making it more capable of rotating on the rigid footform. This allowed the medial edge of the shoe to dig into the ground and continually add rotational traction after breakaway (the initial release of the shoe from the surface).

Table 2.4: Rotational stiffness post-hoc comparison between shoe models

	BladeII	7Fly	Vapor	TRX	Blitz	Superbad	GridIron	BladeD	Qslant	TurfHog
BladeII	-	1.000	0.997	1.000	*0.012*	0.149	0.471	1.000	0.997	0.999
7Fly	1.000	-	1.000	0.988	*0.031*	0.064	0.728	1.000	1.000	0.974
Vapor	0.997	1.000	-	0.900	0.081	*0.024*	0.923	1.000	1.000	0.849
TRX	1.000	0.988	0.900	-	*0.003*	0.417	0.177	0.963	0.903	1.000
Blitz	*0.012*	*0.031*	0.081	*0.003*	-	*<0.001*	0.705	*0.049*	0.079	*0.002*
Superbad	0.149	0.064	*0.024*	0.417	*<0.001*	-	*<0.001*	*0.041*	*0.025*	0.493
GridIron	0.471	0.728	0.923	0.177	0.705	*<0.001*	-	0.832	0.921	0.139
BladeD	1.000	1.000	1.000	0.963	*0.049*	*0.041*	0.832	-	1.000	0.934
Qslant	0.997	1.000	1.000	0.903	0.079	*0.025*	0.921	1.000	-	0.853
TurfHog	0.999	0.974	0.849	1.000	*0.002*	0.493	0.139	0.934	0.853	-

<u>Surface</u>

The values of peak torque and rotational stiffness were significantly affected by the playing surface (Tables 2.3 and 2.4). Both artificial surfaces produced higher torques ($p < 0.001$) than natural grass surfaces. The natural grass surface with engineered, sand based soil produced higher torques ($p = 0.008$) than natural grass with native Michigan soil. The rotational stiffness for both artifical surfaces was higher ($p < 0.001$) than each of the natural grass surfaces. The stiffness of the different systems of artificial or natural grasses was not statistically different from one another.

DISCUSSION:

High rotational traction between football shoes and playing surfaces may yield a potential for injury to the lower extremity (Bonstingl et al., 1975; Lambson et al., 1996; Nigg and Yeadon, 1987; Torg et al., 1974). The current study utilized a mobile apparatus to record the torque and relative rotation at the shoe-surface interface for a variety of currently available, cleated football shoes in combination with synthetic infill surface systems and natural grasses. A wide variation in peak torques between shoe-surface interfaces was not unexpected, based on the current literature. A previous study by Cawley et al. (2003) shows a torque range of 50 and 120 Nm for 7 studded and turf shoe designs on grass. The trend in peak torque across surfaces was also noted to be similar to a previous study by Livesay et al. (2006) that examines several infill surfaces using a lower compressive load and forefoot cleats rigidly mounted to a circular plate. Although those results could not be directly related to the current data, in both studies the grass surfaces produce the lowest peak torques.

The classification of shoe groups based on cleat pattern did not predetermine a shoe's rotational traction characteristics. The only cleat pattern designation that produced peak torques significantly different than all other groups was the turf style cleat. The short elastomeric cleats may not have penetrated the infill layer or soil as deeply as the other models to help limit the degree of rotational traction. The wide range of torques noted both within and across shoe groups emphasized the impact of other factors, beyond cleat pattern, that may affect rotational traction. Therefore, the first hypothesis that related rotational traction to cleat pattern could not be validated in the current study. The second hypothesis that related rotational traction to shoe model was validated with regards to rotational stiffness. The shoe shape, upper material, and construction may all be possible contributors to the varying amounts of rotational stiffness.

One potential limitation of the present study was the surrogate ankle. The deformable elastomer used to represent the torsional stiffness of the ankle joint averaged 11 Nm/deg, exceeding *in vivo* measurements of 1.2 Nm/deg by Mote and Lee (1982). However, the *in vivo* stiffness recorded in the previous study was limited to amplitudes of ±6 degrees, a significant limitation in the overall response of the joint. Assuming the *in vivo* stiffness of the ankle joint can be modeled by a bilinear response similar to the knee joint (Dorius and Hull, 1984), the secondary stiffness of the ankle may be on the order of 3 to 5 times the primary stiffness, yielding a maximum torsional stiffness of 6 Nm/deg for the ankle. The surrogate ankle may also be improved by the incorporation of additional degrees of freedom that may alter loading mechanisms on a surface. Inversion/eversion of the ankle may increase the medial edge loading mechanism and dorsiflexion/plantarflexion may effect the load distribution across the cleats.

Incorporation of these designs into a surrogate ankle may help to generate more physiological responses of the lower leg at the shoe-surface interface.

The artificial surfaces were tested at similar temperatures, while the air temperature for the natural grass testing varied by 21°C. A previous study showed that an increase in air and turf temperature did have an effect on the shoe-surface traction for AstroTurf (Torg et al., 1996). In an extensive literature search, no evidence was gathered regarding a relationship between the ambient air temperature and its effect on traction for a natural grass system. The effect of climate on natural grass systems has been considered in epidemiological studies involving the frequency of injury and the time of season (Orchard, 2002). In a rugby study it was concluded that there was a bias towards a higher frequency of injury in the summer months which was proportionately greater for backs, the players who tend to sustain most non-contact injuries (Gissane et al., 1998). A major contributor to this bias was believed to be ground hardness, brought about by drier and warmer conditions in the summer season. Both natural grass systems in the present study were tested in the same autumn month, and they were regularly watered.

A potential threshold for a "safe" torsional release coefficient of shoes and surfaces was introduced in the 1970s (Torg et al., 1974). In the current study a normal force of 1000 N would generate a theoretical "safe" torque of approximately 95 Nm, based on the previous study results. Most shoe-surface interface values in the current study exceeded this threshold level. This level also exceeds the maximum torque that the ankle can support, approximately 75 Nm, based on cadaver tests (Hirsch and Lewis, 1965). On the other hand, Shoemaker et al. (1988) suggest that muscles may contribute

as much as 70 Nm of resistive torque and help protect the lower extremity from injury during controlled athletic maneuvers.

It is unknown if differences in rotational stiffness at the shoe-surface interface might impact the risk of injury, as suggested in the Livesay et al. (2006) study. The lower rotational stiffness observed for both natural grass systems compared to the artificial surfaces indicated a lower rate of loading. This might allow more time for a protective type of neuromuscular control in the lower extremity that could help stabilize the ankle and knee joints during cutting maneuvers (Livesay et al., 2006). The differences in rotational stiffness across shoes may also influence injury risk. A potential design factor may be the materials used to construct the shoe's upper. A shoe with a pliable upper may allow more time for neuromuscular control, but it may also allow the foot to pronate while the leg is internally rotated. This loading scenario may result in rupture of the anterior tibiofibular ligament, a severe time loss injury (Guise, 1976). Future epidemiological studies of shoe and surface injury rates on infill based surfaces and grass will be important in generating the "real" injury risk for various shoe-surface interfaces.

In conclusion, an extensive amount of work exists concerning the interaction of football cleats with the first-generation of non-infill AstroTurf, yet much remains unknown about the performance characteristics of modern infill, artificial surfaces. The present study investigated the dynamic performance of a number of currently used football shoes and cleat designs on natural grass and infill based artificial surfaces under a compressive load that may be representative of a 95th percentile male during a sports activity. It is important to continue to gain an understanding of the tractional

characteristics of the shoe-surface interface as manufacturers continue to update cleat and surface designs. In order to meet the critical need of improving the design of shoe-surface interfaces many areas still need further research. The effects of moisture and temperature on traction characteristics of infill based artificial surfaces need additional study. It is also unknown whether an internally directed ground reaction torque would engage the cleats in a different manner and generate different torque results. Meyer et al. (2008) demonstrate that this type of loading may generate isolated rupture of the anterior cruciate ligament. From a performance aspect, linear traction testing would assess a player's need for speed and agility (Krahenbuel, 1974; Morehouse and Morrison, 1975). These data could then be used to help improve shoe-surface interfaces and mitigate injury potential while maintaining player performance.

REFERENCES

American Society for Testing and Materials. (2006) Annual Book of ASTM Standards. Standard test method for traction characteristics of the athletic shoe - sports surface interface. F2333-04. ASTM. 15.07:1412-1420.

Andreasson G, Lindenberger U, Renstrom P, Peterson L. (1986) Torque developed at simulated sliding between sport shoes and an artificial turf. Am J Sports Med. 14(3):225-230.

Arnold JA, Coker TP, Heaton LM, Park JP, Harris WP. (1979) Natural history of anterior cruciate tears. Am J Sports Med. 7(6):305-313.

Bonstingl RW, Morehouse CA, Niebel BW. (1975) Torques developed by different types of shoes on various playing surfaces. Med Sci Sports. 7(2):127-131.

Cawley PW, Heidt RS Jr., Scranton PE Jr., Losse GM, Howard ME. (2003) Physiologic axial load, frictional resistance, and the football shoe-surface interface. Foot Ankle Int. 24(7):551-556.

Dorius LK, Hull ML. (1984) Dynamic simulation of the leg in torsion. J Biomech. 17(1):1-9.

Fauno P, Wulff Jakobsen B. (2004) Mechanism of anterior cruciate ligament injuries in soccer. Int J Sports Med. 27:75-79.

Fernandez WG, Yard EE, Comstock RD. (2007) Epidemiology of lower extremity injuries among U.S. high school athletes. Acad Emerg Med. 14(7):641-645.

FieldTurf Inc [Internet]. Product Overview. Available at: http://www.fieldturf.com/product/designConstruction.cfm. Accessed Dec 19, 2007.

Gissane C, Jennings D, White J, Cumine A. (1998) Injury in summer rugby league football: the experiences of one club. Br J Sports Med. 32(3):149-52.

Guise ER. (1976) Rotational ligamentous injuries to the ankle in football. Am J Sports Med. 4(1):1-6.

Hammer D. (1981) Artificial playing surfaces. Athletic Training. 16:127-129.

Hirsch C, Lewis J. (1965) Experimental ankle joint fractures. Acta Orthop Scand. 36:408-417.

Krahenbuel GS. (1974) Speed of movement with varying footwear conditions on synthetic turf and natural grass. Res Q. 45:28-33.

Lambson RB, Barnhill BS, Higgins RW. (1996) Football cleat design and its effect on anterior cruciate ligament injuries. A three year prospective study. Am J Sports Med. 24(2):155-159.

Livesay GA, Reda DR, Nauman EA. (2006) Peak torque and rotational stiffness developed at the shoe-surface interface. Am J Sports Med. 34(3):415-422.

Meyer EG, Baumer TG, Slade JM, Smith WE, Haut RC. (2008) Tibiofemoral contact pressures and osteochondral microtrauma during anterior cruciate ligament rupture due to excessive compressive loading and internal torque of the human knee. Am J Sports Med. 36(10):1966-1977.

Morehouse CA, Morrison WE. (1975) The artificial turf story: A research review. Penn State HPER Series. The Pennsylvania State University. University Park.

Mote CD Jr, Lee CW. (1982) Identification of human lower extremity dynamics in torsion. J Biomech. 15(3):211-222.

Nigg BM, Yeadon MR. (1987) Biomechanical aspects of playing surfaces. J Sports Sci. 5(2):117-145.

Orchard J. (2002) Is there a relationship between ground and climatic conditions and injuries in football? Sports Med. 32(7):419-432.

Powell JW, Schootman M. (1992) A multivariate risk analysis of selected playing surfaces in the National Football League: 1980-1989. An epidemiological study of knee injuries. Am J Sports Med. 20(6):686-694.

Powell JW, Schootman M. (1993) A multivariate risk analysis of natural grass and AstroTurf playing surfaces in the National Football League 1980-1989. Int Turfgrass Soc Res J. 23:201-211.

Robbins D. (1985) Anthropometry of motor vehicle occupants. Volume 3. Transportation Research Institute. DOT/HS 806 717.

Shoemaker SC, Markolf KL, Dorey FJ, Zager S, Namba R. (1988, March) Tibial torque generation in a flexed weight-bearing stance. Clin Orthop Relat Res. 228:164-170.

Shorten MR, Hudson B, Himmelsbach JA. (2003, July 6-12) Shoe-surface traction of conventional and in-filled synthetic turf football surfaces. In: Milburn, P. (ed.) Proc XIX International Congress of Biomechanics, University of Otago, Dunedin, New Zealand. Dunedin, NZ. International Society of Biomechanics. CD ROM abstracts and proceedings.

Southwest Recreational Industries [Internet]. AstroPlay overview. Available at: http://www.srisports.com/field/filled.htm. Accessed Feb 25, 2008.

Stanitski CL, McMaster JH, Ferguson RJ. (1974) Synthetic turf and grass: A comparative study. J Sports Med. 2(1):22-26.

Torg JS, Quedenfeld TC, Landau S. (1974) The shoe-surface interface and its relationship to football knee injuries. J Sports Med. 2(5):261-269.

Torg JS, Stillwell G, Rogers K. (1996) The effect of ambient temperature on the shoe-surface interface release coefficient. Am J Sports Med. 24:79-82.

Chapter 3: The Effects of Various Infills, Fiber Structures, and Shoe Designs on Generating Rotational Traction on an Artificial Surface

ABSTRACT:

The purpose of this study was to investigate the role of infill material and fiber structure on the rotational traction associated with American football shoes on infill-based, third-generation, artificial surfaces. A mobile testing apparatus with a compliant ankle was used to apply rotations and measure the torque produced at the football shoe-surface interface. The mechanical surrogate was used to compare three infill materials in combination with three fiber structures, creating a total of nine unique surfaces. Infill material, fiber structure and shoe design were all found to significantly affect rotational traction. The cryogenically processed, styrene-butadiene rubber infill yielded significantly higher peak torques than the ambient ground, styrene-butadiene rubber and extruded thermoplastic elastomer infills. An artificial surface with a nylon root zone yielded significantly lower peak torques than similar fiber surfaces without a nylon root zone. The size of infill particles and the presence of a nylon root zone may influence the compactness of the infill layer. These features may act to alter the amount of cleat contact with the infill, thereby influencing rotational traction. The amount of cleat contact with the surface may also be determined by the shoe design.

INTRODUCTION:

The popularity of artificial turf has continued to grow since its first emergence in the 1960s. It is now considered by many to be a viable alternative to natural grass, as evidenced by its prevalence in numerous indoor and outdoor stadiums across the world. The latest generation, often termed the "third-generation", of artificial surfaces was introduced in the 1990s. These surfaces are comprised of a soft absorbent infill material (often crushed rubber or a combination of crushed rubber and sand) and longer, more durable pile fibers. This surface is often claimed to better simulate a natural grass field, but since its introduction there is paucity of research regarding the effects of playing on this generation of artificial playing surface.

Injuries to the lower extremity are among the most frequent injuries for all levels of sports and often account for more than 50% of reported injuries (Fernandez et al., 2007). In the National Football League (NFL) ankle and knee sprains combine to account for about 20% of all reported injuries (Powell and Schootman, 1992;1993). These injuries can occur during contact between players or in noncontact situations, such as a rapid change in direction or with a combination of high compressive load and twist during a jump landing (Arnold et al., 1979; Fauno and Wulff Jakobsen, 2004). Frequently the mechanism of injury involves a foot planted on the playing surface with an excessive rotation of the upper body (Guise, 1976).

Traction is defined by the ASTM (American Society for Testing and Materials) committee on Sports Equipment and Facilities to be the resistance to relative motion between a shoe outsole and a sports surface that does not necessarily obey classical (Coulomb) laws of friction (ASTM F2333, 2006). While linear traction is necessary for

high-level performance during any athletic contest (Shorten et al., 2003), it is generally accepted that excessive rotational traction may precipitate ankle and knee injuries (Bonstingl et al., 1975; Lambson et al., 1996; Nigg and Yeadon, 1987; Torg et al., 1974). A previous study of ACL (anterior cruciate ligament) injuries in high school football players documented a significant relationship between cleat design, the amount of rotational traction and the risk of ACL injury on grass (Lambson et al., 1996). The edge cleat design produced significantly higher rotational traction and was associated with an ACL injury rate 3.4 times higher than that of all other designs combined.

Other studies have noted differences of injury rate in the presence or absence of specific risk factors, such as whether the surface was natural grass or an artificial surface. These differences in injury rate may be due to variations in the structure and materials of the turfs (Hammer, 1981), the running speed of the players (Stanitski et al., 1974) or the coefficient of friction between the surface and shoe (Andreasson et al., 1986). The injury risk factor may also depend on the player's position and the type of play at the time of injury, both of which could influence the mechanisms of loading on the lower extremity (Powell and Schootman, 1992;1993).

Although rotational traction has been documented in previous studies (usually as the peak torque magnitude recorded during dynamic testing), it has been primarily focused on natural grass and the first-generation of short-pile artificial turf (Bonstingl et al., 1975; Cawley et al., 2003; Lambson et al., 1996; Torg et al., 1974). The third-generation, artificial surface used in professional, collegiate and high school sports is a sharp contrast to the dense and abrasive first-generation, artifical turf. Artificial surfaces now consist of longer, more grass-like fibers that are surrounded and stabilized by infill

materials, such as rubber and sand. The influence of these individual components on the rotational traction characteristics of an infill artificial surface is unknown.

The purpose of the present study was to investigate the influence of infill material and fiber structure on the rotational traction associated with American football shoes on infill based artificial surfaces. The hypothesis of this study was that artificial surfaces with small infill particles and/or a fiber layout that allow greater infill contact with the cleats will produce higher peak torques than surfaces with larger infill particles and/or a fiber layout that limits the infill contact with the cleats. A better understanding of how different components of the artificial surface affect rotational traction may aide in the design of future surfaces. These data may also have relevance to studies on the risk potential for rotational lower leg injuries on current and future surface designs.

MATERIALS AND METHODS:

Three infill materials were evaluated in this study: A) cryogenically processed, styrene-butadiene rubber (SBR) crumb infill (PermaLife Products, LLC, Guttenberg, New Jersey) (PermaLife.com, 2008), B) ambient ground, SBR crumb infill (PermaLife Products, LLC, Guttenberg, New Jersey) (PermaLife.com, 2008), C) extruded thermoplastic elastomer (TPE) infill (Terra Sports Technology, The Netherlands) (TerraSportsTech.com, 2008). They were tested in combination with three fiber structures: I) monofilament polyethylene fibers (GameDay MT, General Sports Venue, LLC, Rochester, Michigan) (AstroTurfUSA.com, 2008), II) parallel slit polyethylene fibers (GameDay Xpe, General Sports Venue, LLC, Rochester, Michigan) (AstroTurfUSA.com, 2008), III) monofilament polyethylene fibers in conjunction with a

nylon root zone (GameDay 3D, General Sports Venue, LLC, Rochester, Michigan) (AstroTurfUSA.com, 2008). A nylon root zone is a simulated thatch layer at the base of the tufted turf (Figure 3.1). The zone provides fiber support and reduces infill compaction (AstroTurfUSA.com, 2008). All of the fiber structures were constructed with a 3/8" gauge length (the distance between rows of fiber tufts). The nine iterations of artificial turf were installed outdoors with a fulltime maintenance staff and had been in place for approximately one year with limited usage when tested.
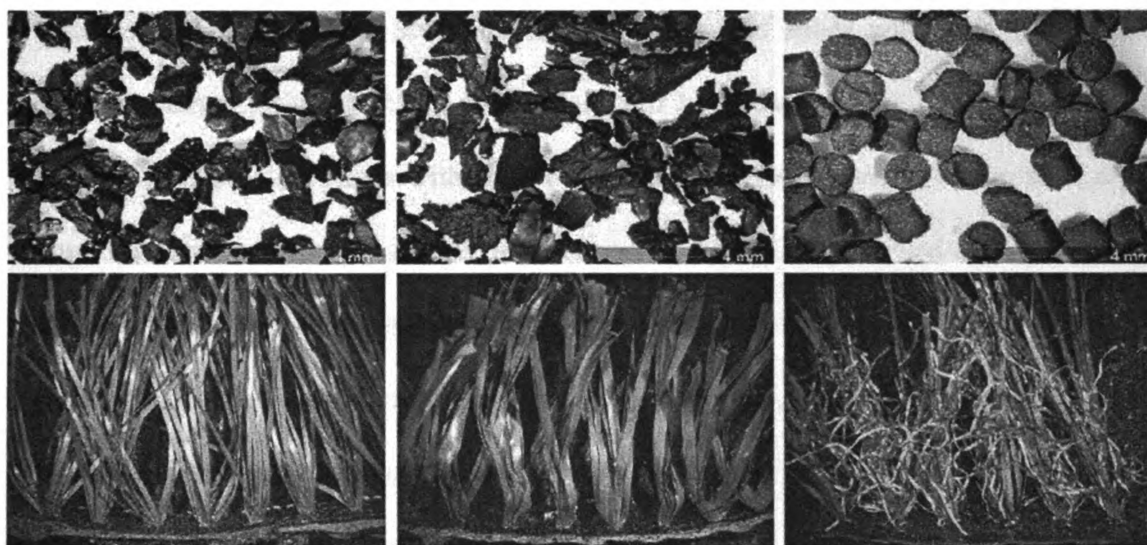
Figure 3.1: Infills (upper left to right) – A (cryogenic SBR), B (ambient SBR), C (extruded TPE); Fibers (lower left to right) – I (monofilament), II (parallel slit), III (monofilament with nylon root zone).

The relative fineness of each infill was analyzed by a fixed volume comparison. The density of each infill was calculated using a 50 cm^3 container and an electronic semi-micro balance (Model R160D, Sartorius, Germany). A fixed volume of 0.2 cm^3 of each infill was then analyzed using SigmaScanPro Image Analysis (Version 5.0.0, SPSS Inc., Chicago, IL). The number of particles was recorded, as well as the maximum diameter of each particle.

Each surface was tested using ten different shoes, yielding 90 different shoe-surface combinations. The shoes were grouped into five categories, based on design properties (Table 3.1): 1) 7 Studded - traditional cleated shoes with seven removable cleats, five covering the forefoot of the sole and two covering the heel region, 2) 12 Studded - molded cleat shoes with twelve cleats around the perimeter of the sole, eight around the forefoot and four around the heel region, 3) Hybrid - molded cleat shoes with four cleats around the heel region and at least fifteen cleats distributed across the forefoot region, 4) Edge – shoes characterized by blade style cleats, 5) Turf - shoes which had a dense pattern of short elastomeric cleats distributed over the entire sole.

Table 3.1: Description of tested football shoes

Category	Mfr.	Model	Height	Cleat material	Number of cleats	Max cleat length (mm)	Image
12 Studded	Nike	Bladell TD	Mid-cut	Elastomeric	14	16.3	
	Adidas	Scorch 7 Fly	Low-cut	TPU	13	12.5	
Edge	Nike	Vapor Jet TD	Low-cut	TPU	12	12.0	
	Adidas	Scorch TRX	Low-cut	TPU	15	13.0	
	Adidas	Corner Blitz 7 MD	Mid-cut	Elastomeric	15	11.0	
Hybrid	Nike	Air Zoom Superbad FT	Mid-cut	Elastomeric	21	11.0	
	Adidas	Grid Iron	Mid-cut	Elastomeric	20	12.0	
7 Studded	Nike	Air Zoom Blade D	Mid-cut	TPU (Steel Tip)	7	12.5	
	Adidas	Quickslant D	Mid-cut	TPU (Steel Tip)	7	12.5	
Turf	Adidas	Turf Hog LE	Mid-cut	Elastomeric	88	6.5	

A testing apparatus was developed to apply a dynamic rotation and measure the torque produced at the shoe/surface interface (Figure 3.2). The apparatus was fabricated to conform to an international standard method for measuring rotational traction characteristics of an athletic shoe-surface interface (ASTM F2333, 2006). The device

consisted of an aluminum frame that could be raised and lowered to the ground with wheels to allow easy mobility. The frame supported the surrogate lower limb, a suspended 425 N weight attached to a 0.25 m radius gear that was used to produce a torque on the shoe. The weight was released by means of a manual lever arm located on the side of the testing device. The drop height of the weight hanger was adjusted so that the input rotation angle of the shaft was 90°. The rate of rotation was chosen to represent a high speed injury situation. During running, the tibia has been documented to internally rotate at ground contact with speeds between 160 and 180°/second (Bellchamber and van den Bogert, 2000; McClay and Manal, 1998; Stacoff et al., 2000). To represent an *in vivo* situation, the rate of rotation was approximately 180°/second. This exceeded the minimum rate of 45°/second required by the ASTM testing standard (ASTM F2333, 2006). The frame was stabilized on the test surfaces by two operators standing on the outboard platforms. The testing apparatus was designed to simulate the anthropomorphic data of a 95th percentile male. This included matching the compressive load to 1 x body weight (1000 N) and fabricating the surrogate lower limb with a tibia length of 44 cm (Robbins, 1985). In addition to reproducing key mass and length measurements for the surrogate lower limb, the ankle was designed to be compliant with regards to internal/external rotation by means of a deformable elastomeric washer.
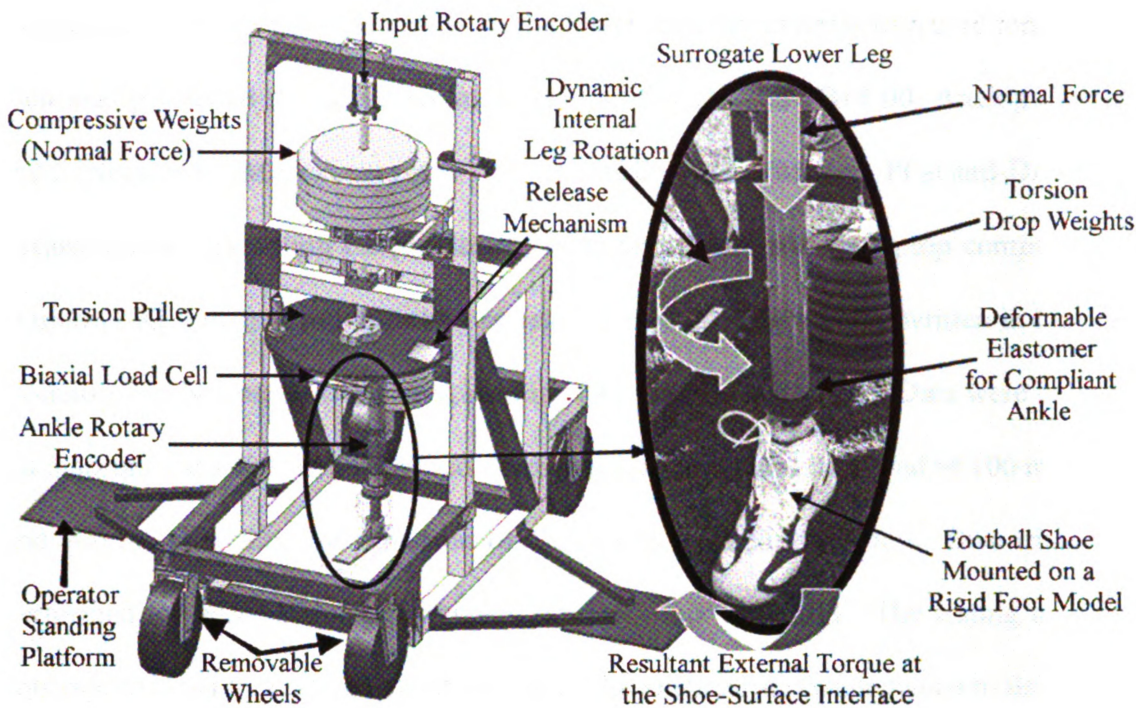
Figure 3.2: Description of rotational traction testing apparatus

To represent a possible worst-case injury scenario, the current study replicated a loading condition having full cleat contact with the ground. The peak torque measured in tests with full cleat contact has been shown to be typically 70% higher than tests with only toe cleats engaged (Bonstingl et al., 1975). A rigid model of the right foot was fabricated and attached below the ankle position on the testing device. The foot represented a U.S. size 13 shoe, and the center of rotation (COR) on the test device was adjustable. The COR was set at the midfoot, a distance of 14 cm from the heel for all tests.

The device generated a dynamic internal rotation of the leg, resulting in an externally applied ground reactionary torque on the foot. A torsional load cell (Model 1216CEW-2K, Interface, Scottsdale, AZ) calibrated for 170Nm full-scale capacity was

placed below the gear and connected to the lower leg shaft in order to record torque. The data was processed through a strain gage amplifier (Model 3B18-00, Analog Devices, Inc., Norwood, MA) connected to an A2D card (Model PC-Card-DAS16/16, Measurement Computing Corp., Norton, MA) and recorded on a laptop computer with Windows XP Professional operating system. A custom program was written in LabView (Version 7.0, National Instruments, Austin, TX) for data collection. Data were collected for 5 seconds at 1000 Hz and the recorded data from each trial consisted of 100 ms before and 900 ms after a torque threshold of 3 Nm was reached in the test. Five trials were performed for each unique combination of shoe, fiber and infill. The testing apparatus was repositioned to a new adjacent section of the artificial surface between trials. The air temperature was also recorded on each day of testing.

Data from all trials were analyzed to determine the peak torque. A two way ANOVA was performed with SigmaStat (Version 2.03, SPSS Inc., Chicago, IL) to assess the effect of infill (n=3) and fiber structure (n=3) on the peak torque, with repeated measures across trials (n=50). When the differences in the mean values among the infill and/or fiber groups were found to be greater than would be expected by chance, Tukey post-hoc tests were performed to detect statistically significant differences between infill (A,B,C) and fiber (I,II,III). The effect of cleat pattern (n=5) was assessed by a one way ANOVA with Tukey post-hoc tests, when appropriate. Statistical significance was set at $p < 0.05$ for all analyses.

RESULTS:

The testing apparatus collected torque-time data on the ninety shoe-surface interface combinations (Table 3.2). The value of peak torque was significantly affected by the type of infill and fiber structure. Infill A yielded significantly higher peak torques ($p < 0.001$) than other infill types (Figure 3.3). There was no statistical difference between infills B and C. Fiber III produced significantly lower peak torques ($p < 0.001$) than other fiber types (Figure 3.4). There was no statistical difference between fibers I and II.

Table 3.2: Peak torque – Nm; mean of five trials (SD)

| | Cleated Shoe | | | | | | | | | | |
| Surface | 12 Studded | | | Edge | | Hybrid | | 7 Studded | | Turf | MEAN |
	Blade II	7Fly	Vapor	TRX	Blitz	Superbad	Gridiron	Blade D	Qslant	TurfHog	
I - A	125.5 (10.5)	114.2 (8.6)	119.6 (7.5)	121.2 (1.8)	119.0 (2.3)	101.8 (4.4)	112.0 (5.6)	100.2 (4.8)	105.6 (5.6)	71.4 (3.2)	109.0 (16.0)
II - A	116.4 (5.3)	112.2 (6.0)	122.8 (4.8)	121.0 (11.4)	126.0 (5.3)	102.8 (4.4)	118.2 (8.6)	94.6 (1.7)	100.2 (7.9)	87.4 (3.2)	110.2 (13.9)
III - A	117.0 (1.6)	107.6 (4.7)	104.8 (6.0)	118.2 (4.7)	104.4 (2.5)	93.8 (10.0)	104.2 (5.9)	87.0 (4.8)	95.0 (9.8)	90.2 (4.9)	102.2 (11.6)
I - B	128.0 (9.9)	112.0 (3.3)	120.0 (4.2)	107.6 (8.6)	105.2 (4.3)	96.8 (6.6)	95.6 (3.2)	95.0 (6.6)	92.6 (4.8)	75.2 (3.8)	102.8 (15.5)
II - B	112.8 (7.5)	102.0 (8.1)	110.4 (7.6)	105.4 (5.3)	106.2 (2.9)	97.6 (6.7)	105.0 (8.2)	91.6 (6.7)	89.2 (2.2)	84.4 (5.5)	100.5 (10.7)
III - B	110.8 (4.2)	85.4 (5.6)	98.4 (6.4)	113.0 (8.6)	99.8 (4.5)	90.0 (3.7)	94.6 (5.7)	86.2 (7.0)	85.4 (3.8)	75.0 (2.9)	93.9 (12.5)
I - C	117.0 (9.9)	97.2 (9.1)	110.4 (5.5)	105.8 (6.9)	98.2 (2.4)	98.2 (8.1)	91.0 (3.4)	91.6 (4.1)	92.4 (3.6)	70.0 (2.4)	97.2 (13.5)
II - C	113.4 (5.2)	97.2 (7.8)	110.8 (6.8)	102.4 (4.6)	108.8 (3.4)	95.2 (1.3)	100.6 (2.7)	91.4 (3.3)	83.4 (5.8)	84.0 (3.2)	98.7 (11.0)
III - C	102.2 (6.1)	97.0 (9.4)	104.6 (2.3)	98.2 (3.4)	105.6 (1.7)	93.0 (6.1)	102.0 (5.8)	96.4 (9.9)	85.0 (4.8)	84.6 (4.0)	96.9 (8.9)
MEAN	115.9 (7.7)	102.8 (9.5)	111.3 (8.2)	110.3 (8.4)	108.1 (8.9)	96.6 (4.1)	102.6 (8.6)	92.7 (4.4)	92.1 (7.4)	80.2 (7.4)	

Figure 3.3: Box plot of peak torque across shoes for each infill. The line near the center of the box represents the median value, the box represents the inter-quartile range and the whiskers represent the range. * indicates significant difference compared to other infills.
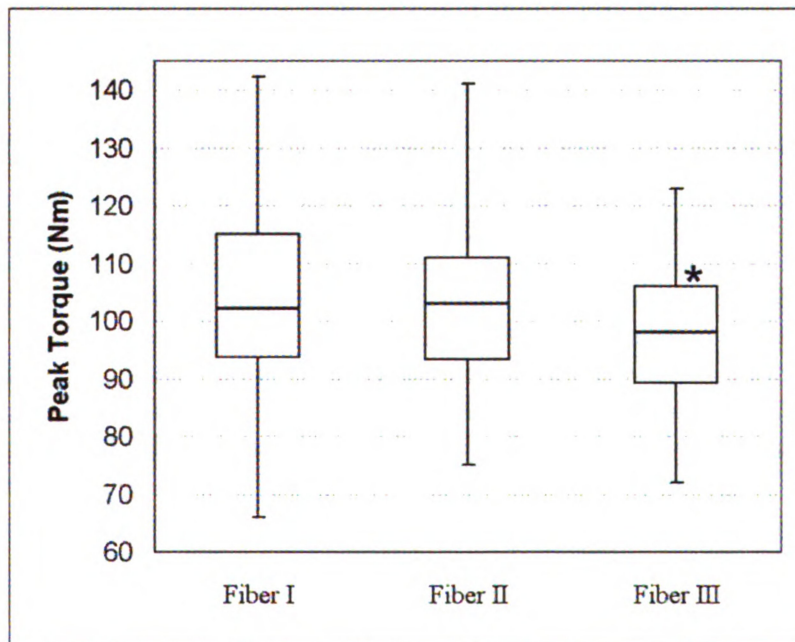
Figure 3.4: Box plot of peak torque across shoes for each fiber. The line near the center of the box represents the median value, the box represents the inter-quartile range and the whiskers represent the range. * indicates significant difference compared to other fibers.

The cleat pattern significantly affected peak torque. The 12 Studded and Edge cleat groups yielded the highest peak torques, while the Turf shoe, composed of a dense pattern of short elastomeric cleats, produced the lowest torques ($p < 0.001$) (Figure 3.5). The peak torques between the Hybrid and 7 Studded cleat groups were not significantly different.
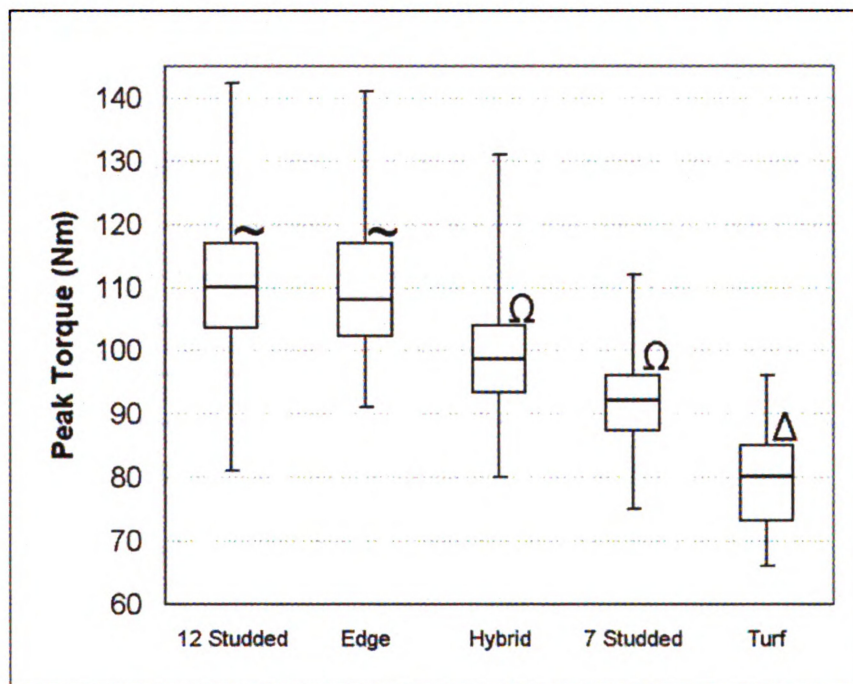
Figure 3.5: Box plot of peak torque across surfaces for each shoe type. The line near the center of the box represents the median value, the box represents the inter-quartile range and the whiskers represent the range. ~ indicates significant difference with respect to Hybrid, 7 Studded, and Turf designs. Ω indicates significant difference with respect to 12 Studded, Edge and Turf designs. Δ indicates significant difference with respect to all other cleat designs.

Size and volume measurements of the three infills were recorded (Table 3.3). All

testing was conducted in Michigan in early autumn. No testing was performed if

moisture was observed on the surface, or if it had recently rained. The experiments were

performed over a one month period, resulting in air temperature variations (Table 3.4).

Infill A was tested at an average temperature of 20.4 ± 3.1°C, infill B at 31.7 ± 2.1°C and

infill C at 26.9 ± 3.5°C. Fiber I was tested at an average temperature of 24.4 ± 5.9°C,

fiber II at 26.1 ± 4.5°C, and fiber III at 28.4 ± 5.4°C.

Table 3.3: Infill size as measured using particles in a 50 cc container

Infill	Mean Diameter (mm)	Number of Particles
A	1.73	114
B	2.39	73
C	2.40	22

Table 3.4: Air temperature during rotational traction testing – degrees C; mean
temperature (SD)

Surface	Temperature (°C)
I - A	18.6 (1.9)
II - A	21.2 (4.6)
III - A	21.4 (0.7)
I - B	31.7 (0.0)
II - B	29.8 (0.9)
III - B	33.7 (2.1)
I - C	22.9 (2.8)
II - C	27.4 (0.5)
III - C	30.2 (0.5)

DISCUSSION:

High rotational traction between football shoes and playing surfaces may yield a potential for injury to the lower extremity (Bonstingl et al., 1975; Lambson et al., 1996; Nigg and Yeadon, 1987; Torg et al., 1974). The current study utilized a mobile testing apparatus to record torque at the shoe-surface interface for different combinations of infill material and fiber structure. The torques were measured on each surface using ten different cleated shoes, yielding ninety unique shoe-surface permutations.

In the current study peak torques were significantly affected by infill type. The differences in torque may be due to the fineness of the infill, which is determined by the manufacturing process. A finer particle, such as infill A, may develop a relatively compacted structure of infill that leads to more cleat contact and greater rotational traction. In contrast, the rounded cylindrical shape of infill C may not pack as tightly as infill A to limit the degree of rotational traction. There were no statistical differences in peak torque between fibers I and II. This suggested that there was no difference in rotational traction between monofilament and parallel slit fiber systems. The most influential variable in the generation of torque may have been the presence or absence of the nylon root zone. The nylon root zone needed less infill for system stability that may have affected its compactness. This may have limited cleat contact with the infill and provided a less compacted type of infill layer. This may explain the lower peak torques observed with fiber III.

The differences in peak torque noted between the cleat patterns illustrated the impact of shoe design on rotational traction. Shoe designs with numerous and/or large cleats around the peripheral margin of the sole (12 Studded and Edge) yielded higher

peak torques than shoes with fewer or smaller cleats (Hybrid, 7 Studded, and Turf). The turf design shoe (TurfHog) produced significantly lower torques than all other designs. The short elastomeric cleats may not have penetrated the infill layer as deeply as the other models to help limit the degree of rotational traction. The statistical difference between cleat pattern groups found in this analysis was not apparent in a previous study by the same investigators which utilized the same testing methodology and cleated shoes (Villwock et al., 2009). The previous study (Villwock et al., 2009) involved a rubber infill surface, a rubber/sand infill surface, and two natural grass surfaces. This resulted in an overall standard deviation in peak torque of 19.9 Nm. In the present study all of the artificial surfaces were composed of 100% rubber infill, resulting in an overall standard deviation in peak torque of 12.7 Nm. This may have allowed differences in rotational traction based on cleat pattern to be more statistically apparent.

A limitation of the current study was air temperature variation, which occurred as a result of a month required to complete testing. Infill A, which yielded significantly higher torques than infills B and C, was tested at a lower temperature than infills B and C. Fiber III, which yielded significantly lower torques than fibers I and II, was tested at a higher temperature than fibers I and II. It is interesting to note that the infill and fiber types which produced the lowest torques were tested at the highest air temperatures. If air temperature had influenced these results, the resultant effects would seem to be in sharp contrast to a study performed by Torg et al. (1996) which documents that an increase in air and turf temperature results in an increase of shoe-surface interface traction. The correlation in that previous study was based on soft rubber shoes on AstroTurf No.8, a short pile non-infill surface that is not comparable to the surfaces in

this study. Based on this fundamental difference in design, the influence of temperature variation in the current study is unknown.

If the rotational traction characteristics of natural grass are the gold standard upon which artificial surfaces should be compared, several of the surfaces in the current study compared well to this standard. The previous study by this group, utilizing the same testing methodology and cleated shoes, recorded an average peak torque on a natural grass surface of 95.9 ± 18 Nm (Villwock et al., 2009). The artificial surface constructed with fiber III and infill B generated a lower peak torque, averaging 93.9 Nm. All three fiber structures with infill C also produced peak torques within 3 Nm of the natural grass surface. It is unknown if these similarities in peak torque may result in similar injury rates. A threshold for "safe" torsional release coefficients of shoes and surfaces was introduced in the 1970s (Torg et al., 1974). In the current study a normal force of 1000 N would correspond to a theoretical "safe" torque of approximately 95 Nm. Most shoe-surface interface values in the current study exceeded this threshold. This threshold level also exceeds the maximum torque that the ankle can support of approximately 75 Nm, based on cadaver tests (Hirsch and Lewis, 1965). On the other hand, Shoemaker et al. (1988) suggests that muscles may contribute as much as 70 Nm of resistive torque and help protect the lower extremity during controlled athletic maneuvers. Future epidemiological studies of surface injury rates on these infill-based, third-generation, artificial surfaces will be important for generating the "real" injury risk.

In conclusion, the current study identified several attributes of third-generation, artificial surfaces, such as infill size and the presence of a root zone, which influenced rotational traction. Cleat pattern was also identified as a shoe design factor responsible

for affecting rotational traction on third-generation, artificial surfaces. A vast amount of literature exists concerning the interaction of football cleats with natural grass and the first-generation, non-infill AstroTurf systems. Yet much remains unknown about the tractional characteristics of modern infilled artificial surfaces. From a performance aspect, linear traction testing would assess a player's need for speed and agility. These data could then be used along with rotational traction information to help improve shoe-surface interfaces and mitigate injury potential while maintaining player performance.

REFERENCES

American Society for Testing and Materials. (2006) Annual Book of ASTM Standards. Standard test method for traction characteristics of the athletic shoe - sports surface interface. F2333-04. ASTM. 15.07:1412-1420.

Andreasson G, Lindenberger U, Renstrom P, Peterson L. (1986) Torque developed at simulated sliding between sport shoes and an artificial turf. Am J Sports Med. 14(3):225-230.

Arnold JA, Coker TP, Heaton LM, Park JP, Harris WP. (1979) Natural history of anterior cruciate tears. Am J Sports Med. 7(6):305-313.

Bellchamber TL, van den Bogert AJ. (2000) Contributions of proximal and distal moments to axial tibial rotation during walking and running. J Biomech. 33(11):1397-1403.

Bonstingl RW, Morehouse CA, Niebel BW. (1975) Torques developed by different types of shoes on various playing surfaces. Med Sci Sports. 7(2):127-131.

Cawley PW, Heidt RS Jr., Scranton PE Jr., Losse GM, Howard ME. (2003) Physiologic axial load, frictional resistance, and the football shoe-surface interface. Foot Ankle Int. 24(7):551-556.

Fauno P, Wulff Jakobsen B. (2004) Mechanism of anterior cruciate ligament injuries in soccer. Int J Sports Med. 27:75-79.

Fernandez WG, Yard EE, Comstock RD. (2007) Epidemiology of lower extremity injuries among U.S. high school athletes. Acad Emerg Med. 14(7):641-645.

General Sports Venue, LLC [Internet]. Rochester (MI): Product overview. Available at: http://www.astroturfusa.com/product/. Accessed December 6, 2007.

Guise ER. (1976) Rotational ligamentous injuries to the ankle in football. Am J Sports Med. 4(1):1-6.

Hammer D. (1981) Artificial playing surfaces. Athletic Training. 16:127-129.

Hirsch C, Lewis J. (1965) Experimental ankle joint fractures. Acta Orthop Scand. 36:408-417.

Lambson RB, Barnhill BS, Higgins RW. (1996) Football cleat design and its effect on anterior cruciate ligament injuries. A three year prospective study. Am J Sports Med. 24(2):155-159.

McClay I, Manal K. (1988) A comparison of three-dimensional lower extremity kinematics during running between excessive pronators and normals. Clin Biomech. 13(3):195-203.

Nigg BM, Yeadon MR. (1987) Biomechanical aspects of playing surfaces. J Sports Sci. 5(2):117-145.

PermaLife Products, LLC [Internet]. Guttenberg (NJ): PermaLife SportsFill. Available at: http://www.permalife.com/SportsFillProducts.asp. Accessed December 6, 2007.

Powell JW, Schootman M. (1992) A multivariate risk analysis of selected playing surfaces in the National Football League: 1980-1989. An epidemiological study of knee injuries. Am J Sports Med. 20(6):686-694.

Powell JW, Schootman M. (1993) A multivariate risk analysis of natural grass and AstroTurf playing surfaces in the National Football League 1980-1989. Int Turfgrass Soc Res J. 23:201-211.

Robbins D. (1985) Anthropometry of motor vehicle occupants. Volume 3. Transportation Research Institute. DOT/HS 806 717.

Shoemaker SC, Markolf KL, Dorey FJ, Zager S, Namba R. (1988, March) Tibial torque generation in a flexed weight-bearing stance. Clin Orthop Relat Res. 228:164-170.

Shorten MR, Hudson B, Himmelsbach JA. (2003, July 6-12) Shoe-surface traction of conventional and in-filled synthetic turf football surfaces. In: Milburn, P. (ed.) Proc XIX International Congress of Biomechanics, University of Otago, Dunedin, New Zealand. Dunedin, NZ. International Society of Biomechanics. CD ROM abstracts and proceedings.

Stacoff A, Nigg BM, Reinschmidt C, van den Bogert AJ, Lundberg A. (2000) Tibiocalcaneal kinematics of barefoot versus shod running. J Biomech. 33(11):1387-1395.

Stanitski CL, McMaster JH, Ferguson RJ. (1974) Synthetic turf and grass: A comparative study. J Sports Med. 2(1):22-26.

TerraSportsTech [Internet]. (The Netherlands): Terra-XPS brochure. Available at: http://www.terrasportstech.com/upload/File/terraxps_english.pdf. Accessed December 6, 2007.

Torg JS, Quedenfeld TC, Landau S. (1974) The shoe-surface interface and its relationship to football knee injuries. J Sports Med. 2(5):261-269.

Torg JS, Stillwell G, Rogers K. (1996) The effect of ambient temperature on the shoe-surface interface release coefficient. Am J Sports Med. 24:79-82.

Villwock MR, Meyer EG, Powell JP, Fouty AJ, Haut RC. (2009) Football playing surface and shoe design affect rotational traction. Am J Sports Med. 37(3):518-525.

Chapter 4: External Rotation Ankle Injuries - Investigating Ligamentous Ruptures

ABSTRACT:

A majority of experiments that investigate external rotation injuries of the ankle joint produce fracture rather than the soft tissue injuries reported in many clinical studies. In addition, two different methods of foot fixation have been used to study the biomechanical response and tolerance of the human ankle to external rotation of the foot/ankle complex. It was hypothesized that experiments with a younger specimen population will result in a high frequency of ligamentous injuries, prior to bone fracture during excessive levels of external rotation of the foot/ankle complex. The torque, rotation, and mode of soft tissue injury may also be a function of the type of fixation used to constrain the foot. Seven ankle pairs were tested by externally rotating the foot/ankle complex until diagnosed injury. Two different methods of foot fixation were studied: potted and taped constraint. Motion analysis of the fibula, tibia and talus was performed in four ankle pairs. The mean failure torque was 72 Nm. Differences in the failure mode were noted between the potted and taped groups. The posterior talofibular ligament was involved in the injury when the foot was constrained in potting material. The deltoid ligament failed when the foot was constrained using the taped and potted methods, but the frequency of deltoid injury was higher for the taped foot. The higher rate of deltoid injury for the taped foot may be attributable to the additional talar motion during external rotation of the foot/ankle complex. The ankles tested with a potted foot failed at lower levels of foot rotation. This may imply that shoes with tight, stiff uppers may influence foot mechanics and therefore the potential for and location of soft tissue injury.

INTRODUCTION:

Ankle sprains are one of the most common sports injuries (Lassiter et al., 1989; McConkey, 1987), accounting for ten percent to forty-five percent of sport-related injuries (Fallat et al., 1998; MacAuley, 1999). The severity of injury varies greatly and the player's recovery time is related to the structures involved and their degree of damage. In the NFL (National Football League), excessive external rotation of the foot/ankle complex is often associated with significant time loss injuries (Boytim et al., 1991; Guise, 1976). These injuries typically involve the ligamentous structures of the ankle joint. The importance of individual ligamentous contributions to resistive torque during external rotation of the foot/ankle complex has been investigated in numerous sectioning studies (Johnson & Markolf, 1983; Rasmussen et al., 1982; Xenos et al., 1995). This involves surgically cutting a ligament and quantifying its contribution to restraint of a particular joint motion, as sequential levels of disruption are introduced in the joint. Buckle transducers and strain gauges have also been used to show that there are relatively high forces developed in the ankle ligaments during external rotation of the foot (Bahr et al., 1998; Shybut et al., 1983). Yet, in contrast to the soft tissue injuries that are reported in many clinical studies on the ankle (Boytim et al., 1991; Edwards & DeLee, 1984; Hopkinson et al., 1990), experimental studies have typically generated a high frequency of bone fractures when the foot is externally rotated (Lauge-Hansen, 1950; Markolf et al., 1989; Schaffer & Manoli, 1987)

In the current literature there are conflicting reports as to the location of the primary ligamentous restraint to external rotation of the foot/ankle complex. Numerous studies on the mechanisms of ankle injury deal with injuries to the syndesmosis and

anterior ligamentous structures (Hirsch & Lewis, 1965; Markolf et al., 1989; Stiehl et al., 1992), but a previous study using sectioning techniques also describes the important role of the posterior talofibular ligament (PTaFL) in the ankle's resistance to external rotation of the foot/ankle complex (Stormont et al., 1985). In addition, Colville et al. (1990) measure strain in various ankle ligaments and conclude that the greatest strain experienced during dorsiflexion-external rotation is in the PTaFL. Clinicians also indicate a high frequency of cases involving injury to this posterior ligamentous structure (Colville et al., 1990; Fallat et al., 1998). Yet, some report that the PTaFL is rarely injured except in association with complete dislocation of the talus (Molus & Martin, 2008).

There is limited documentation of laboratory studies that externally rotate the foot and induce isolated ligamentous injury of the ankle. Markolf et al. (1989), for example, applied supination-external rotation to the foot and documents five cases of lateral ligamentous injury without bone fracture. Yet, no further description of the specific ligaments damaged is included in the manuscript. Rasmussen (1985) applied dorsiflexion-external rotation to the foot resulting in posterior talofibular ligament (PTaFL) rupture. Yet, failure levels of torque and rotation are not provided in the study. Other experimental studies produce ligamentous injury, but always in combination with bone fractures (Hirsch and Lewis, 1965; Lauge-Hansen, 1950; Stiehl et al., 1992).

In a majority of manuscripts that describe external rotation injuries of the ankle joint, the age and gender of the cadaveric test specimens has not been reported (Hirsch and Lewis, 1965; Markolf et al., 1989; Schaffer and Manoli, 1987). These variables may substantially affect both the failure load and the mode of failure in the joint, since most

ankle sprains occur in persons under the age of 35 years (Nilsson, 1983). Stiehl et al. (1992) investigated external rotation injuries of the ankle using male specimens with an age of 67 ± 19 years. The experiment generated fibular fractures in combination with ligamentous injuries. The advanced age of these test specimens may explain the high frequency of bone fractures that were produced in the study.

Within the current literature, two different methods of foot fixation have also been used to study the biomechanical response and tolerance of the human ankle to external rotation of the foot. Stormont et al. (1985) rigidly fix the foot in a potting alloy and perform a sectioning experiment. The study concludes that the primary ligamentous restraints to external rotation of the foot are the calcaneofibular (CaFL) and posterior talofibular (PTaFL) ligaments. In contrast, Stiehl et al. (1992) constrain the foot with fiberglass cast tape and externally rotate the foot 90 degrees. The study produces injury to the anterior ligamentous structures, including the deltoid ligament, anterior tibiofibular ligament (ATiFL), and interosseous ligament in association with fracture of the fibula and tibia. These contrasting data on the locations of the primary soft tissue restraints during external rotation of the foot may be attributable to differences in the method of foot fixation. Foot constraint may influence subtalar motion and the movement of the bony structures within the foot, thereby influencing the mode of injury during external rotation of the foot.

It was hypothesized that experiments with a younger specimen population will result in a high frequency of ligamentous injuries, prior to bone fracture during excessive levels of external rotation of the foot. Measurement of the rotational moments, angular rotations, and modes of soft tissue injury may also be a function of the type of

experimental fixation used to constrain the foot. These experimental data may provide new information for the clinical diagnosis of injury to the ankle following excessive external rotations. The biomechanical data may also be used to help develop a biofidelic ankle surrogate that can be used in the evaluation of athletic shoe-surface interfaces for studies of injury risk (Villwock et al., 2009).

MATERIALS AND METHODS:

Torsion experiments were conducted on lower limbs from seven male cadavers (aged 40 ± 11 years). The limbs were procured through university sources, stored at -20 degrees Celsius and thawed to room temperature for 24 hours prior to testing. The tibia and fibula were sectioned approximately 15 cm distal to the center of the knee. The proximal end of the tibia and fibula shafts were cleaned with 70% alcohol and potted in a rectangular aluminum tray with room temperature curing epoxy (Fibre Strand, Martin Senior Corp., Cleveland, OH). Two different manners of foot fixation were used in this series of experiments. Ten lower extremities were tested with the foot potted in a rectangular aluminum tray with room temperature curing epoxy (Fibre Strand) (Figure 4.1). Screws were placed into the calcaneous and the entire foot was surrounded and supported with the potting material, but care was taken to leave space around the medial and lateral malleoli. Four additional lower extremities were tested by constraining the foot with athletic tape (Elastikon, Johnson & Johnson, New Brunswick, NJ) onto a 22-cm x 10-cm polycarbonate plate which was then inserted into a rigid fixture (Figure 4.2). A tapered elastomeric insert (Shore Hardness 10A) with a maximum thickness of 2.5 cm was placed beneath the arch of the foot to simulate support that may be provided by a

shoe. Both methods of foot fixation were positioned in different degrees of flexion by means of interchangeable wedges placed underneath the foot plate. The foot was everted (10 to 15 degrees about an anteroposterior axis) in all tests (Figure 4.3).
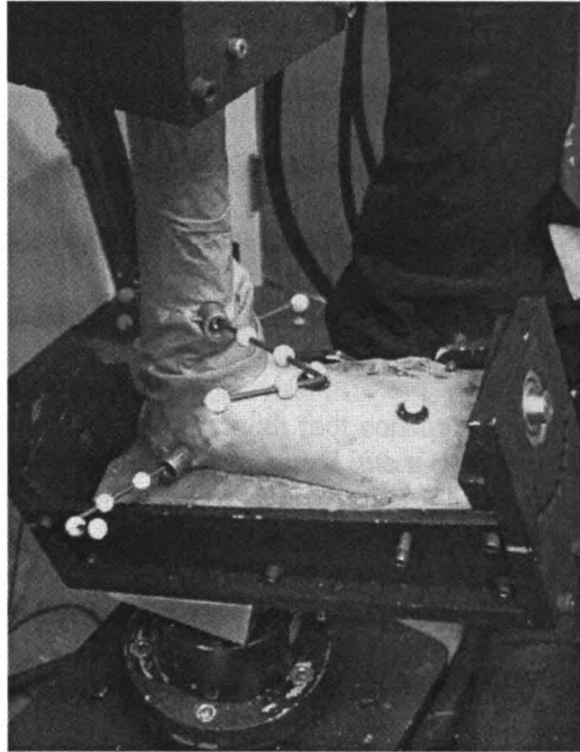
Figure 4.1: Close-up of cadaveric lower extremity mounted in testing device with foot constrained in potting material. Reflective marker arrays were used to conduct motion analysis using a Vicon system.
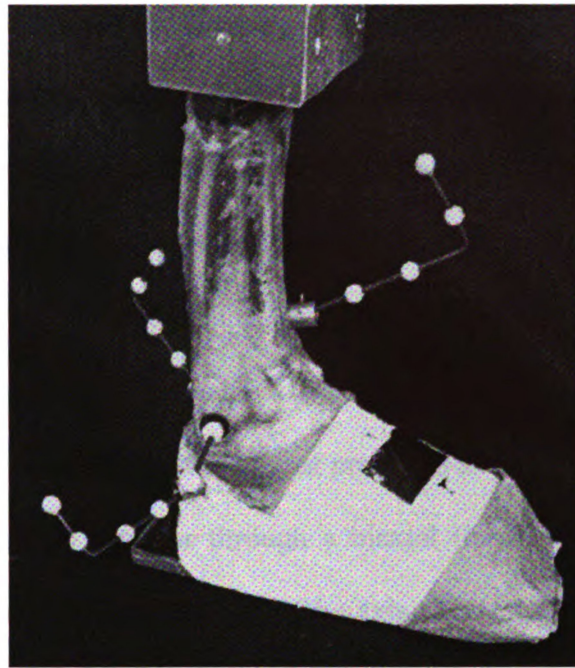
Figure 4.2: Cadaveric lower extremity with foot constrained to polycarbonate plate with athletic tape. The polycarbonate plate is inserted into a rigid fixture for testing. Reflective marker arrays were used to conduct motion analysis using a Vicon system.
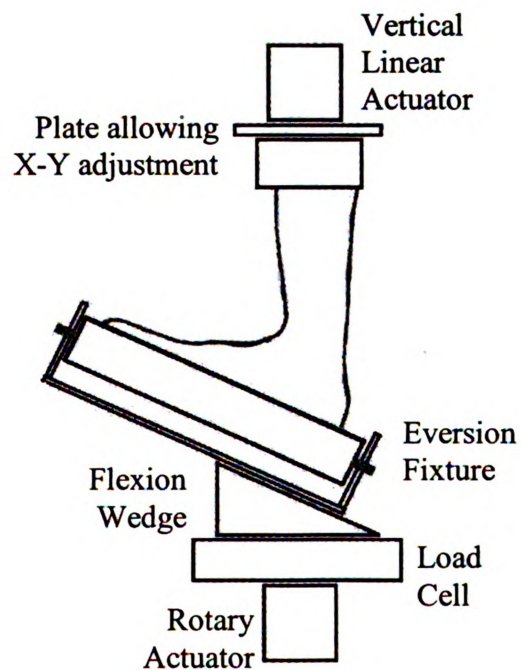
Figure 4.3: Experimental setup performed on biaxial materials testing machine.

ro

(M

(M

M

M

(M

wa

12

wi

ex

de

sp

tib

wi

stu

suc

fai

(C

ext

Ox

A custom, hydraulic, biaxial testing machine was built by mounting a 244 Nm rotary actuator (Model SS-001-1V, Micromatic, Berne IN) onto a linear actuator frame (Model 312.21, MTS Corp., Eden Prairie, MN) with a vertically oriented linear actuator (Model 204.52, MTS Corp.). The actuators had separate controllers (Model 458.2 Microconsole for the linear actuator and Model 442 Controller for the rotary actuator, MTS Corp.). The rotational displacement was programmed by a waveform generator (Model 458.91 Microprofiler, MTS Corp.) that produced a haversine waveform. The foot was attached to the rotary actuator through a biaxial (torsion-axial) load cell (Model 1216CEW-2K, Interface, Scottsdale, AZ). The axis of rotation of the foot was aligned with the ankle center between the medial and lateral malleoli. The proximal end of the extremity was secured to the rotation locked linear actuator with a custom fixture designed to allow sufficient positioning for dorsiflexion and eversion of the foot. Each specimen was mounted with the tibia axis aligned with the linear actuator.

Compressive preloads of two to three times body weight were applied through the tibia prior to the application of an external torque. A dynamic angular rotation was input with a position controlled waveform. Two different rates of rotation were used in this study, 0.5 Hz and 2 Hz. The rotation was increased by increments of five degrees in successive tests until diagnosed ligamentous injury or bone fracture. The mode of injury, failure load and failure angle of foot rotation were documented for each specimen.

The last eight ankles (four pairs) were subjected to pre-test computed topography (CT) scans and a subsequent motion analysis of the fibula, tibia and talus during the external rotation tests using a Vicon motion capture system (Oxford Metrics Ltd., Oxford, United Kingdom). The CT scans were performed with reflective marker arrays

fixed to the fibula and tibia (Figures 4.1 and 4.2). The fibula array was attached to the lateral malleolus and the tibia array was positioned several centimeters proximal to the inferior articular surface. This allowed determination of transverse plane positions of the fibula and tibia markers with respect to their geometric centers using an open source DICOM viewer and analysis tool (OsiriX, Version 2.7.5, Open Source General Public License). Virtual points were identified in Vicon Bodybuilder (Oxford Metrics Ltd.) at these designated bone centers and tracked during each test to measure the translation of the distal segments of the fibula and tibia. The anterior-posterior translation, medial-lateral translation and internal/external rotation of the fibula and tibia were documented at peak foot rotation. This allowed the motion of the fibula relative to the tibia to be calculated, providing a measure of the motion at the syndesmosis. The rotations of the talus were measured by the inclusion of an additional array that was positioned on the superoposterior surface of the talus for the dorsiflexed specimens and on the superoanterior surface of the talus for the plantarflexed specimen. These analyses were performed on the test data from the experiment immediately preceding the test resulting in diagnosed gross failure of the ankle.

Following the experimental testing, all soft tissue injuries and bone fractures were documented during a careful gross dissection of the joint. One way ANOVAs were performed with SigmaStat (Version 2.03, SPSS Inc., Chicago, IL) to compare failure torque and failure angle of foot rotation between the potted and taped ankles. Statistical significance was set at $p < 0.05$ for these analyses.

RE

a m

talo

4.4)

the

mid

tibi

RESULTS:

The mean failure torque of the ankles with a potted foot was 69.8 ± 12.4 Nm with a mean failure angle of 41.8 ± 6.9 degrees (Table 4.1). Isolated avulsion of the posterior talofibular ligament (PTaFL) from the fibula was noted in four of the ten ankles (Figure 4.4). Distal fibular fractures were generated in three ankles, two of which passed through the anterior tibiofibular ligament (ATiFL) (Figure 4.5). Single incidents were noted of mid-substance PTaFL rupture, anterior deltoid ligament rupture (tibiotalar and tibionavicular), and a spiral fracture of the tibia and fibula.

Table 4.1: Torque and angle of foot/ankle complex rotation at failure (foot constrained in potting material).
* indicates torque and angle information lost due to data acquisition program malfunction.

Specimen	Age	Ht (m)	Wt (kg)	Rotation Rate (Hz)	Flexion (deg)	Torque (N·m)	Angle (deg)	Injury Description
32388R		Unknown		0.5	20	55	34	Fib avulsion of PTaFL
32388L				2	20	60	35	Fib avulsion of PTaFL
32416R	34	1.83	68	2	20	*	*	Distal fib fracture through ATiFL
32416L				0.5	20	95	55	Distal fib fracture
32516R	47	1.47	113	0.5	20	61	45	Distal fib fracture through ATiFL
32516L				0.5	20	62	35	Spiral fracture of tibia and fibula
32489R	40	1.78	113	2	10	68	40	Fib avulsion of PTaFL
32489L				2	10	76	45	Fib avulsion of PTaFL
32532L	19	1.88	86	0.5	20	80	50	Anterior deltoid (tibionavicular, tibiotalar)
32498R	47	1.78	64	2	-10	71	40	PTaFL
					AVG	69.8	42.1	
					(SD)	-12.4	-7.3	
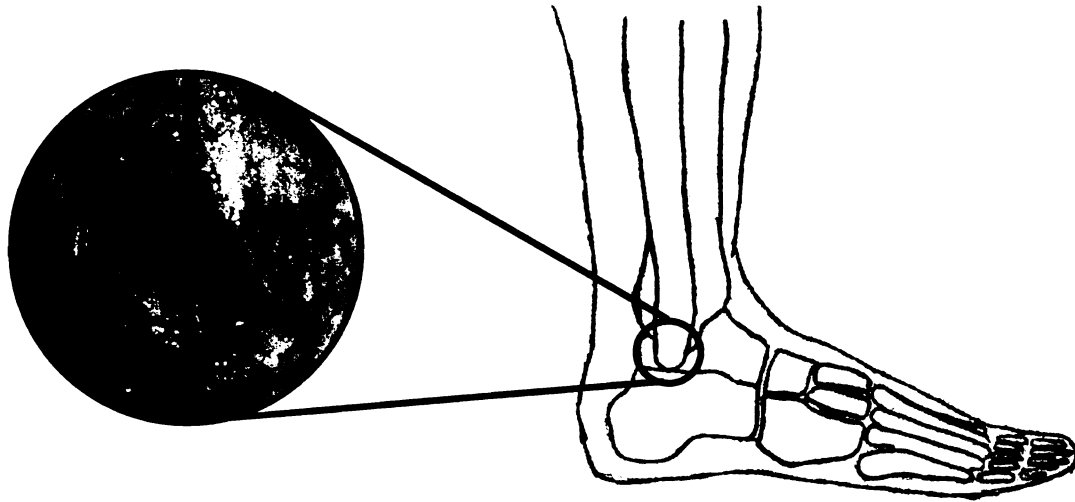
Figure 4.4: Fibular avulsion of the posterior talofibular ligament
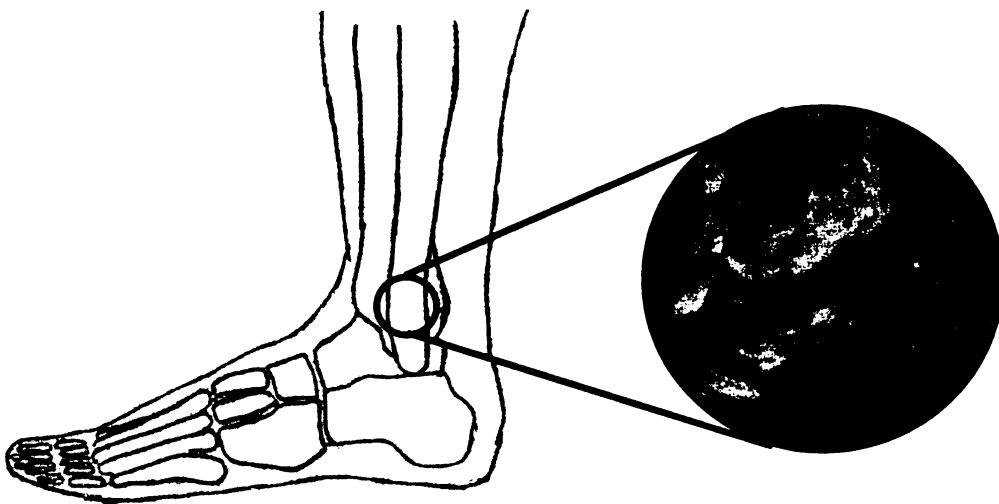
Figure 4.5: Fibular fracture through the anterior tibiofibular ligament

The mean failure torque of the ankles with a taped foot was 78.5 ± 18.1 Nm with a mean failure angle of 65.5 ± 10.7 degrees (Table 4.2). Damage to the anterior portion of the deltoid ligament (tibiotalar and/or tibionavicular) was noted in three of the four ankles (Figure 4.6). Fibular fracture through the ATiFL was observed in one ankle. There was no significant difference in failure torque between the potted and taped foot groups, but a significant difference was noted in angle of foot/ankle complex rotation at failure ($p < 0.001$) between the two groups.

Table 4.2: Torque and angle of foot/ankle complex rotation at failure (foot constrained with athletic tape)

Specimen	Age	Ht (m)	Wt (kg)	Rotation Rate (Hz)	Flexion (deg)	Torque (N·m)	Angle (deg)	Injury Description
32532R	19	1.88	86	0.5	20	84	63	Anterior deltoid (tibnav, tibtal)
32498L	47	1.78	64	0.5	20	85	52	Distal fib fracture through ATiFL
32462R	52	1.75	104	0.5	20	93	77	Anterior deltoid (tibnav), PTaFL
32462L				2	0	52	70	Anterior deltoid (tibnav, tibtal)
					AVG	78.5	65.5	
					(SD)	-18.1	-10.7	

69

trans

(Tab

was

aver

exter

taped

with
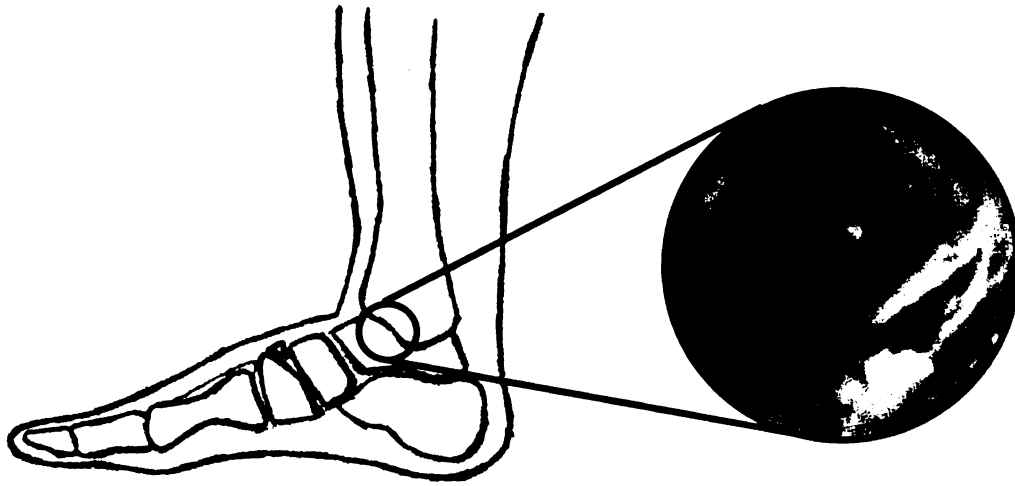
Figure 4.6: Anterior deltoid rupture

Prior to failure, the external rotation moment caused medial and posterior translation of the fibula relative to the tibia, when compared to non-weight bearing (Tables 4.3 and 4.4). The fibula translated medially an average of 3.02 mm when the foot was potted, and 4.31 mm when the foot was taped. The posterior translation of the fibula averaged 5.15 mm for both the potted and taped foot. The distal segment of the fibula externally rotated in relation to the tibia an average of five degrees in both the potted and taped foot experiments. The talus exhibited greater external rotation and plantarflexion with the taped foot in comparison to the potted foot (Tables 4.3 and 4.4).

Table 4.3: Motion analysis results from trial immediately preceding failure (potted foot group). Positive translation is in the medial and posterior direction. Positive flexion is plantarflexion.

Specimen	Torque (N·m)	Angle (deg)	Medial Translation (mm)		Posterior Translation (mm)		External Rotation (deg)			Flexion (deg) Talus	Inversion (deg) Talus
			Fibula	Tibia	Fibula	Tibia	Fibula	Tibia	Talus		
32489R	61	35	5.2	1.6	2.7	-1.2	7.9	5.3	17.4	2.6	3.7
32489L	68	40	4.9	1.3	1.5	-3.9	9.7	4.1	16.6	0.9	3.6
32532L	69	45	2.5	-0.3	5.1	-0.8	14.2	4.4	23.5	4.6	2.8
32498R	60	35	3.1	1	7.9	2.4	10.5	8.3	18.5	0.9	2.3
AVG (SD)	64.5 (4.7)	38.8 (4.8)	3.9 (1.3)	0.9 (0.8)	4.3 (2.8)	-0.9 (2.6)	10.6 (2.7)	5.5 (1.9)	19.0 (3.1)	2.3 (1.8)	3.1 (0.7)

Table 4.4: Motion analysis results from trial immediately preceding failure (taped foot group). Positive translation is in the medial and posterior direction. Positive flexion is plantarflexion.

Specimen	Torque (N·m)	Angle (deg)	Medial Translation (mm)		Posterior Translation (mm)		External Rotation (deg)			Flexion (deg) Talus	Inversion (deg) Talus
			Fibula	Tibia	Fibula	Tibia	Fibula	Tibia	Talus		
32489R	81	58	8.9	5.5	4.6	0.2	9.0	7.6	18.8	7.2	1.8
32489L	75	47	9.1	2.6	3.4	-2.4	18.7	12.6	23.0	1.5	3.2
32532L	75	73	9.7	4.1	3.7	-4.4	16.7	11.1	39.0	10.0	4.1
32498R	58	65	-3.8	-5.5	-2.4	-4.7	15.0	6.3	48.2	5.1	-3.4
AVG (SD)	72.3 (9.9)	60.8 (11.0)	6.0 (6.5)	1.7 (4.9)	2.3 (3.2)	-2.8 (2.2)	14.9 (4.2)	9.4 (2.9)	32.2 (13.7)	6.0 (3.6)	1.4 (3.4)

DISCUSSION:

This study measured the rotational moments and angular rotations of the ankle that resulted in gross injury to ligaments and/or bone fracture during external rotation of the foot/ankle complex. The mean failure torque in this experiment, approximately 72 Nm, compared well with the current literature. Hirsch and Lewis (1965) document a mean failure torque of 75 Nm to produce fracture of the ankle joint during pronation-external rotation of the foot, and Stiehl et al. (1992) record a mean failure torque for male specimens of 65 Nm to generate ankle fractures during external rotation of the foot. The modes of failure in the current study (posterior talofibular ligament (PTaFL) avulsions, deltoid ligament tears and fibular fractures) were also comparable to the documented modes of failure in the current literature. The anterior tibiofibular ligament (ATiFL) was only involved in the injury in the event of a distal fibular fracture. Rasmussen (1985) forced dorsiflexion-external rotation injuries in two ankles. In both preparations, the PTaFL was involved in the injury. Stiehl et al. (1992) externally rotated the foot and documented fibular fracture in combination with a torn ATiFL and deltoid ligament in eight of twelve specimens.

Differences in the failure mode were noted between the potted and taped groups. The PTaFL was involved in the injury when the foot was constrained in potting material. The deltoid ligament failed when the foot was constrained using the taped and potted methods, but the frequency of deltoid injury was higher for the taped foot. These results support the hypothesis that the location of injury may be a function of the type of experimental fixation used to constrain the foot. The importance of the PTaFL when the foot was potted is in agreement with a sectioning study performed with similar

constraints that documents the contribution of the PTaFL in the ankle's resistance to external rotation (Stormont et al., 1985). The frequency of deltoid injury with the taped foot is also comparable to the rate observed by Stiehl et al. (1992) in which the authors constrain the foot with fiberglass tape and externally rotate the foot. In the real world, this may imply that shoes with tight, stiff uppers, as described by Villwock et al. (2009), may influence foot mechanics and therefore the potential for changes in the location of soft tissue injury. Similar effects on ankle injury based on boot stiffness have been previously documented in snowboarding (Delorme et al., 2005).

The motion analysis contributes to an understading of the mechanisms of injury. The higher rate of deltoid injury for the taped foot may be attributable to the additional talar motion during external rotation of the foot/ankle complex. The increased plantarflexion of the talus in the taped foot may have released tension in the PTaFL and increased tension in the anterior deltoid, thereby allowing additional external rotation and further increasing strain in the anterior deltoid ligament. The limited talar motion when the foot was potted may be due to subtalar constraint imposed by the potting material. Conversely, the increased talar motion when the foot was taped may be due to the ability of the arch to collapse.

It is interesting to note that the potted specimen with the deltoid injury was the youngest specimen (19 years of age), and exhibited greater external talus rotation along with greater external fibula rotation than the other potted specimens. The increase in fibular rotation may be attributed to the better bone quality of this specimen. The fibula may have been less brittle and able to respond to the increase in PTaFL tension, thereby avoiding the avulsion type injury noted in several ankles. The strain in the anterior

deltoid ligament may also have been increased by the additional plantarflexion of the talus noted in this specimen compared to the other potted specimens.

The potted and taped foot groups failed at comparable levels of torque, but significantly different levels of foot/ankle complex rotation were recorded in the study. The ankles with a potted foot failed at smaller input rotations. Research by Lundberg et al. (1989a; 1989b) suggests that rotations of the bones within the foot during eversion and external rotation may act as torsion dissipating devices. This implies that a rotation dependent injury mechanism may be influenced by constraint of the foot (Figure 4.7). For example, a shoe that allows subtalar motion and natural movement of the bone structures within the foot may require greater foot rotation to generate an injury.

Figure 4.7: Rotation dependent injury mechanism may involve the player lying prone as another player lands on his ankle, forcing the foot to externally rotate.

In a study by Taylor et al. (1992) that examined 44 football players with syndesmotic sprains, a positive diagnosis was based on tenderness around the

syndesmosis. The pain associated with a syndesmotic sprain may be the result of excessive strain in the ATiFL resulting in microdamage, rather than a visible rupture. Colville et al. (1990) measure strain in the lateral ankle ligaments during dorsiflexion and external rotation of the foot and document strains in the PTaFL approximately twice those in the ATiFL, while strain in the posterior tibiofibular ligament (PTiFL) is negligible. This may explain the number of PTaFL injuries in the current study, with no cases of isolated syndesmotic injury. The results of this analysis indicated that the ankles exhibit posterior (5.1 mm) and medial (3.0 to 4.3 mm) translations of the fibula relative to the tibia, with external rotation (5.1 to 5.5 degrees) of the fibula relative to the tibia. These motions exceeded those recorded in the literature for a healthy population subjected to a 7.5 Nm external rotation moment (Beumer et al., 2003). Healthy volunteers in that study experienced an average fibular displacement in relation to the tibia of 1.48 mm in the medial direction, 1.87 mm in the posterior direction, and an external rotation of 3.85 degrees. Although the fibula translations recorded in the current study were greater than those for healthy volunteers, the clinical implications of these cadaver data and their potential for generating microdamage in the syndesmosis and associated tenderness indicative of a high ankle sprain are yet unknown.

A limitation of this study was the frequency of bone avulsion injuries at the insertion of the posterior talofibular ligament. While a younger aged specimen population was used to try and limit bone fracture, avulsions still occurred. If the avulsion injuries were avoided, the anterior deltoid may have been the vulnerable soft tissue, or "weakest link", for the specimens tested with a potted foot. Other studies have shown, in fact, that the PTaFL is stronger than portions of the anterior deltoid ligament

(Butler & Walsh, 2004; Siegler et al., 1988). If the bone quality would have been more representative of the typical, younger athlete, the anterior deltoid may have been the location of primary failure, as seen in specimen 32532L. The number of avulsions may also be attributed to the speed of testing which was limited to control inertial effects in the current experimental setup. Past research on the knee suggest that the mode of ligamentous injury may be dependent on the strain rate. Avulsions may occur more often at low rates, while midsubstance failures are frequently documented at high rates (Crowninshield & Pope, 1976). Another limitation of the current study was that the foot restraint, in terms of the potential shoe design issue, was not more completely studied at this time.

In conclusion, following excessive external rotation of the foot/ankle complex this study documented isolated ligament ruptures in the PTaFL and anterior portions of the deltoid ligament. Damage to the ATiFL only occurred in combination with fibular fracture. Fibular motions during external rotation of the foot exceeded those measured *in vivo* for a healthy population, but the potential clinical implications of these data and their potential for generating tenderness in the syndesmosis, indicative of a "high ankle" sprain, are currently unknown. Finally, the amount of constraint offered by a shoe and its upper may influence the potential for and determine the location of soft tissue injuries in the anterior or the posterior aspects of the ankle following excessive levels of external rotation of the foot/ankle complex on an athletic field.

REFERENCES

Bahr R, Pena F, Shine J, Lew WD, Engebretsen L. (1998) Ligament force and joint motion in the intact ankle: a cadaveric study. Knee Surg Sports Traumatol Arthrosc. 6:115-121.

Beumer A, Valstar ER, Garling EH, Niesing R, Ranstam J, Lofvenberg R, Swierstra BA. (2003) Kinematics of the distal tibiofibular syndesmosis. Acta Orthop Scand. 74(3):337-343.

Boytim MJ, Fischer DA, Neumann L. (1991) Syndesmotic ankle sprains. Am J Sports Med. 19(3):294-298.

Brosky T, Nyland J, Nitz A, Caborn DN. (1995) The ankle ligaments: consideration of syndesmotic injury and implications for rehabilitation. J Orthop Sports Phys Ther. 21:197-205.

Butler AM, Walsh WR. (2004) Mechanical response of ankle ligaments at low loads. Foot Ankle. 25:8-12.

Colville MR, Marder RA, Boyle JJ, Zarins B. (1990) Strain measurements in lateral ankle ligaments. Am J Sports Med. 18(2):196-200.

Crowninshield RD, Pope MH. (1976) The strength and failure characteristics of the rat medial collateral ligament. J Trauma. 16:99-105.

Delorme S, Tavoularis S, Lamontagne M. (2005) Kinematics of the Ankle Joint Complex in Snowboarding. Journal of Applied Biomechanics. 21:394-403.

Ebraheim NA, Elgafy H, Padanilam T. (2003) Syndesmotic disruption in low fibular fractures associated with deltoid ligament injury. Clin Orthop Relat Res. 409:260-267.

Edwards GS, DeLee JC. (1984) Ankle diastasis without fracture. Foot Ankle. 4(6):305-312.

Fallat L, Grimm DJ, Saracco, JA. (1998) Sprained ankle syndrome: Prevalence and analysis of 639 acute injuries. J Foot Ankle Surg. 37:280-285.

Fritschy D. (1989) An unusual ankle injury in top skiers. Am J Sports Med. 17:282-286.

Guise ER. (1976) Rotational ligamentous injuries to the ankle in football. Am J Sports Med. 4(1):1-6.

Hirsch C, Lewis J. (1965) Experimental ankle joint fractures. Acta Orthop Scand. 36:408-417.

Hopkinson WJ, St. Pierre P, Ryan JB, Wheeler JH. (1990) Syndesmosis sprains of the ankle. Foot Ankle. 10(6):325-330.

Johnson EE, Markolf KL. (1983) The contribution of the anterior talofibular ligament to ankle laxity. J Bone Joint Surg Am. 65(1):81-88.

Lassiter TE Jr, Malone TR, Garrett WE Jr. (1989) Injury to the lateral ligaments of the ankle. Orthop Clin North Am. 20:629-640.

Lauge-Hansen N. (1950) Fractures of the Ankle II. Combined Experimental-Surgical and Experimental-Roentgenologic Investigations. Arch Surg. 60:957-985.

Lundberg A, Svensson OK, Bylund C, Goldie I, Selvik G. (1989a) Kinematics of the ankle/foot complex – Part 2: pronation and supination. Foot Ankle. 9(5):248-253.

Lundberg A, Svensson OK, Bylund C, Selvik G. (1989b) Kinematics of the ankle/foot complex – Part 3: influence of leg rotation. Foot Ankle. 9(6):304-309.

Lynch, SA. (2002) Assessment of the injured ankle in the athlete. J Ath Train. 37(4):406-412.

MacAuley D. (1999) Ankle injuries: same joint, different sports. Med Sci Sports Exerc. 31(7 suppl):S409-411.

Markolf KL, Schmalzried TP, Ferkel RD. (1989) Torsional strength of the ankle in vitro. The supination-external-rotation injury. Clin Orthop Relat Res. 246:266-272.

McConkey JP. (1987) Ankle sprains, consequences and mimics. Med Sport Sci. 23:39-55.

Miller CD, Shelton WR, Barrett GR, Savoie FH, Dukes AD. (1995) Deltoid and syndesmosis ligament injury of the ankle without fracture. Am J Sports Med. 23(6):746-750.

Molus MA, Martin DF. (2008) Talofibular ligament injury. Retrieved December 17, 2008, from eMedicine WebMD Web site: http://emedicine.medscape.com/article /86396-overview.

Nilsson S. (1983) Sprains of the lateral ankle ligaments, part II: epidemiological and clinical study with special reference to different forms of conservative treatment. J Oslo City Hosp. 33(2-3):13-36.

Norkus SA, Floyd RT. (2001) The Anatomy and Mechanisms of Syndesmotic Ankle Sprains. J Ath Train. 36(1):68-73.

Pankovich AM. (1976) Maisonneuve fracture of the fibula. J Bone Joint Surg Am. 58:337-342.

Rasmussen O, Tovborg-Jensen I, Boe S. (1982) Distal tibiofibular ligaments. Acta Orthop Scand. 53:681-686.

Rasmussen O. (1985) Stability of the ankle joint. Analysis of the function and traumatology of the ankle ligaments. Acta Orthop Scand. 56(Suppl 211):1-75.

Sarrafian SK. (1983) Anatomy of the foot and ankle: descriptive, topographic, functional. Philadelphia, PA: JB Lippincott; 143-198.

Schaffer JJ, Manoli A. (1987) The Antiglide Plate for Distal Fibular Fixation. J Bone Joint Surg Am. 69-A(4):596-604.

Siegler S, Block J, Schneck CD. (1988) The mechanical characteristics of the collateral ligaments of the human ankle joint. Foot and Ankle. 8:234-242.

Shybut GT, Hayes W, White AA. (1983) Normal pattern of ligament loading among the lateral collateral ankle ligaments. Trans Orthop Res Soc. 8:15.

Stiehl JB, Skrade DA, Johnson RP. (Dec, 1992) Experimentally produced ankle fractures in autopsy specimens. Clin Orthop Relat Res. 285:244-249.

Stormont DM, Morrey BF, An KN, Cass JR. (1985) Stability of the loaded ankle. Relation between articular restrain and primary and secondary static restraints. Am J Sports Med. 13(5):295-300.

Taylor DC, Bassett FH. (1993) Syndesmosis ankle sprains: diagnosing the injury and aiding recovery. Physician Sportsmed. 21(12):39-46.

Taylor DC, Englehardt DL, Bassett FH. (1992) Syndesmosis sprains of the ankle. The influence of heterotopic ossification. Am J Sports Med. 20(2):146-150.

Turco VJ. (1977) Injuries to the ankle and foot in athletics. Orthop Clinics North Am. 8:669-682.

Villwock MR, Meyer EG, Powell JP, Fouty AJ, Haut RC. (2009) Football playing surface and shoe design affect rotational traction. Am J Sports Med. [Epub ahead of print] PMID: 19168808.

Williams GN, Jones MH, Amendola A. (2007) Syndesmotic ankle sprains in athletes. Am J Sports Med. 35(7):1197-1207.

Xenos JS, Hopkinson WJ, Mulligan ME, Olson EJ, Popovic NA. (1995) The tibiofibular syndesmosis: evaluation of the ligamentous structures, methods of fixation, and radiographic assessment. J Bone Joint Surg Am. 77:847-856.

Chapter 5: Development and Evaluation of a Surrogate Ankle for Use with a Rotational Traction Measurement Apparatus.

ABSTRACT:

Biofidelic devices are used in the automobile industry to assess injury risk during a vehicular accident. Similar biofidelic devices may have broad applicability in the field of sports injury prevention and could be used to enhance player safety. Ankle sprains constitute one of the most common sports injuries. Past studies have suggested that high rotational traction at the shoe-surface interface may increase the likelihood of lower extremity injury. Researchers have assessed this risk by measuring the peak torque during an applied rotation. On the other hand, ankle sprains may be dependent upon the amount of strain developed in the ankle ligaments during rotation of the foot/ankle complex, not the magnitude of torque. The current study quantifies the torsional stiffness of the human foot/ankle complex based on cadaver experiments. The development of a surrogate foot/ankle complex is then detailed and compared to the human response. Lastly, the results of a rotational traction study on a couple football shoe-surface interfaces are presented using the surrogate ankle. The testing resulted in a new outcome variable, peak twist of the ankle, that may allow assessment of the risk of injury to the ankle due to excessive rotational traction at the shoe-surface interface.

INTRODUCTION:

Information gathered from healthy volunteer studies and cadaver research has been used to create anthropometric test devices for the automobile industry in order to predict injury risk during a vehicular accident (Forman et al., 2006; McDonald et al., 2003; Tornvall et al., 2007). These test devices, or "crash test dummies", are usually instrumented to record data about the dynamic behavior of the dummy during a crash. Similar biofidelic devices may have broad applicability in the field of sports injury prevention and could be used to enhance player safety.

In the National Football League (NFL), ankle sprains account for about 10% of all sports-related reported injuries (Powell and Schootman, 1993). It is generally accepted that excessive rotational traction may precipitate some of these lower extremity injuries (Bonstingl et al., 1975; Lambson et al., 1996; Nigg and Yeadon, 1987; Torg et al., 1974). Previous studies that analyze injury risk due to traction at the shoe-surface interface have measured the peak torque during an applied rotation of the shoe (Cawley et al., 2003; Lambson et al., 1996; Livesay et al., 2006; Torg et al., 1974). Yet, tissue strain may be a better indicator of injury tolerance than load due to the viscoelastic nature of the soft tissues involved in ankle injuries (Boytim et al., 1991; Edwards and DeLee, 1984). For example, previous studies have shown that the ultimate tensile strength (UTS) of soft tissues, including ligaments and tendons, increases as strain rate increases, while the ultimate strain is not affected (France et al., 1987; Ng et al., 2004). The ligamentous damage experienced in an ankle sprain may be brought about by mechanical disruption due to excessive elongation and deformation of one or more ligaments. Therefore,

81

measurement of ankle twist during an applied axial rotation at the shoe-surface interface may provide a better indicator of ankle injury risk than torque alone.

The development of a biofidelic ankle may be used as a tool to assess ankle injury risk due to the shoe-surface interface. The goal of this study was to quantify the torsional stiffness of the human foot/ankle complex, then design a surrogate foot/ankle complex to mimic the human response. The surrogate would then be incorporated into an existing rotational traction apparatus used to assess peak torque at the shoe-surface interface (Villwock et al., 2009a; 2009b). Measurement of the ankle twist during an applied external rotation moment applied to the shoe may provide an additional tool that can help assess the risk of ankle injury due to the shoe-surface interface characteristics.

MATERIALS AND METHODS:

The data from a previous cadaver experiment was re-analyzed to determine the torsional stiffness of the human ankle joint (Villwock et al., 2009c). The previous tests involved externally rotating ten ankle joints until failure. Briefly, the foot was potted in room temperature curing epoxy (Fibre Strand, Martin Senior Corp., Cleveland, OH). Screws were placed into the calcaneous and the entire foot was surrounded and supported with the potting material. Prior to each test, the foot was everted and the ankle was placed into various degrees of flexion. Compressive preloads of 2-3 times body weight were applied. The specimens were loaded by incrementally increasing the angle of rotation by five degrees until a grossly diagnosable injury. Graphs were then constructed of torque versus ankle rotation for each successive experiment. The torque-rotation data was taken from each subfailure experiment. The failure experiment was not included for

the determination of torsional stiffness. The primary stiffness was determined by a linear regression through the experimental data up to 20 degrees of foot/ankle complex rotation. The secondary stiffness was determined by a linear regression through the data above 35 degrees of foot/ankle complex rotation. The overall stiffness was calculated from a linear regression through the entire data set.

The surrogate lower leg from the rotational traction testing apparatus (Figure 5.1) was then re-designed to match the torsional stiffness from the cadaver experiments. The leg consisted of a hollow aluminum tibia connected to a rigid foot made from room temperature curing epoxy (Fibre Strand, Martin Senior Corp., Cleveland, OH). The foot was connected to the tibia and allowed to rotate about the tibia axis through a small channel (Figure 5.2). The length of the channel and the material used to fill the channel could be modified, allowing control of torsional stiffness at the ankle. The elastomeric materials were neoprene (Part # 8981K16, McMaster-Carr, Elmhurst, Il) in various degrees of hardness. These bumpers were 0.25 inches thick, 0.75 inches tall and filled the entire length of the channel (2.5 inches).
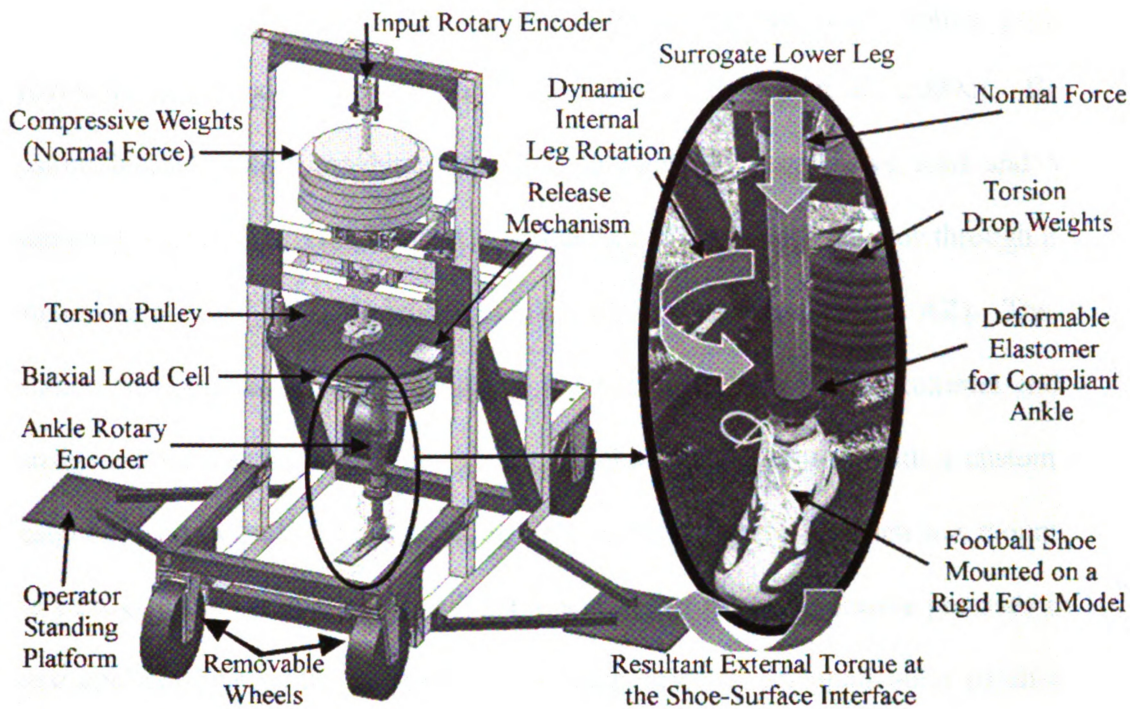
Figure 5.1: Rotational traction testing apparatus (Villwock et al., 2009a; 2009b)
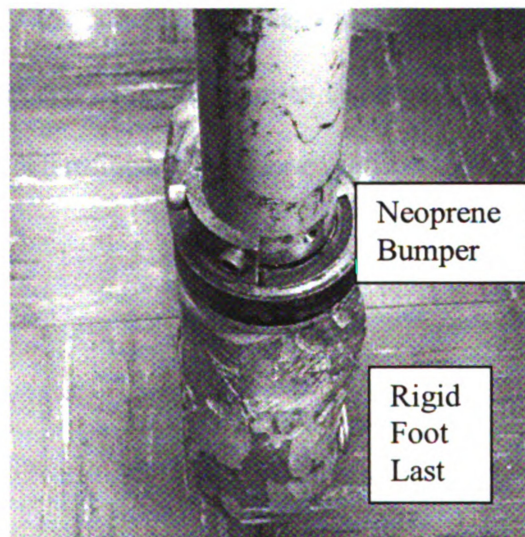
Figure 5.2: Posterior view of the surrogate lower extremity. An angular displacement transducer inside of the tibia shaft recorded foot/ankle complex rotation. The channel was filled with neoprene rubber to simulate the torsional stiffness of the ankle.

The surrogate lower leg was evaluated using the same testing protocol as previously described in the cadaver ankle study (Villwock et al., 2009c). Briefly; a custom biaxial testing machine was used to apply a compressive load and a rotary moment (Figure 5.3). The foot last was attached to the rotary actuator through a biaxial (torsion-axial) load cell (Model 1216CEW-2K, Interface, Scottsdale, AZ). The axis of rotation was aligned with the center of the surrogate tibia. The proximal end of the surrogate tibia was secured to the rotation locked linear actuator with a custom fixture designed to allow sufficient positioning for alignment. Each specimen was mounted with the surrogate tibia axis aligned with the linear actuator. Compressive preloads of 100N were applied through the surrogate tibial shaft prior to the application of an external torque. A dynamic angular rotation was input with a rotation controlled waveform at 1 Hz. The rotation was increased in increments of five degrees in successive tests until the torque exceeded 110 Nm. At the conclusion of each experiment, the ankle was manually rotated until contact with the end of the channel to ensure a consistent starting position. The torsional stiffness was determined in a manner similar to that previously described for the cadaver specimens.

85
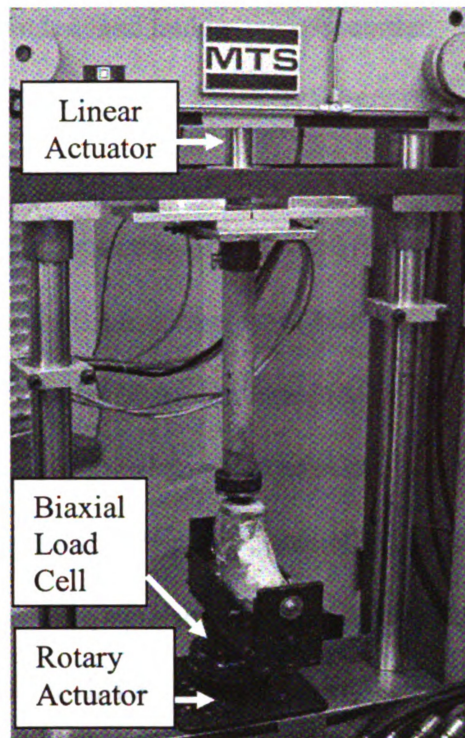
Figure 5.3: Surrogate lower extremity mounted on the material testing machine.

The traction measurement apparatus (Figure 5.1) was then utilized to evaluate the biofidelic ankle on an indoor playing surface (AstroPlay, Southwest Recreational Industries, Leander, Texas). The surface was installed in an indoor sports complex six years prior to the tests. Four shoes were evaluated on the surface. These shoes were from the upper and lower ranges of peak torque and rotational stiffness in a previously documented study on this surface (Villwock et al., 2009a): Nike Blade II TD, Adidas Turf Hog LE, Adidas Corner Blitz 7 MD and Nike Air Zoom Superbad FT. The testing procedure followed the format previously described (Villwock et al., 2009a). Briefly, a 1000 N compressive load was applied followed by a 90 degree internal rotation of the surrogate leg, resulting in an externally directed ground reaction torque on the foot. The entire cleat pattern was in contact with the ground, and the center of rotation was at the

midfoot. Rotations of the leg and ankle were recorded using angular displacement transducers (Model 0605-S7104010201, Trans-Tek Inc., Ellington, CT). Five trials were performed for each shoe-surface combination. The test apparatus was repositioned between trials to a new, adjacent section of turf.

Peak torque and rotational stiffness, as previously defined (Villwock et al., 2009a), were documented and used in the statistical analyses. In addition, the peak rotation of the ankle during each trial was recorded and analyzed. A one way ANOVA was performed with SigmaStat (Version 2.03, SPSS Inc., Chicago, IL) to assess differences between shoe models, with repeated measures across trials (n=5). Tukey post-hoc tests were used to evaluate differences in the mean values between shoes when such effects were throught to be greater than would be expected by chance. Statistical significance was set at $p < 0.05$ for all analyses.

RESULTS:

Data from the previous cadaver study by Villwock et al. (2009c) was re-analyzed to determine the torsional stiffness of the human ankle. A torque versus foot/ankle complex rotation plot was constructed (Figure 5.4). The primary stiffness was determined to be 1.24 ± 0.49 Nm/deg, increasing to a secondary stiffness of 2.03 ± 0.64 Nm/deg, with an overall stiffness response of 1.68 ± 0.26 Nm/deg
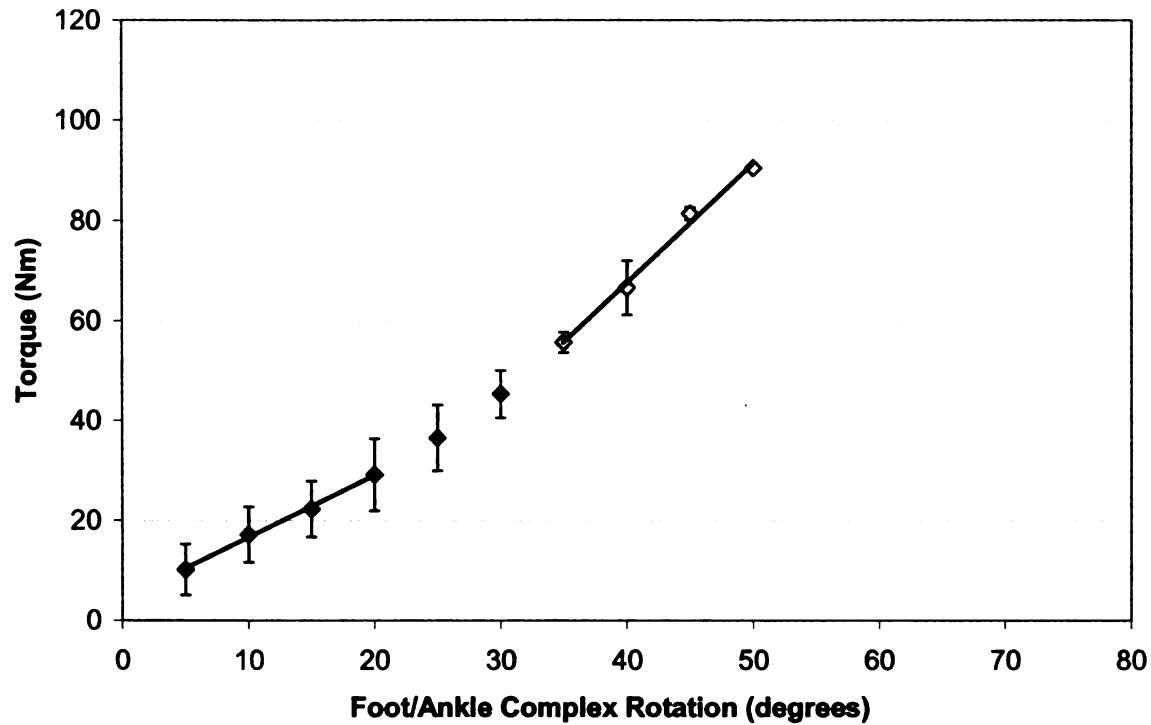
Figure 5.4: Torque versus foot/ankle complex rotation from a cadaver study by Villwock et al. (2009c). This graph depicts the average results, with standard deviations, calculated from ten cadaver lower extremities in five degree incremental trials. Trendlines are included for the primary and secondary torsional stiffnesses. The data used to construct this graph does not include the failure-level experiments.

The surrogate ankle design was evaluated with several neoprene bumpers representing various levels of hardness. The torque versus foot/ankle complex rotation was plotted for each rubber (Fig 5.5). The primary stiffness ranged from 0.9 to 2.4 Nm/degree, the secondary stiffness ranged from 1.0 to 3.8 Nm/degree, and the overall stiffness ranged from 1.2 to 3.0 Nm/degree: The high and low stiffnesses were produced with the 60A and 30A durometer materials, respectively (Table 5.1).

Table 5.1: Torsional stiffness values (Nm/deg). The primary stiffness was determined in a linear regression through all data points up to 20 degrees of foot/ankle complex rotation. The secondary stiffness was then determined in a linear regression through all data points above 35 degrees of foot/ankle complex rotation. The overall stiffness was based on a linear regression through the entire data set.

Neoprene Hardness	Primary	Secondary	Overall
30A	0.92	1.04	1.20
40A	0.98	2.26	1.80
50A	1.63	2.74	2.40
60A	2.42	3.80	3.00
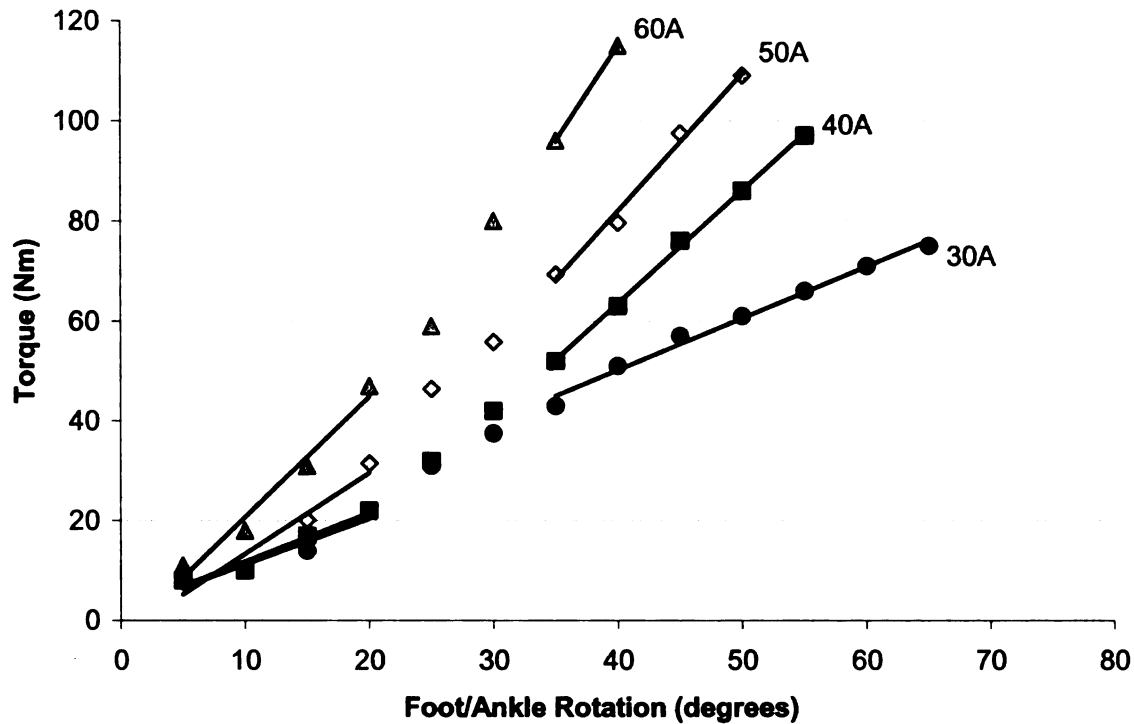
Figure 5.5: Torque versus foot/ankle complex rotation data from the surrogate tests. The results are from neoprene rubber bumpers of varying hardness, as measured on the durometer Shore A hardness scale. Trendlines are included for the primary and secondary torsional stiffness.

For reasons to be discussed later, the traction measurement apparatus (Figure 5.1) was tested on an AstroPlay installation with neoprene 50A used as the elastomeric bumper in the ankle joint. The Adidas Turfhog produced the lowest peak torque, 80 Nm (Figure 5.6). The Adidas Blitz generated the highest rotational stiffness, 5.1 Nm/degree, and the highest rotation of the ankle at 36.5 degrees (Figures 5.7 and 5.8).
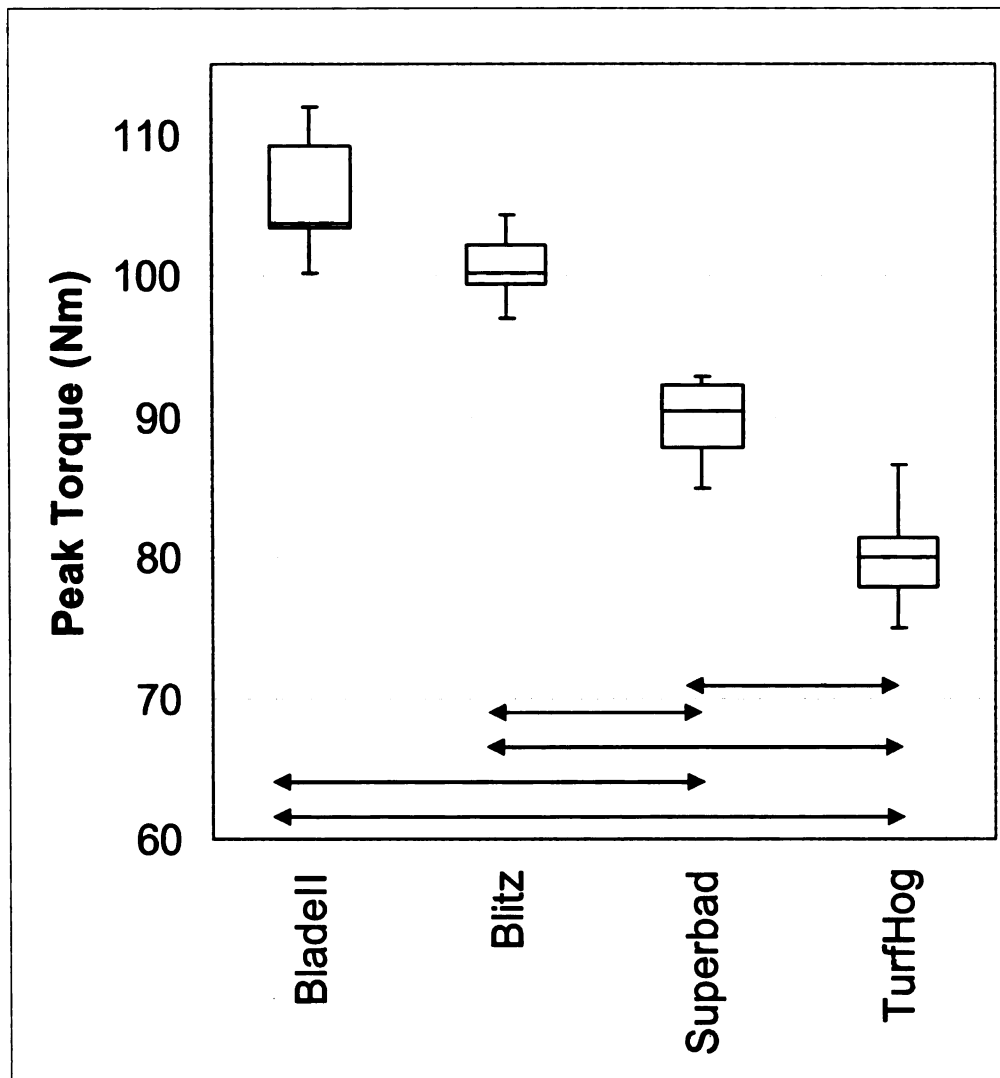
Figure 5.6: Box plot of peak torque (Nm) for each shoe. The line near the center of the box represents the median value, the box represents the inter-quartile range and the whiskers represent the range. Arrows represent significant differences ($p < 0.05$).
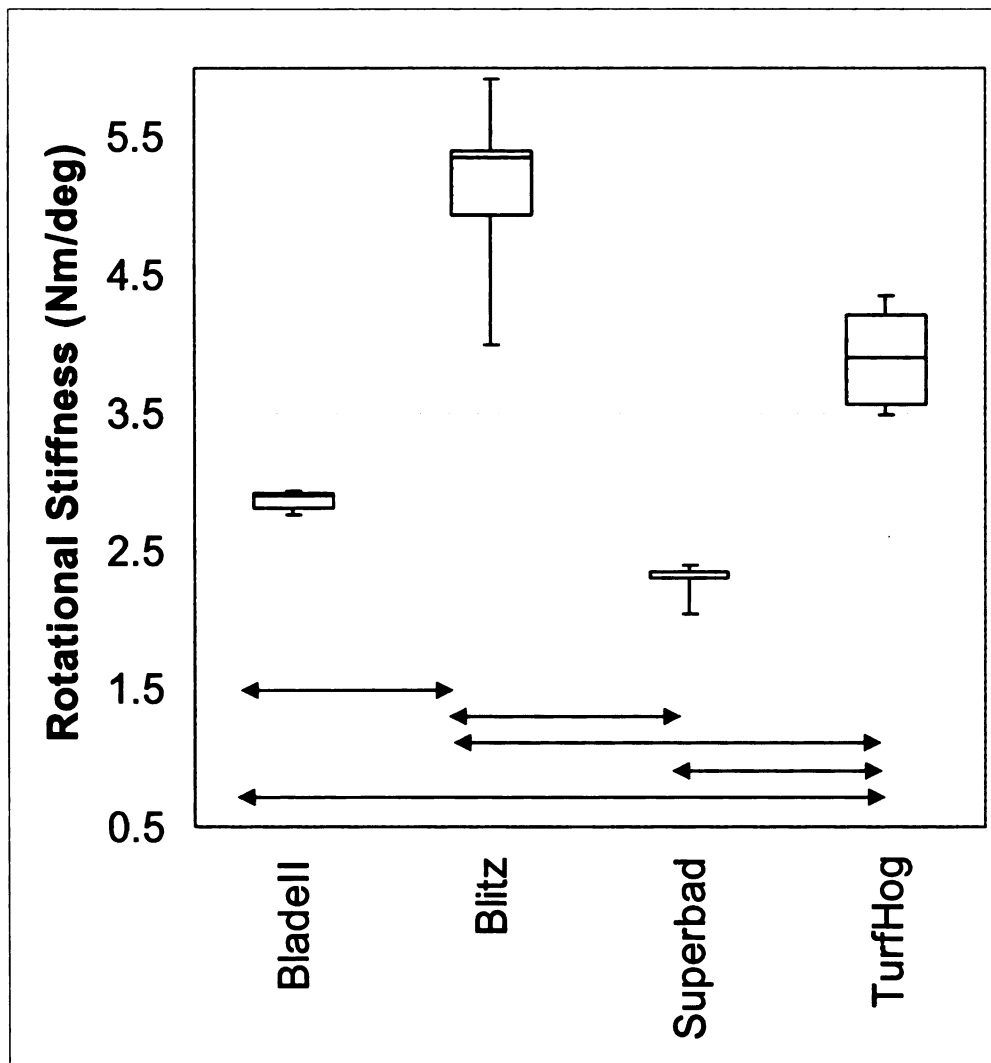
Figure 5.7: Box plot of rotational stiffness (Nm/deg) for each shoe. The line near the center of the box represents the median value, the box represents the inter-quartile range and the whiskers represent the range. Arrows represent significant differences (p <0.05).
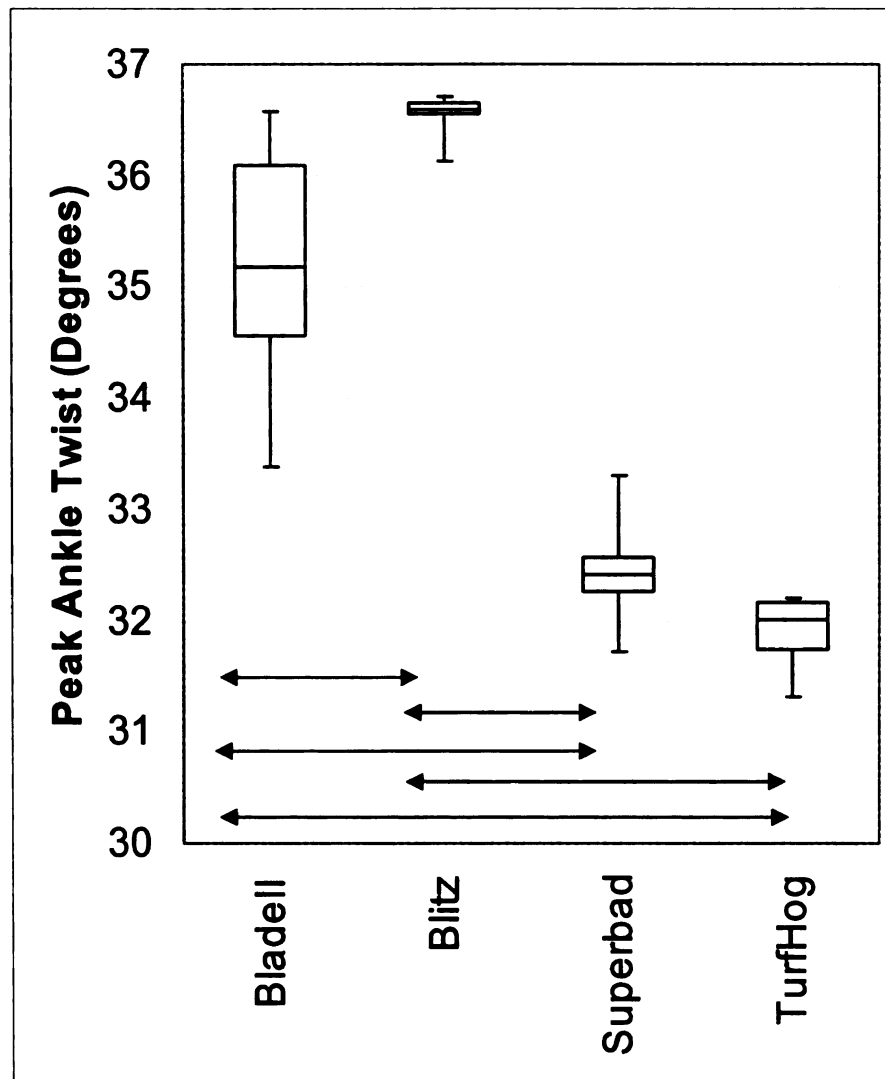
Figure 5.8: Box plot of peak rotation of the ankle (degrees) for each shoe. The line near the center of the box represents the median value, the box represents the inter-quartile range and the whiskers represent the range. Arrows represent significant differences (p <0.05).

DISCUSSION:

The torsional stiffness values from the cadavers in the current study were comparable to those presented in the literature. Stiehl et al. (1992) externally rotate the foot/ankle complex until failure and measure the torsional stiffness during the first 20 degrees of rotation. The authors note an average value for male specimens of 1.21 Nm/degree, compared to the average value in the current study of 1.24 Nm/degree over the same range of rotation. Schaffer and Manoli (1987) externally rotate the foot/ankle complex until failure and measure the torsional stiffness, ignoring the initial response. The authors note an average value of 2.14 Nm/degree, which was comparable to the secondary stiffness of 2.03 Nm/degree in the current study.

The surrogate ankle joint was constructed with neoprene rubber. This material was chosen for its resiliency and durability (McMaster.com, 2008). The variations in hardness affected the torsional stiffness of the ankle. The material that provided a response most similar to the cadaver tests had a hardness of 40A. However, the *in vivo* response of the ankle joint may be influenced by muscle activation. Mote and Lee (1982) measure the torsional stiffness at the ankle joint in a healthy volunteer. The response was limited to external rotations below 6 degrees, resulting in a stiffness of 1.27 Nm/degree when the subject was 100 percent weight bearing. This measurement is comparable to the results of the cadaver tests in the current study. The authors note that the percentage of weight bearing and the amount of muscle tension could vary the torsional stiffness of the ankle. For example, the torsional stiffness of the ankle increases from a state of minimal to maximal muscle activity by approximately twenty-eight percent (Mote and Lee, 1982).

The neoprene that most closely resembled the *in vivo* response of the ankle may then be the 50A durometer material. This material provided slightly greater torsional stiffness than the cadaver ankle, amounting to an increase in stiffness of thirty-one percent for the primary range and thirty-five percent over the secondary range. This is similar to the twenty-eight percent increase noted due to muscle activation in the *in vivo* study by Mote and Lee (1982). No specifications had been defined for the internal/external rotational degree of freedom for the Thor-Lx crash test dummy (Shams et al., 1999), but Neoprene 50A was chosen as the elastomer bumper in the biofidelic ankle for the THOR-FLx crash test dummy (Shams et al., 2002).

The surrogate ankle was evaluated with the rotational traction testing apparatus on an AstroPlay surface using Neoprene 50A as the deformable elastomer in the ankle joint. The results of these experiments were compared to a previous study with an identical testing protocol, but a more rigid ankle joint (Villwock et al., 2009a). The rotational stiffness values documented in this study for each shoe were within 1 Nm/degree of those presented previously by Villwock et al. (2009a). The magnitude of peak torque was similar for the Nike Blade II, Adidas Blitz and Adidas TurfHog in comparison to the previous study (Villwock et al., 2009a). The greatest discrepancy in peak torque between the two studies existed for the Nike Superbad shoe, which generated a peak torque that was twenty-five percent lower in the current study. It is believed that the higher torque in the previous study was due to the high torsional stiffness (approximately 11 Nm/degree) of the surrogate ankle joint (Villwock et al., 2009a). With a stiff ankle joint, a majority of the ninety degree input leg rotation occurred between the shoe and surface. In the current study, the ankle joint was more compliant and had a torsional stiffness of 2.4

Nm/degree with the neoprene 50A bumper. This resulted in more of the input leg rotation occurring at the ankle joint and less rotation between the shoe and surface. In the case of a shoe with a pliable upper (Nike Superbad), this provided less opportunity for the leading edge of the shoe to twist and plow into the surface causing an increase in torque (Villwock et al., 2009a). The discrepancy of torque between the two studies for the Nike Superbad shoe illustrates the influence that the magnitude of rotation has on the risk of ankle injury for certain shoe-surface interface combinations. Future development of the testing apparatus may include the incorporation of a torque controlled input, rather than a fixed level of leg rotation. This would allow the input to simulate the torque threshold documented in previous cadaver tests, and measure the amount of ankle and shoe rotation that occurs for a given shoe-surface interface.

Twist of the ankle joint was a new variable introduced in this rotational traction study. The significantly higher rotation of the ankle with the Adidas Blitz shoe on the AstroPlay surface may be due to the shoe's rigid upper material and its high rotational stiffness. The high rotational stiffness associated with the Adidas Blitz resulted in the ankle joint experiencing larger magnitudes of torque early in the rotation and may have generated the additional twist of the ankle joint.

It is interesting to note that the peak torque for each of these shoe models exceeded the torque-tolerance, based on cadaver data at 72 Nm (Villwock et al., 2009c). However, the peak twist in the ankle for each of the shoe models did not exceed the tolerance data of 42 degrees based on these previous cadaver tests (Villwock et al., 2009c). This might imply that rotation of the ankle may be a more realistic variable to monitor for injury risk assessment, since not everyone gets ankle injuries in these shoes.

Further studies, in concert with injury studies from the field, will be needed to better determine if torque or rotation of the foot/ankle complex would be the best measure of injury potential in the ankle using the surrogate test device.

Development of the surrogate lower extremity should also include the incorporation of a biofidelic knee joint. This would allow comparisons between ankle and knee twist to determine which joint may be more at risk of injury, given an applied rotation or torque via specific shoe-surface interface conditions. The response of the lower extremity to excessive internal rotation of the foot/ankle complex should also be studied as this mechanism is often associated with anterior cruciate ligament injury (Meyer et al., 2008). Development of additional degrees of freedom for the ankle might be another advancement that may generate more physiological responses of the lower leg at the shoe-surface interface. For example, medial and lateral ankle sprains could be due to shear forces applied to the lower extremity while the foot is planted on the surface (Boytim et al., 1991).

If ultimate strain is a better indicator of soft tissue injury risk in the ankle (and knee) than ultimate stress, measuring the magnitude of peak torque at the shoe-surface interface may not be an adequate injury predictor. Measuring rotation in the ankle may provide a measure by which peak torque and rotational stiffness are both integral to the outcome variable: injury risk assessment. In this regard, a biofidelic ankle would be crucial for evaluation of the potential for injury to the ankle (or knee) due to mismatches in shoe-surface interface designs.

REFERENCES

Bonstingl RW, Morehouse CA, Niebel BW. (1975) Torques developed by different types of shoes on various playing surfaces. Med Sci Sports. 7(2):127-131.

Boytim MJ, Fischer DA, Neumann L. (1991) Syndesmotic ankle sprains. Am J Sports Med. 19(3):294-298.

Cawley PW, Heidt RS Jr., Scranton PE Jr., Losse GM, Howard ME. (2003) Physiologic axial load, frictional resistance, and the football shoe-surface interface. Foot Ankle Int. 24(7):551-556.

Edwards GS, DeLee JC. (1984) Ankle diastasis without fracture. Foot Ankle. 4(6):305-312

Forman J, Lessley D, Shaw CG, Evans J, Kent R, Rouhana SW, Prasad P. (2006) Thoracic response of belted PMHS, the Hybrid III, and the THOR-NT mid-sized male surrogates in low speed, frontal crashes. Stapp Car Crash J. 50:191-215.

France EP, Paulos LE, Abbott PJ, Roberts PF, Muhic LA, Lemaster JH, Kazarian LE. (1987) Failure characteristics of the medial collateral ligament of the knee: Effects of high strain rate. Aviat Space Environ Med. 58:488.

Lambson RB, Barnhill BS, Higgins RW. (1996) Football cleat design and its effect on anterior cruciate ligament injuries. A three year prospective study. Am J Sports Med. 24(2):155-159.

Livesay GA, Reda DR, Nauman EA. (2006) Peak torque and rotational stiffness developed at the shoe-surface interface. Am J Sports Med. 34(3):415-422.

McDonald JP, Shams T, Rangarajan N, Beach D, Huang T, Freemire J, Artis M, Wang Y, Haffner M. (2003) Design and development of a THOR based female crash test dummy. Stapp Car Crash J. 47:551-570.

McMaster-Carr [Internet]. Commercial-strength neoprene rubber technical information. Supply catalog p. 3440. Available at: http://www.mcmaster.com/ Accessed Nov 7, 2008.

Meyer EG, Baumer TG, Slade JM, Smith WE, Haut RC. (2008) Tibiofemoral contact pressures and osteochondral microtrauma during anterior cruciate ligament rupture due to excessive compressive loading and internal torque of the human knee. Am J Sports Med. 36(10):1966-1977.

Mote CD Jr, Lee CW. (1982) Identification of human lower extremity dynamics in torsion. J Biomech. 15(3):211-222.

Ng BH, Chou SM, Lim BH, Chong A. (2004) Strain rate effect on the failure properties of tendons. Proc Inst Mech Eng [H]. 218(3):203-206.

Nigg BM, Yeadon MR. (1987) Biomechanical aspects of playing surfaces. J Sports Sci. 5(2):117-145.

Powell JW, Schootman M. (1993) A multivariate risk analysis of natural grass and AstroTurf playing surfaces in the National Football League 1980-1989. Int Turfgrass Soc Res J. 23:201-211.

Schaffer JJ, Manoli A. (1987) The antiglide plate for distal fibular fixation. J Bone Joint Surg Am. 69-A(4):596-604.

Shams T, Beach D, White R, Rangarajan N, Haffner M, Eppinger R, Pritz H, Kuppa S, Beebe M. (1999) Development and design of THOR-Lx: The Thor lower extremity. Proc 43rd Stapp Car Crash Conference. Society of Automotive Engineers. Warrendale, PA: 141-160.

Shams T, Beach D, Huang T, Rangarajan N. (2002) Development of THOR-FLx: A biofidelic lower extremity for use with 5th percentile female crash test dummies. Stapp Car Crash J. 46:267-283.

Stiehl JB, Skrade DA, Johnson RP. (Dec, 1992) Experimentally produced ankle fractures in autopsy specimens. Clin Orthop Relat Res. 285:244-249.

Torg JS, Quedenfeld TC, Landau S. (1974) The shoe-surface interface and its relationship to football knee injuries. J Sports Med. 2(5):261-269.

Tornvall FV, Holmqvist K, Davidsson J, Svensson MY, Haland Y, Ohrn H. (2007) A new THOR shoulder design: a comparison with volunteers, the Hybrid III, and THOR NT. Traffic Inj Prev. 8(2):205-215.

Villwock MR, Meyer EG, Powell JP, Fouty AJ, Haut RC. (2009a) Football playing surface and shoe design affect rotational traction. Am J Sports Med. 37(3):518-525.

Villwock MR, Meyer EG, Powell JP, Fouty AJ, Haut RC. (2009b) The effects of various infills, fiber structures, and shoe designs on generating rotational traction on an artificial surface. J Sports Eng Tech. 223(1):11-19.

Villwock MR, Meyer EG, Powell JP, Haut RC. (2009c) A biomechanical investigation of ankle injury under external foot/ankle complex rotation using the human cadaver model. J Appl Biomech. In Review.

Chapter 6: Conclusions and Recommendations for Future Research

Conclusions:

This thesis explores the football shoe-surface interface and its potential relationship to injury risk. It attempts to understand the mechanics of the third-generation, artificial surface. Other investigators have assessed peak torque on artificial surfaces, but no one has tried to identify the surface variables which contribute to rotational traction. By understanding the mechanics of the materials, guidelines may be proposed in an effort to consider injury prevention during the design phase of artifical surfaces and shoes. This thesis also proposes a novel device that can be used to predict ankle injury risk based on ankle deformation rather than peak torque.

Chapter 1 documented the need for further analyses into the risk of potential injury while playing football on a third-generation, artificial surface based on torque. Specifically, the need for rotational traction measurements of modern football shoes on infill based artificial surfaces using physiological loading conditions. Chapter 2 investigated the rotational traction of ten football shoes on the most commonly used surfaces in American football. It was hypothesized in this chapter that artificial surfaces would generate higher rotational tractions than natural grass surfaces. It was also hypothesized that rotational traction characteristics would be associated with the football shoe cleat pattern and materials used in the shoe's upper. The results demonstrated that the AstroPlay and FieldTurf surfaces in this study yielded significantly higher peak torque and rotational stiffness in comparison to the natural grass surfaces. In addition, the natural grass surfaces were significantly different from each other, with the sand

based soil surface producing higher peak torque than the native Michigan soil surface. With the exception of the turf style shoe design, cleat pattern was not found to influence rotational traction measurements. The model of shoe, however, did significantly affect rotational stiffness. This may be due to differences in the structural integrity and material composition of the shoe's upper.

Chapter 3 further investigated the influence of infill material and fiber structure on generating rotational traction on third-generation, artificial surfaces. It hypothesized that rotational traction of the artificial surface would be largely influenced by the infill layer. It was found that the infill produced by cryogenic fragmentation generated significantly higher torque than the ground or extruded rubber. It was believed that the compact structure of the infill layer due to the small size of the cryogenic particles increased the cleated shoe's resistance to rotation. The presence of a nylon root zone in the fiber structure was also found to significantly reduce peak torque. This variable most likely affected torque generation by reducing the compactness of the infill layer. The effect of cleat pattern was statistically apparent in this analysis due to the similar structure of the tested surfaces. The cleat patterns identified by larger perimeter cleats (12 Studded and Edge) produced significantly higher torques than the other design groups.

Chapter 4 documented ankle injuries that result from excessive external rotation, possibly related to foot fixation in American football. It was hypothesized that experiments with a younger cadaveric population would produce a higher frequency of ligamentous injury without bone fracture. A difference in foot fixation in the current literature was also thought to influence the mode of soft tissue injury. The results documented isolated ligamentous injury to the posterior talofibular ligament and the

101

anterior portion of the deltoid ligament. The higher incidence of deltoid injuries when the foot was taped may indicate that the amount of constraint offered by shoes could influence the potential for and location of soft tissue injury in the ankle during external rotation.

Chapter 5 detailed the development of a biofidelic ankle that can be used to predict the risk of ankle injury as a result of foot fixation on a playing surface. The biofidelic surrogate not only measures peak torque, but assesses the amount of rotational deformation that occurs at the ankle joint. Strain, unlike stress, may not be affected by strain rate. Thus, the surrogate's ability to measure ankle rotation may be a more valuable predictor of soft tissue injury risk than peak torque alone. Additional experiments may be needed to validate this notion.

Recommendations for Future Research:

The research on ankle injury in this thesis evokes many questions about its impact on real-world injury situations. Additional ankle research using a paired study may be useful to address the potential injury issues that might be attributable to foot fixation and subtalar constraint. Constraining the cadaver foot/ankle complex in available footwear constructed with uppers of various rigidities may examine the real-world practicality of how foot mechanics (e.g. subtalar motion) may be restricted in certain models of shoes. The measurement of strain in the various ankle ligaments as a function of the rate of rotation and degree of constraint from shoe uppers is also important in understanding the mechanism and location of injury. Additional research may explain how these differences affect the body's physiological response to foot fixation on a playing surface.

The data presented in this thesis provides a foundation for understanding the traction characteristics of third-generation, artificial surfaces. There is still much that remains unknown about their performance. The focus of the present work was in measuring rotational traction, under the assumption that excessive rotational traction produces an increased risk of lower extremity injury. There may always be a trade-off in artificial surface design between reducing rotational traction for increased "safety", and increasing linear traction for improved speed and performance. In order to properly assess the relationship between rotational traction and linear traction, the measurement of linear traction on the tested surfaces in this thesis will be necessary.

Future directions for rotational traction testing of shoe designs include documenting torque as a function of the center of rotation, and documenting how the torque may vary between an internally directed ground reaction torque and external ground reaction torque. Future directions for surface testing include measuring the effects of moisture and temperature on infill artificial surfaces. As manufacturers continue to update cleat and surface designs it is important to understand how specific variables affect traction characteristics with the ultimate goal of improving the shoe-surface interface by mitigating injury potential while maintaining or even improving player performance.

The biofidelic ankle discussed in this thesis may provide an additional tool for assessment of the risk of ankle injury due to foot fixation on the playing surface. However, for this tool to be accepted it must be known if torque or rotation of the foot/ankle complex is a better measure of injury potential. The answer to this question may arise from ankle research that monitors the strain in the various ligaments during an

applied external rotation. The incorporation of a biofidelic knee into the surrogate lower extremity might also provide insight into determination of the "weakest link" under various shoe-surface interface conditions.

It is not possible to fully evaluate the risk of injury on a surface without considering its hardness. The risk of concussion from head to surface impact represents a serious potential injury. Analysis of the deceleration forces associated with such collisions will provide another assessment of the relative risk of injury due to the player and surface interaction.

The documentation of hardness values and traction characteristics provide quantitative measures for comparing the mechanical performance of the player-surface interface. An additional step is to study how these mechanical variations might translate into biomechanical differences in player movement patterns during sport specific maneuvers. This may provide for a clearer understanding of the specific injury mechanisms that can be associated with the football shoe-surface interface and aide in the development of future injury prevention technologies and training strategies.

Through iterative shoe-surface designs and biomechanical testing, it may be possible to not only match the shoe-surface design to the sport, but match the shoe-surface interaction to the player. Continued research and development into understanding the complex behavior at the football shoe-surface interface may benefit the career and lives of athletes for years to come.

Appendix A: Peak torque, rotational stiffness and temperature data from Chapters 2 and 3

Table A1: Peak torque of Gameday Grass surfaces with cryogenic infill (Nm)

Mfg	Model	Trial	Gameday Fiber: MT Infill: Cryo	Gameday Fiber: Tapex Infill: Cryo	Gameday Fiber: XPe Infill: Cryo	Gameday Fiber: 3D Infill: Cryo
Nike	BladeII TD Mid Football	1	142	137	123	118
		2	115	122	111	119
		3	128	123	111	115
		4	120	123	119	116
		5	122	127	118	117
		MEAN	125.5	126.4	116.4	117.0
		SD	10.5	6.2	5.3	1.6
		TEMP	66°F	66°F	78°F	71°F
Nike	Vapor Jet TD Low Fotball	1	107	133	126	113
		2	127	126	122	106
		3	122	115	127	98
		4	121	123	115	107
		5	121	120	124	100
		MEAN	119.6	123.4	122.8	104.8
		SD	7.5	6.7	4.8	6.0
		TEMP	66°F	66°F	78°F	70°F
Nike	Air Zoom Superbad FT Mid Football	1	95	106	104	87
		2	104	98	99	104
		3	100	103	104	80
		4	104	101	98	100
		5	106	110	109	98
		MEAN	101.8	103.6	102.8	93.8
		SD	4.4	4.6	4.4	10.0
		TEMP	66°F	66°F	78°F	74°F
Nike	Air Zoom Blade D Mid Football	1	99	107	94	88
		2	102	110	96	85
		3	106	100	95	80
		4	93	101	96	89
		5	101	107	92	93
		MEAN	100.2	105.0	94.6	87.0
		SD	4.8	4.3	1.7	4.8
		TEMP	66°F	66°F	78°F	70°F
Adidas	Turf Hog LE Mid Football	1	77	79	89	87
		2	69	90	85	94
		3	70	93	92	96
		4	70	84	87	84
		5	71	95	84	90
		MEAN	71.4	88.2	87.4	90.2
		SD	3.2	6.6	3.2	4.9
		TEMP	68°F	66°F	59°F	70°F

Table A2: Peak torque of Gameday Grass surfaces with cryogenic infill continued (Nm)

Mfg	Model	Trial	Gameday Fiber: MT Infill: Cryo	Gameday Fiber: Tapex Infill: Cryo	Gameday Fiber: XPe Infill: Cryo	Gameday Fiber: 3D Infill: Cryo
Adidas	Corner Blitz 7 D Mid Football	1	117	124	128	108
		2	117	123	132	105
		3	121	129	129	102
		4	122	130	119	105
		5	118	116	122	102
		MEAN	119.0	124.4	126.0	104.4
		SD	2.3	5.6	5.3	2.5
		TEMP	68°F	66°F	59°F	70°F
Adidas	Scorch TRX Low Football	1	120	123	116	121
		2	121	124	141	111
		3	123	117	120	116
		4	123	130	114	121
		5	119	126	114	122
		MEAN	121.2	124.0	121.0	118.2
		SD	1.8	4.7	11.4	4.7
		TEMP	68°F	66°F	71°F	70°F
Adidas	Scorch 7 Fly Low Football	1	114	116	106	101
		2	127	123	110	109
		3	108	116	110	110
		4	105	116	113	105
		5	117	112	122	113
		MEAN	114.2	116.6	112.2	107.6
		SD	8.6	4.0	6.0	4.7
		TEMP	68°F	66°F	71°F	70°F
Adidas	Grid Iron Mid Football	1	104	109	108	104
		2	115	119	119	114
		3	111	116	120	103
		4	111	122	113	98
		5	119	117	131	102
		MEAN	112.0	116.6	118.2	104.2
		SD	5.6	4.8	8.6	5.9
		TEMP	59°F	64°F	59°F	70°F
Adidas	Quickslant D Mid Football	1	105	100	95	83
		2	105	95	106	96
		3	97	100	96	95
		4	112	113	93	91
		5	109	108	111	110
		MEAN	105.6	103.2	100.2	95.0
		SD	5.6	7.2	7.9	9.8
		TEMP	59°F	64°F	71°F	70°F

Table A3: Peak torque of Gameday Grass surfaces with extruded infill (Nm)

Mfg	Model	Trial	Gameday Fiber: MT Infill: Ext.	Gameday Fiber: Tapex Infill: Ext.	Gameday Fiber: XPe Infill: Ext.	Gameday Fiber: 3D Infill: Ext.
Nike	BladeII TD Mid Football	1	113	109	110	106
		2	105	104	107	107
		3	119	98	120	106
		4	116	101	117	99
		5	132	113	113	93
		MEAN	117.0	105.0	113.4	102.2
		SD	9.9	6.0	5.2	6.1
		TEMP	89°F	97°F	84°F	91°F
Nike	Vapor Jet TD Low Fotball	1	117	99	117	108
		2	102	100	118	105
		3	113	107	111	103
		4	111	119	105	102
		5	109	109	103	105
		MEAN	110.4	106.8	110.8	104.6
		SD	5.5	8.1	6.8	2.3
		TEMP	89°F	97°F	84°F	91°F
Nike	Air Zoom Superbad FT Mid Football	1	104	95	96	101
		2	89	91	97	95
		3	106	94	95	93
		4	90	94	94	92
		5	102	91	94	84
		MEAN	98.2	93.0	95.2	93.0
		SD	8.1	1.9	1.3	6.1
		TEMP	89°F	97°F	84°F	97°F
Nike	Air Zoom Blade D Mid Football	1	88	95	95	109
		2	92	90	95	86
		3	92	86	89	98
		4	88	95	89	87
		5	98	84	89	102
		MEAN	91.6	90.0	91.4	96.4
		SD	4.1	5.0	3.3	9.9
		TEMP	89°F	97°F	84°F	97°F
Adidas	Turf Hog LE Mid Football	1	72	77	84	80
		2	66	79	84	84
		3	70	81	80	84
		4	72	83	89	84
		5	70	81	83	91
		MEAN	70.0	80.2	84.0	84.6
		SD	2.4	2.3	3.2	4.0
		TEMP	89°F	91°F	86°F	89°F

Table A4: Peak torque of Gameday Grass surfaces with extruded infill continued (Nm)

Mfg	Model	Trial	Gameday Fiber: MT Infill: Ext.	Gameday Fiber: Tapex Infill: Ext.	Gameday Fiber: XPe Infill: Ext.	Gameday Fiber: 3D Infill: Ext.
Adidas	Corner Blitz 7 D Mid Football	1	102	105	114	105
		2	97	110	110	107
		3	97	102	107	107
		4	99	104	108	106
		5	96	98	105	103
		MEAN	98.2	103.8	108.8	105.6
		SD	2.4	4.4	3.4	1.7
		TEMP	89°F	91°F	86°F	97°F
Adidas	Scorch TRX Low Football	1	117	109	105	103
		2	100	104	108	94
		3	106	98	96	100
		4	106	101	100	97
		5	100	113	103	97
		MEAN	105.8	105.0	102.4	98.2
		SD	6.9	6.0	4.6	3.4
		TEMP	89°F	91°F	88°F	89°F
Adidas	Scorch 7 Fly Low Football	1	105	110	100	92
		2	108	109	107	110
		3	96	92	92	97
		4	89	91	100	85
		5	88	97	87	101
		MEAN	97.2	99.8	97.2	97.0
		SD	9.1	9.1	7.8	9.4
		TEMP	89°F	91°F	88°F	89°F
Adidas	Grid Iron Mid Football	1	90	105	98	93
		2	97	103	100	100
		3	89	100	99	103
		4	90	95	105	107
		5	89	105	101	107
		MEAN	91.0	101.6	100.6	102.0
		SD	3.4	4.2	2.7	5.8
		TEMP	89°F	97°F	86°F	89°F
Adidas	Quickslant D Mid Football	1	93	89	89	81
		2	87	95	80	83
		3	93	85	86	81
		4	97	84	87	88
		5	92	89	75	92
		MEAN	92.4	88.4	83.4	85.0
		SD	3.6	4.3	5.8	4.8
		TEMP	89°F	97°F	86°F	97°F

Table A5: Peak torque of Gameday Grass surfaces with ambient infill (Nm)

Mfg	Model	Trial	Gameday Fiber: MT Infill: Amb.	Gameday Fiber: Tapex Infill: Amb.	Gameday Fiber: XPe Infill: Amb.	Gameday Fiber: 3D Infill: Amb.
Nike	BladeII TD Mid Football	1	130	114	103	111
		2	141	120	121	112
		3	124	120	116	106
		4	114	121	107	108
		5	131	128	117	117
		MEAN	128.0	120.6	112.8	110.8
		SD	9.9	5.0	7.5	4.2
		TEMP	75°F	90°F	81°F	86°F
Nike	Vapor Jet TD Low Fotball	1	124	128	120	105
		2	115	113	107	94
		3	123	120	108	91
		4	116	120	116	97
		5	122	123	101	105
		MEAN	120.0	120.8	110.4	98.4
		SD	4.2	5.4	7.6	6.4
		TEMP	66°F	90°F	81°F	88°F
Nike	Air Zoom Superbad FT Mid Football	1	96	90	109	91
		2	102	97	95	89
		3	86	98	92	84
		4	98	92	94	93
		5	102	94	98	93
		MEAN	96.8	94.2	97.6	90.0
		SD	6.6	3.3	6.7	3.7
		TEMP	66°F	90°F	81°F	88°F
Nike	Air Zoom Blade D Mid Football	1	96	106	92	93
		2	97	101	82	78
		3	84	94	92	93
		4	102	101	91	87
		5	96	97	101	80
		MEAN	95.0	99.8	91.6	86.2
		SD	6.6	4.5	6.7	7.0
		TEMP	66°F	90°F	81°F	86°F
Adidas	Turf Hog LE Mid Football	1	73	84	82	79
		2	80	82	92	74
		3	76	78	82	73
		4	70	75	88	72
		5	77	79	78	77
		MEAN	75.2	79.6	84.4	75.0
		SD	3.8	3.5	5.5	2.9
		TEMP	75°F	90°F	81°F	86°F

Table A6: Peak torque of Gameday Grass surfaces with ambient infill continued (Nm)

Mfg	Model	Trial	Gameday Fiber: MT Infill: Amb.	Gameday Fiber: Tapex Infill: Amb.	Gameday Fiber: XPe Infill: Amb.	Gameday Fiber: 3D Infill: Amb.
Adidas	Corner Blitz 7 D Mid Football	1	110	115	103	100
		2	102	104	108	100
		3	109	107	109	107
		4	100	100	103	97
		5	105	102	108	95
		MEAN	105.2	105.6	106.2	99.8
		SD	4.3	5.9	2.9	4.5
		TEMP	77°F	85°F	81°F	86°F
Adidas	Scorch TRX Low Football	1	102	112	102	103
		2	102	111	114	117
		3	117	112	102	123
		4	117	107	102	117
		5	100	104	107	105
		MEAN	107.6	109.2	105.4	113.0
		SD	8.6	3.6	5.3	8.6
		TEMP	77°F	90°F	83°F	86°F
Adidas	Scorch 7 Fly Low Football	1	111	109	109	81
		2	113	111	101	84
		3	108	103	90	85
		4	117	94	100	82
		5	111	107	110	95
		MEAN	112.0	104.8	102.0	85.4
		SD	3.3	6.7	8.1	5.6
		TEMP	77°F	85°F	83°F	86°F
Adidas	Grid Iron Mid Football	1	96	98	107	88
		2	93	99	100	91
		3	92	99	109	103
		4	97	111	94	96
		5	100	101	115	95
		MEAN	95.6	101.6	105.0	94.6
		SD	3.2	5.4	8.2	5.7
		TEMP	77°F	85°F	81°F	86°F
Adidas	Quickslant D Mid Football	1	96	95	88	83
		2	97	85	87	83
		3	95	87	92	89
		4	89	97	91	82
		5	86	90	88	90
		MEAN	92.6	90.8	89.2	85.4
		SD	4.8	5.1	2.2	3.8
		TEMP	77°F	85°F	81°F	86°F

Table A7: Peak torque of FieldTurf, AstroPlay, and natural grass surfaces (Nm)

Mfg	Model	Trial	AstroPlay MSU Indoor	Field Turf UM Indoor	Practice Grass (Native Soil)	Stadium Grass (Sand Soil)
Nike	BladeII TD Mid Football	1	113	125	94	108
		2	135	132	84	117
		3	119	147	81	111
		4	118	136	80	121
		5	123	139	99	121
		MEAN	121.6	135.8	87.6	115.6
		SD	8.3	8.2	8.4	5.9
		TEMP	70°F	70°F	90°F	52°F
Nike	Vapor Jet TD Low Fotball	1	119	130	88	99
		2	115	130	103	99
		3	109	130	101	98
		4	120	133	100	111
		5	129	135	101	95
		MEAN	118.4	131.6	98.6	100.4
		SD	7.3	2.3	6.0	6.1
		TEMP	70°F	70°F	90°F	52°F
Nike	Air Zoom Superbad FT Mid Football	1	123	118	69	104
		2	117	126	76	102
		3	120	120	77	103
		4	115	112	78	105
		5	124	111	68	93
		MEAN	119.8	117.4	73.6	101.4
		SD	3.8	6.1	4.7	4.8
		TEMP	70°F	70°F	90°F	52°F
Nike	Air Zoom Blade D Mid Football	1	122	121	81	130
		2	135	117	81	100
		3	135	114	85	112
		4	126	127	83	102
		5	136	119	85	118
		MEAN	130.8	119.6	83.0	112.4
		SD	6.4	4.9	2.0	12.3
		TEMP	70°F	70°F	90°F	52°F
Adidas	Turf Hog LE Mid Football	1	77	82	63	62
		2	72	78	60	57
		3	78	79	55	56
		4	82	88	60	58
		5	83	80	62	65
		MEAN	78.4	81.4	60.0	59.6
		SD	4.4	4.0	3.1	3.8
		TEMP	70°F	70°F	90°F	52°F

Table A8: Peak torque of AstroPlay, FieldTurf,and natural grass surfaces continued (Nm)

Mfg	Model	Trial	AstroPlay MSU Indoor	Field Turf UM Indoor	Practice Grass (Native Soil)	Stadium Grass (Sand Soil)
Adidas	Corner Blitz 7 D Mid Football	1	107	124	85	77
		2	108	118	73	71
		3	108	120	83	70
		4	107	124	74	79
		5	116	123	74	74
		MEAN	109.2	121.8	77.8	74.2
		SD	3.8	2.7	5.7	3.8
		TEMP	70°F	70°F	90°F	52°F
Adidas	Scorch TRX Low Football	1	119	133	80	99
		2	128	118	81	105
		3	113	133	69	97
		4	115	125	88	100
		5	110	136	81	92
		MEAN	117.0	129.0	79.8	98.6
		SD	7.0	7.4	6.8	4.7
		TEMP	70°F	70°F	88°F	52°F
Adidas	Scorch 7 Fly Low Football	1	115	124	88	110
		2	108	120	98	102
		3	102	120	94	121
		4	109	118	90	108
		5	105	120	105	96
		MEAN	107.8	120.4	95.0	107.4
		SD	4.9	2.2	6.8	9.4
		TEMP	70°F	70°F	88°F	52°F
Adidas	Grid Iron Mid Football	1	106	104	83	86
		2	114	111	84	94
		3	117	113	87	83
		4	104	117	82	82
		5	107	117	71	79
		MEAN	109.6	112.4	81.4	84.8
		SD	5.6	5.4	6.1	5.7
		TEMP	70°F	70°F	90°F	52°F
Adidas	Quickslant D Mid Football	1	102	116	96	102
		2	112	108	96	107
		3	108	113	92	102
		4	111	110	105	108
		5	96	120	83	104
		MEAN	105.8	113.4	94.4	104.6
		SD	6.7	4.8	8.0	2.8
		TEMP	70°F	70°F	90°F	52°F

Table A9: Rotational stiffness of Gameday Grass surfaces with cryogenic infill (Nm/degree)

Mfg	Model	Trial	Gameday Fiber: MT Infill: Cryo	Gameday Fiber: Tapex Infill: Cryo	Gameday Fiber: XPe Infill: Cryo	Gameday Fiber: 3D Infill: Cryo
Nike	BladeII TD Mid Football	1	4.29	3.07	3.28	3.26
		2	2.71	4.01	4.02	2.71
		3	4.29	4.28	3.72	3.32
		4	3.88	4.48	3.83	2.37
		5	3.65	3.96	2.92	3.08
		MEAN	3.8	4.0	3.6	2.9
		SD	0.7	0.5	0.4	0.4
		TEMP	66°F	66°F	78°F	71°F
Nike	Vapor Jet TD Low Fotball	1	2.79	3.26	3.13	3.07
		2	3.48	3.16	3.50	2.61
		3	3.14	3.06	2.97	2.79
		4	3.24	3.11	3.14	3.10
		5	3.26	2.77	3.36	3.11
		MEAN	3.2	3.1	3.2	2.9
		SD	0.3	0.2	0.2	0.2
		TEMP	66°F	66°F	78°F	70°F
Nike	Air Zoom Superbad FT Mid Football	1	2.67	2.46	3.02	2.06
		2	2.40	3.27	2.57	2.18
		3	2.22	2.18	2.32	1.63
		4	2.96	2.38	2.79	2.70
		5	2.76	1.99	3.05	1.86
		MEAN	2.6	2.5	2.8	2.1
		SD	0.3	0.5	0.3	0.4
		TEMP	66°F	66°F	78°F	74°F
Nike	Air Zoom Blade D Mid Football	1	3.44	3.05	2.44	2.06
		2	3.33	4.62	3.55	2.48
		3	3.30	3.66	3.12	1.34
		4	3.28	4.61	4.19	2.12
		5	3.22	4.30	3.37	3.90
		MEAN	3.3	4.1	3.3	2.4
		SD	0.1	0.7	0.6	0.9
		TEMP	66°F	66°F	78°F	70°F
Adidas	Turf Hog LE Mid Football	1	3.88	2.76	3.70	3.06
		2	4.29	3.63	3.02	3.39
		3	4.32	3.76	2.21	3.08
		4	2.68	3.17	3.71	3.86
		5	4.53	3.64	2.97	3.56
		MEAN	3.9	3.4	3.1	3.4
		SD	0.7	0.4	0.6	0.3
		TEMP	68°F	66°F	59°F	70°F

Table A10: Rotational stiffness of Gameday Grass surfaces with cryogenic infill continued (Nm/degree)

Mfg	Model	Trial	Gameday Fiber: MT Infill: Cryo	Gameday Fiber: Tapex Infill: Cryo	Gameday Fiber: XPe Infill: Cryo	Gameday Fiber: 3D Infill: Cryo
Adidas	Corner Blitz 7 D Mid Football	1	4.26	3.98	4.63	3.71
		2	5.40	4.87	5.28	3.58
		3	5.32	4.83	4.68	4.26
		4	5.35	5.28	5.55	4.27
		5	5.32	4.19	4.76	4.76
		MEAN	5.1	4.6	5.0	4.1
		SD	0.5	0.5	0.4	0.5
		TEMP	68°F	66°F	59°F	70°F
Adidas	Scorch TRX Low Football	1	3.35	3.31	2.91	2.71
		2	3.63	3.28	3.65	2.48
		3	3.70	3.77	3.39	3.21
		4	3.07	3.23	2.89	2.95
		5	3.17	3.23	3.77	3.10
		MEAN	3.4	3.4	3.3	2.9
		SD	0.3	0.2	0.4	0.3
		TEMP	68°F	66°F	71°F	70°F
Adidas	Scorch 7 Fly Low Football	1	3.20	2.90	4.56	2.94
		2	3.97	3.36	3.27	2.92
		3	4.42	3.53	3.67	3.90
		4	3.50	3.39	3.72	3.14
		5	4.68	3.74	4.23	4.04
		MEAN	4.0	3.4	3.9	3.4
		SD	0.6	0.3	0.5	0.5
		TEMP	68°F	66°F	71°F	70°F
Adidas	Grid Iron Mid Football	1	3.88	3.79	4.06	3.58
		2	4.80	4.45	4.80	4.29
		3	5.49	4.50	4.32	4.78
		4	4.52	4.78	3.29	4.21
		5	4.97	4.91	2.94	4.29
		MEAN	4.7	4.5	3.9	4.2
		SD	0.6	0.4	0.8	0.4
		TEMP	59°F	64°F	59°F	70°F
Adidas	Quickslant D Mid Football	1	2.19	3.77	3.00	2.61
		2	4.02	3.39	4.20	2.80
		3	3.65	3.40	2.47	1.88
		4	2.95	4.15	2.27	1.82
		5	3.80	3.75	2.95	1.83
		MEAN	3.3	3.7	3.0	2.2
		SD	0.8	0.3	0.8	0.5
		TEMP	59°F	64°F	71°F	70°F

Table A11: Rotational stiffness of Gameday Grass surfaces with extruded infill (Nm/degree)

Mfg	Model	Trial	Gameday Fiber: MT Infill: Ext.	Gameday Fiber: Tapex Infill: Ext.	Gameday Fiber: XPe Infill: Ext.	Gameday Fiber: 3D Infill: Ext.
Nike	BladeII TD Mid Football	1	3.51	2.93	3.20	2.43
		2	4.17	3.68	3.92	2.77
		3	3.60	3.28	3.90	3.08
		4	4.21	3.36	4.10	3.19
		5	3.50	2.99	4.08	3.51
		MEAN	3.8	3.2	3.8	3.0
		SD	0.4	0.3	0.4	0.4
		TEMP	89°F	97°F	84°F	91°F
Nike	Vapor Jet TD Low Fotball	1	3.44	2.26	3.65	2.84
		2	3.84	2.92	3.24	3.06
		3	3.10	2.82	3.30	2.86
		4	3.19	2.84	3.34	3.01
		5	3.74	3.44	2.93	2.50
		MEAN	3.5	2.9	3.3	2.9
		SD	0.3	0.4	0.3	0.2
		TEMP	89°F	97°F	84°F	91°F
Nike	Air Zoom Superbad FT Mid Football	1	2.22	2.93	2.06	2.29
		2	1.93	2.26	1.88	1.66
		3	2.26	2.80	2.04	2.05
		4	2.43	2.25	2.00	2.11
		5	2.20	2.28	2.18	2.25
		MEAN	2.2	2.5	2.0	2.1
		SD	0.2	0.3	0.1	0.3
		TEMP	89°F	97°F	84°F	97°F
Nike	Air Zoom Blade D Mid Football	1	3.40	2.99	3.03	2.93
		2	4.45	1.61	2.21	3.33
		3	3.77	2.95	3.96	2.16
		4	3.08	3.13	3.44	1.93
		5	3.58	3.54	2.92	1.82
		MEAN	3.7	2.8	3.1	2.4
		SD	0.5	0.7	0.6	0.7
		TEMP	89°F	97°F	84°F	97°F
Adidas	Turf Hog LE Mid Football	1	2.90	2.82	2.90	3.10
		2	3.30	2.88	2.98	3.46
		3	2.42	3.27	3.39	3.31
		4	2.80	2.70	3.68	2.86
		5	3.28	2.72	3.50	4.24
		MEAN	2.9	2.9	3.3	3.4
		SD	0.4	0.2	0.3	0.5
		TEMP	89°F	91°F	86°F	89°F

Table A12: Rotational stiffness of Gameday Grass surfaces with extruded infill continued (Nm/degree)

Mfg	Model	Trial	Gameday Fiber: MT Infill: Ext.	Gameday Fiber: Tapex Infill: Ext.	Gameday Fiber: XPe Infill: Ext.	Gameday Fiber: 3D Infill: Ext.
Adidas	Corner Blitz 7 D Mid Football	1	3.30	3.44	3.71	3.63
		2	3.92	4.29	3.82	4.49
		3	3.87	4.15	3.73	4.85
		4	3.75	3.81	3.86	3.88
		5	3.78	4.40	4.03	4.38
		MEAN	3.7	4.0	3.8	4.2
		SD	0.2	0.4	0.1	0.5
		TEMP	89°F	91°F	86°F	97°F
Adidas	Scorch TRX Low Football	1	2.44	2.15	2.74	2.73
		2	2.70	2.28	3.51	2.50
		3	1.97	2.95	3.26	2.72
		4	2.28	2.35	3.76	2.64
		5	2.58	2.49	3.22	2.86
		MEAN	2.4	2.4	3.3	2.7
		SD	0.3	0.3	0.4	0.1
		TEMP	89°F	91°F	88°F	89°F
Adidas	Scorch 7 Fly Low Football	1	2.81	4.05	3.24	2.98
		2	3.51	3.41	3.86	3.09
		3	3.14	3.55	4.27	3.30
		4	3.54	3.26	3.51	3.30
		5	3.86	3.48	3.92	3.63
		MEAN	3.4	3.5	3.8	3.3
		SD	0.4	0.3	0.4	0.3
		TEMP	89°F	91°F	88°F	89°F
Adidas	Grid Iron Mid Football	1	3.32	3.73	3.99	3.36
		2	4.86	3.72	4.91	4.23
		3	4.72	3.58	4.35	4.17
		4	4.28	3.76	4.36	3.90
		5	3.49	4.31	4.45	3.59
		MEAN	4.1	3.8	4.4	3.9
		SD	0.7	0.3	0.3	0.4
		TEMP	89°F	97°F	86°F	89°F
Adidas	Quickslant D Mid Football	1	3.47	2.44	3.10	3.31
		2	2.95	2.66	1.78	2.55
		3	2.08	2.78	3.14	3.10
		4	1.76	2.86	3.18	1.76
		5	4.37	2.61	2.95	1.92
		MEAN	2.9	2.7	2.8	2.5
		SD	1.1	0.2	0.6	0.7
		TEMP	89°F	97°F	86°F	97°F

Table **A13**: Rotational stiffness of Gameday Grass surfaces with ambient infill (Nm/degree)

Mfg	Model	Trial	Gameday Fiber: MT Infill: Amb.	Gameday Fiber: Tapex Infill: Amb.	Gameday Fiber: XPe Infill: Amb.	Gameday Fiber: 3D Infill: Amb.
Nike	BladeII TD Mid Football	1	3.24	3.18	2.51	2.77
		2	3.62	3.35	3.04	2.35
		3	3.64	3.20	3.10	3.15
		4	3.48	3.49	3.57	3.59
		5	3.66	3.52	3.98	2.52
		MEAN	3.5	3.3	3.2	2.9
		SD	0.2	0.2	0.6	0.5
		TEMP	75°F	90°F	81°F	86°F
Nike	Vapor Jet TD Low Fotball	1	Rotary Fixture Malfunction (Rotational Data Lost)	3.22	3.88	2.70
		2		3.19	3.31	2.67
		3		3.43	2.65	2.62
		4		3.71	3.80	2.60
		5		3.55	3.60	2.13
		MEAN		3.4	3.4	2.5
		SD		0.2	0.5	0.2
		TEMP		90°F	81°F	88°F
Nike	Air Zoom Superbad FT Mid Football	1		2.15	2.32	2.24
		2		1.96	2.50	2.10
		3		2.18	2.08	1.75
		4		2.88	2.12	1.89
		5		2.09	2.24	1.86
		MEAN		2.3	2.3	2.0
		SD		0.4	0.2	0.2
		TEMP		90°F	81°F	88°F
Nike	Air Zoom Blade D Mid Football	1		3.32	3.06	2.06
		2		3.78	3.07	3.20
		3		3.20	3.14	1.78
		4		3.74	3.39	2.35
		5		2.81	2.91	1.77
		MEAN		3.4	3.1	2.2
		SD		0.4	0.2	0.6
		TEMP		90°F	81°F	86°F
Adidas	Turf Hog LE Mid Football	1	2.98	3.07	2.88	2.34
		2	3.43	3.13	2.64	3.02
		3	3.05	3.34	3.15	2.55
		4	3.07	3.51	3.28	3.28
		5	Data Lost	3.48	2.83	2.79
		MEAN	3.1	3.3	3.0	2.8
		SD	0.2	0.2	0.3	0.4
		TEMP	75°F	90°F	81°F	86°F

Table A14: Rotational stiffness of Gameday Grass surfaces with ambient infill continued (Nm/degree)

Mfg	Model	Trial	Gameday Fiber: MT Infill: Amb.	Gameday Fiber: Tapex Infill: Amb.	Gameday Fiber: XPe Infill: Amb.	Gameday Fiber: 3D Infill: Amb.
Adidas	Corner Blitz 7 D Mid Football	1	4.83	3.31	3.19	3.45
		2	4.84	3.26	3.60	3.84
		3	4.35	3.59	4.03	3.36
		4	4.50	2.90	3.24	3.19
		5	3.29	3.68	3.80	3.40
		MEAN	4.4	3.3	3.6	3.4
		SD	0.6	0.3	0.4	0.2
		TEMP	77°F	85°F	81°F	86°F
Adidas	Scorch TRX Low Football	1	2.61	2.98	1.76	2.52
		2	2.39	2.86	3.63	2.87
		3	2.99	3.00	2.86	2.77
		4	2.40	3.41	3.28	2.04
		5	3.03	2.74	3.29	3.01
		MEAN	2.7	3.0	3.0	2.6
		SD	0.3	0.3	0.7	0.4
		TEMP	77°F	90°F	83°F	86°F
Adidas	Scorch 7 Fly Low Football	1	3.18	3.10	2.75	3.06
		2	3.31	4.01	3.70	3.31
		3	3.37	3.91	3.47	1.81
		4	3.59	3.66	3.35	3.66
		5	3.90	3.22	3.35	2.69
		MEAN	3.5	3.6	3.3	2.9
		SD	0.3	0.4	0.4	0.7
		TEMP	77°F	85°F	83°F	86°F
Adidas	Grid Iron Mid Football	1	3.21	3.06	3.98	2.70
		2	4.03	3.90	4.72	3.65
		3	4.14	3.55	3.59	3.65
		4	3.59	4.18	3.50	3.39
		5	4.61	3.34	4.48	3.48
		MEAN	3.9	3.6	4.1	3.4
		SD	0.5	0.4	0.5	0.4
		TEMP	77°F	85°F	81°F	86°F
Adidas	Quickslant D Mid Football	1	2.39	3.03	2.82	2.57
		2	1.89	3.67	2.40	3.01
		3	2.26	3.32	3.50	1.93
		4	1.79	2.51	1.78	1.90
		5	2.19	3.43	2.87	2.99
		MEAN	2.1	3.2	2.7	2.5
		SD	0.3	0.4	0.6	0.5
		TEMP	77°F	85°F	81°F	86°F

Table A15: Rotational stiffness of AstroPlay, FieldTurf, and natural grass surfaces (Nm/degree)

Mfg	Model	Trial	AstroPlay MSU Indoor	Field Turf UM Indoor	Practice Grass (Native Soil)	Stadium Grass (Sand Soil)
Nike	BladeII TD Mid Football	1	3.37	3.46	1.65	1.97
		2	2.89	3.89	1.61	2.23
		3	4.04	4.10	1.77	2.07
		4	2.96	3.97	1.38	2.48
		5	2.85	4.35	1.85	2.24
		MEAN	3.2	4.0	1.7	2.2
		SD	0.5	0.3	0.2	0.2
		TEMP	70°F	70°F	70°F	70°F
Nike	Vapor Jet TD Low Fotball	1	3.12	3.61	1.71	2.24
		2	3.63	4.50	2.43	1.86
		3	3.64	3.94	1.98	3.00
		4	3.81	3.72	1.99	2.14
		5	3.76	4.13	1.97	2.24
		MEAN	3.6	4.0	2.0	2.3
		SD	0.3	0.4	0.3	0.4
		TEMP	70°F	70°F	70°F	70°F
Nike	Air Zoom Superbad FT Mid Football	1	2.59	2.53	1.60	1.58
		2	2.25	2.15	1.60	1.81
		3	2.31	2.26	1.42	1.55
		4	2.34	2.71	1.41	1.92
		5	2.27	2.78	1.16	1.76
		MEAN	2.4	2.5	1.4	1.7
		SD	0.1	0.3	0.2	0.2
		TEMP	70°F	70°F	70°F	70°F
Nike	Air Zoom Blade D Mid Football	1	4.03	2.86	1.57	2.70
		2	3.20	2.58	2.90	3.32
		3	2.57	3.11	3.10	2.39
		4	4.12	3.31	1.93	3.21
		5	2.87	3.65	2.03	2.79
		MEAN	3.4	3.1	2.3	2.9
		SD	0.7	0.4	0.7	0.4
		TEMP	70°F	70°F	70°F	70°F
Adidas	Turf Hog LE Mid Football	1	3.26	2.81	1.83	2.17
		2	3.37	3.17	2.35	1.29
		3	3.37	2.97	2.01	1.43
		4	3.31	3.24	3.37	1.72
		5	3.49	3.10	1.56	1.47
		MEAN	3.4	3.1	2.2	1.6
		SD	0.1	0.2	0.7	0.3
		TEMP	70°F	70°F	70°F	70°F

Table A16: Rotational stiffness of AstroPlay, FieldTurf, and natural grass surfaces continued (Nm/degree)

Mfg	Model	Trial	AstroPlay MSU Indoor	Field Turf UM Indoor	Practice Grass (Native Soil)	Stadium Grass (Sand Soil)
Adidas	Corner Blitz 7 D Mid Football	1	3.91	4.23	2.92	2.53
		2	4.86	5.42	3.87	2.45
		3	4.26	5.30	2.28	2.76
		4	4.38	5.10	3.08	2.22
		5	4.32	5.37	4.07	2.79
		MEAN	4.3	5.1	3.2	2.5
		SD	0.3	0.5	0.7	0.2
		TEMP	70°F	70°F	70°F	70°F
Adidas	Scorch TRX Low Football	1	2.83	2.99	2.05	2.02
		2	3.21	2.94	2.03	2.08
		3	3.14	3.05	2.04	2.06
		4	3.16	3.05	2.41	1.66
		5	3.44	2.99	2.76	2.02
		MEAN	3.2	3.0	2.3	2.0
		SD	0.2	0.0	0.3	0.2
		TEMP	70°F	70°F	70°F	70°F
Adidas	Scorch 7 Fly Low Football	1	3.01	3.62	2.02	1.62
		2	3.97	3.63	2.36	2.08
		3	4.47	3.79	1.77	2.46
		4	3.72	3.52	2.18	2.11
		5	3.66	3.92	1.68	1.64
		MEAN	3.8	3.7	2.0	2.0
		SD	0.5	0.2	0.3	0.4
		TEMP	70°F	70°F	70°F	70°F
Adidas	Grid Iron Mid Football	1	3.75	3.43	3.16	1.97
		2	4.33	4.09	2.06	2.88
		3	4.67	4.83	1.84	1.84
		4	4.31	4.37	2.21	2.86
		5	4.53	4.16	2.55	2.75
		MEAN	4.3	4.2	2.4	2.5
		SD	0.4	0.5	0.5	0.5
		TEMP	70°F	70°F	70°F	70°F
Adidas	Quickslant D Mid Football	1	3.45	3.34	2.36	2.63
		2	2.47	3.61	1.60	3.40
		3	3.35	3.24	2.81	2.22
		4	3.52	3.66	3.55	2.34
		5	3.69	3.08	1.99	3.09
		MEAN	3.3	3.4	2.5	2.7
		SD	0.5	0.2	0.8	0.5
		TEMP	70°F	70°F	70°F	70°F

Appendix B: Standard operating procedure for measurement of rotational traction on the football shoe-surface interface.

Purpose:

The purpose of the torsional traction test is to measure the traction properties between footwear and ground surfaces.

*Prescripts of **A & B** denote responsibilities of each person*

Shoes:

1. All shoes must be size 13 mens unless more lasts are made.

2. **B** Each shoe is to be put on the manikin foot and tied very tightly.

3. **B** Shoe laces should be secured away from the ground-shoe interface.

Pre-Test Setup:

1. Unpack the tester

   a. Position the tester over the first test site

   b. **A** Unhitch the trailer mover

   c. **B** Lean the tester toward the hitch

   d. **A** Remove the pins holding on the rear wheel assembly

   e. **B** Set the tester back down

2. **A** Hook up the computer using the A2D board.

3. Zero the torque sensor.

Prior to First Test:

1. Suspend a known weight from the pulley.

2. Document the live readout from the load cell.

3. Ensure that the load cell is reading the proper torque.

   Torque = Force*Moment Arm = Weight(in Newtons)*0.25m

4. If there is a discrepancy, the load cell must be replaced before testing as it is damaged.

First Test Setup:

1. Attach the top of the manikin leg to the plate under the plexi-glass disk allowing for desired rotation.

   a. Attach directly above the heel if heel rotation is desired, likewise above the forefoot if forefoot rotation is desired.

2. **B** Attach the 95 pounds of weights to the cable.

3. Feed the cable around the plexi-glass disk.

4. **A** Pull the height lever back so the cable is even with the pulley.

5. **B** Use the leverage bar to cock the disk until the release latch holds it in place.

6. **B** When the weights are elevated the foam pad should be placed below them to prevent ground damage.

7. The shoe should now be pointing straight forward.

8. **A** Carefully lower the apparatus until the weight is completely on the shoe.

   a. **A** Both the height lever and release lever are adjusted at the same time.

9. Once the test is ready to start, both testers should be standing with both feet on the fold down pads.

10. A The computer record program should be started and the release lever pulled to run the test.

*F*ollowing Test Setups:

1. A Pull the height lever back so the cable is even with the pulley.

2. B Use the leverage bar to cock the disk until the release latch holds it in place.

3. B Lean the tester toward the hitch and use your feet to place the leverage bar under the tester.

4. B Set the tester back down

5. A Using the trailer mover, lift the hitch end and slide 14-18 inches toward the hitch.

    a. B The tester should be balanced on the leverage bar while sliding.

6. B Lean the tester toward the hitch and remove the leverage bar from under the tester.

7. B Fully rotate the ankle back to the starting position by contacting the stop.

8. A Carefully lower the apparatus until the weight is completely on the shoe.

    a. A Both the height lever and release lever are adjusted at the same time.

9. Once the test is ready to start, both testers should be standing with both feet on the fold down pads.

10. A The computer record program should be started and the release lever pulled to run the test.

11. Five tests are completed with each shoe/ground interface. After which either the shoe is changed or the tester is moved to another ground surface.

Last Test Setup:

1. Suspend a known weight from the pulley

2. Document the live readout from the load cell.

3. Ensure that the load cell is reading the proper torque.

   Torque = Force*Moment Arm = Weight(in Newtons)*0.33m

4. If there is a discrepancy, the data from the current day of testing must be discarded and the load cell replaced as it is damaged.

Software Setup:

1. The labview program for the rotational traction test is called "NFL torsion for LV7.vi"

2. Pressing the play button on the top left of the screen will transfer the program to live mode. This will read the live data from the angular transducers and load cell.

3. The program is executed by pressing start. The digital trigger must be "disabled" for the start button to initiate the test.

4. The torque is measured in channel 1. The leg and ankle rotation are channels 2 and 3, respectively.
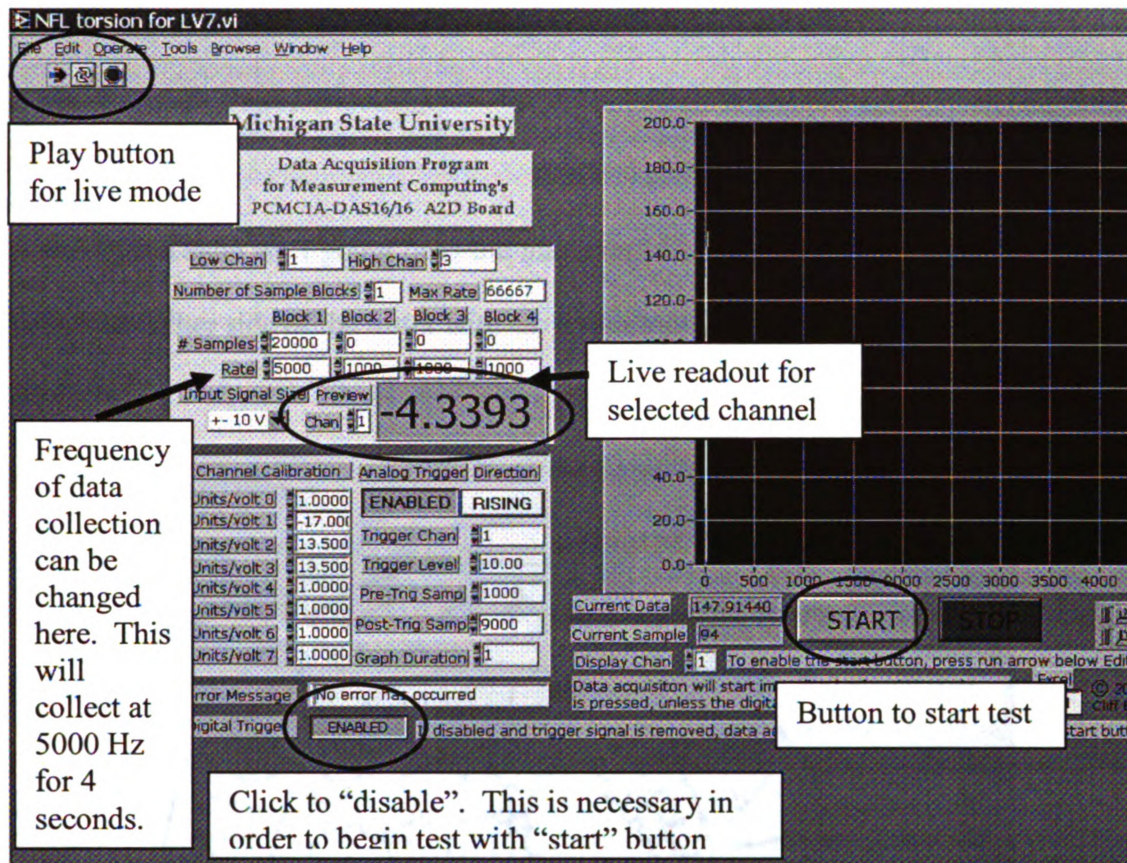
Figure B1: Live readout of the labview program during a rotational traction test.

Data Analysis:

1. For data analysis, refer to the separate SOP entitled "SOP_Traction_Analysis_Macro.doc"

Things to remember during testing:

- Do not test over grass with paint on it unless all of the tests are conducted that way.

Helpful tips for troubleshooting:

- If the shoe isn't going onto the manikin foot easily it is sometimes helpful to lift the other side of the tester with the trailer mover.
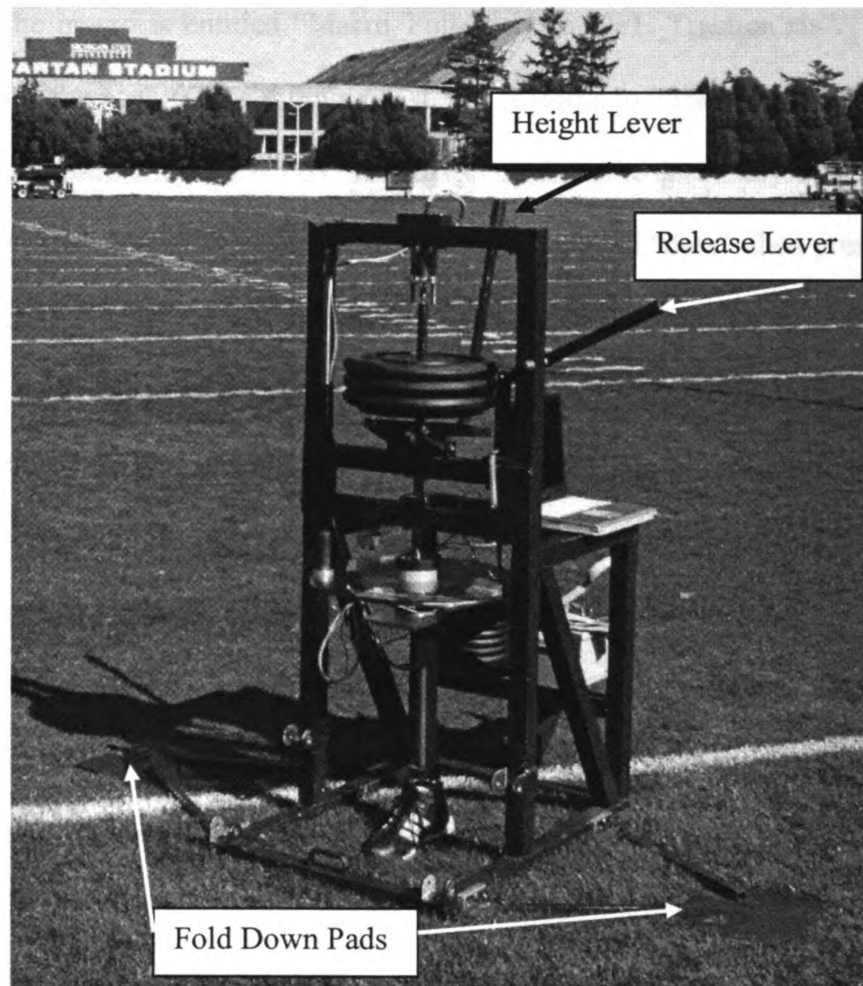

Figure B2: Key components of the rotational traction apparatus.

Appendix C: Standard operating procedure for analysis of rotational traction data

The labview program "NFL torsion for LV7.vi" is used to collect data for a rotational traction experiment. Upon execution, the program generates a .csv file and subsequently, an excel file for each trial. One of the worksheets in the excel file is titled "data" and contains the data in columns A:H.. For data analysis, a custom macro was created. The macro is entitled "Macro_FullAnalyses_NFL_Traction.xls". This macro will calculate the peak torque during a trial, the stiffness to 75% of the peak torque, and the peak ankle rotation (cells W1:3). In order to perform the data analysis, open the excel file which you wish to analyze, select the worksheet named "data", then press ctrl + q to execute the macro. For the macro to execute, the original file containing the macro must be opened. This means that you must open "Macro_FullAnalyses_NFL_Traction.xls" prior to performing the analysis. The code for the macro is included below.

In addition, the macro can calculate the ankle rotation associated with a chosen torque value. The default is 72.5 Nm corresponding to the average failure torque of the NFL ankle cadaver tests performed in our laboratory, it can be changed by entering a new value in cell S6. It is unknown if this additional analysis provides any important information. It has been included for comparison purposes.

Macro Code

```
Range("I1").Select

ActiveCell.FormulaR1C1 = "Torque < 3"

Range("J1").Select

ActiveCell.FormulaR1C1 = "Torque < Fail"

Range("K1").Select

ActiveCell.FormulaR1C1 = "Torque < 75%PT"

Range("L1").Select

ActiveCell.FormulaR1C1 = "Leg < 85"

Range("M1").Select

ActiveCell.FormulaR1C1 = "Find 3"

Range("N1").Select

ActiveCell.FormulaR1C1 = "Find Fail"

Range("O1").Select

ActiveCell.FormulaR1C1 = "Find 75%PT"

Range("P1").Select

ActiveCell.FormulaR1C1 = "Find Leg85"

Range("R1").Select

ActiveCell.FormulaR1C1 = "Match 3Nm"

Range("R2").Select

ActiveCell.FormulaR1C1 = "Match Fail"

Range("R3").Select

ActiveCell.FormulaR1C1 = "Match 75%PT"
```

```
Range("R4").Select

ActiveCell.FormulaR1C1 = "Match Leg85"

Range("V1").Select

ActiveCell.FormulaR1C1 = "Peak Torque"

Range("W1").Select

ActiveCell.FormulaR1C1 = "=MAX(R[1]C[-21]:(INDEX(C2,R4C19,0)))"

Range("V2").Select

ActiveCell.FormulaR1C1 = "Stiffness"

Range("W2").Select

ActiveCell.FormulaR1C1 = _


"=SLOPE((INDEX(C2,R1C19,0)):(INDEX(C2,R3C19,0)),(INDEX(C7,R1C19,0)):(IND
EX(C7,R3C19,0)))"

    Range("I2").Select

    Range("R6").Select

    ActiveCell.FormulaR1C1 = "Cadaver Failure Torque"

    Range("S6").Select

    ActiveCell.FormulaR1C1 = "75"

    Range("I2").Select

    ActiveCell.FormulaR1C1 = "=IF(RC[-7]<3,1,0)"

    Range("I2").Select

    Selection.AutoFill Destination:=Range("I2:I10001")

    Range("I2:I10001").Select
```

```
Range("J2").Select

ActiveCell.FormulaR1C1 = "=IF(RC[-8]<R6C19,1,0)"

Range("J2").Select

Selection.AutoFill Destination:=Range("J2:J10001")

Range("J2:J10001").Select

Range("K2").Select

ActiveCell.FormulaR1C1 = "=IF(RC[-9]<(0.75*R1C23),1,0)"

Range("K2").Select

Selection.AutoFill Destination:=Range("K2:K10001")

Range("K2:K10001").Select

Range("L2").Select

ActiveCell.FormulaR1C1 = "=IF(RC[-7]<85,1,0)"

Range("L2").Select

Selection.AutoFill Destination:=Range("L2:L10001")

Range("L2:L10001").Select

Range("M2").Select

ActiveCell.FormulaR1C1 = "=IF(AND(RC[-4]=1,R[1]C[-4]=0),1,0)"

Range("M2").Select

Selection.AutoFill Destination:=Range("M2:M10001")

Range("M2:M10001").Select

Range("N2").Select

ActiveCell.FormulaR1C1 = "=IF(AND(RC[-4]=1,R[1]C[-4]=0),1,0)"

Range("N2").Select
```

```
Selection.AutoFill Destination:=Range("N2:N10001")

Range("N2:N10001").Select

Range("O2").Select

ActiveCell.FormulaR1C1 = "=IF(AND(RC[-4]=1,R[1]C[-4]=0),1,0)"

Range("O2").Select

Selection.AutoFill Destination:=Range("O2:O10001")

Range("O2:O10001").Select

Range("P2").Select

ActiveCell.FormulaR1C1 = "=IF(AND(RC[-4]=1,R[1]C[-4]=0),1,0)"

Range("P2").Select

Selection.AutoFill Destination:=Range("P2:P10001")

Range("P2:P10001").Select

Range("S1").Select

ActiveCell.FormulaR1C1 = "=MATCH(1,C[-6],0)"

Range("S2").Select

ActiveCell.FormulaR1C1 = "=MATCH(1,C[-5],0)"

Range("S3").Select

ActiveCell.FormulaR1C1 = "=MATCH(1,C[-4],0)"

Range("S4").Select

ActiveCell.FormulaR1C1 = "=MATCH(1,C[-3],0)"

Range("S5").Select

ActiveWindow.ScrollColumn = 9

Range("W1:W2").Select
```

```
With Selection.Interior

    .ColorIndex = 35

    .Pattern = xlSolid

End With

Range("V6").Select

ActiveCell.FormulaR1C1 = "Comparison at Cadaver Failure Torque"

Range("V7").Select

ActiveCell.FormulaR1C1 = "Torque"

Range("V8").Select

ActiveCell.FormulaR1C1 = "Leg Rotation"

Range("V9").Select

ActiveCell.FormulaR1C1 = "Ankle Rotation"

Range("V10").Select

ActiveCell.FormulaR1C1 = "Shoe Rotation"

Range("W7").Select

ActiveCell.FormulaR1C1 = "=INDEX(C2,R2C19)"

Range("W8").Select

ActiveCell.FormulaR1C1 = "=INDEX(C5,R2C19)"

Range("W9").Select

ActiveCell.FormulaR1C1 = "=INDEX(C6,R2C19)"

Range("W10").Select

ActiveCell.FormulaR1C1 = "=INDEX(C7,R2C19)"

Range("W7:W10").Select
```

```
With Selection.Interior

    .ColorIndex = 36

    .Pattern = xlSolid

End With

Columns("V:V").EntireColumn.AutoFit

ActiveWindow.SmallScroll ToRight:=4

End Sub
```

Appendix D: Standard operating procedure for torsional experiments of the cadaver ankle

Preparation

- Thaw a pair of legs overnight at room temperature.

- Put on a sterile surgical gown and gloves. Tape a seal between the gloves and the gown. Put on a face shield, face mask, hair and shoe covers.

- Spread absorbent pads out on the counter. Have a scalpel, scissors, forceps, bone saw, ruler, marker, saline solution and alcohol nearby and ready for use.

- Get an orange "biohazard" bag out and tape it open inside of the large metal trashcan, for easy disposal of excess tissues.

Dissection Technique

Begin dissection before the legs are completely unthawed, unless the knee specimens will also be used within a day. Measure from the knee center to 15 cm distally and mark with a black marker. Make a circumfrential insision around the tibia and fibula at this point, cutting all the way through to the bone. Use the band saw to cut the bone, seperating the knee from the lower 2/3 of the tibia/fibula and ankle. Return the knee to the freezer for future testing. Allow the lower leg to thaw completely before removing skin and muscle tissue. Be extra careful around the ankle joint because the skin gets thin there and you do not want to cut into the joint capsule. Make an incision through the skin, circumferentially around the leg, just above the ankle. Make a longitudinal cut and

remove the skin from the tibia/fibula by grabbing it with the forceps and reflecting it back while cutting the under layers with a scalpel. Remove the calf muscles from about 15 cm above the ankle and up fading gradually to the Achilles tendon. Remove additional muscle/fatty tissue from front and sides that may get in the way during testing. Be careful to stay away from the front edge of the fibula to avoid damaging the interosseous ligament.

Place the partially dissected leg into the potting jig and adjust the height of the tibia potting fixture so it is even with the transection point. Tighten it in place and mark the bottom edge on the tibia/fibula with a marker or scalpel. Remove all tissue around the outsides of the tibia and fibula shafts above the mark. Be sure to avoid the inside edge where the interosseous membrane attaches. Scrape the tibia/fibula to remove all other soft tissue and clean with alcohol to make a clean potting surface.

Predrill two holes in the tibia near the anterior and posterior edges of the potting and slightly out of plane with each other. Bicortical is preferred, but be sure not to damage the fibula or interosseous membrane when coming through the back side of the tibia. If separation between the transected ends of the tibia and fibula is desired during potting, this can be achieved by inserting one of the screws all the way through the tibia and pushing on the fibula at the desired distance and position. Insert #10*2in stainless steel Phillips pan head self tapping screws into holes leaving at least 0.75 inch sticking out into the potting.

Carefully remove skin around the ankle so that the talus is partially exposed anteriorly. Fatty tissue on the sides of the ankle can also be cleaned of. Leave skin on the foot. Predrill and insert three screws into the Calcaneous (2 laterally and 1 medially)

making sure that they are offset from each other so that they do not create a long hole all the way through or run into each other. This step is not required if the fixation method is athletic tape.

Potting Procedure / Taping Procedure

Double check the height of the tibia fixture and that everything fits correctly and the tibia is aligned straight up and down in the coronal and sagittal planes. Check the ankle joint center's position relative to the footbed. The center of rotation (marked on potting bed for 10 deg dorsiflexion) should match the midline of the ankle axis (between lateral and medial malieoli). If it needs to be adjusted in the anterior/posterior direction use spacer blocks on the upper potting cup to move it back in alignment. The longitudinal axis of the foot (a line between the calcaneal tuberosity and the space between the first two toes) should also be centered on the footbed. When the ankle and proximal ends are positioned correctly, attach the front plate to the upper potting cup and then the distal end cap plates from either side to hold the tibia centered (Figure C1). Use duct tape to seal all gaps around the tibia and fibula to prevent potting material from leaking out. Make sure the potting fixture is lubricated with oil for easy removal of the potted bones. Mix an appropriate amount of potting material (half a large cup) and activator (use less so there is more time before it hardens) in a separate plastic container to fill the potting fixture.
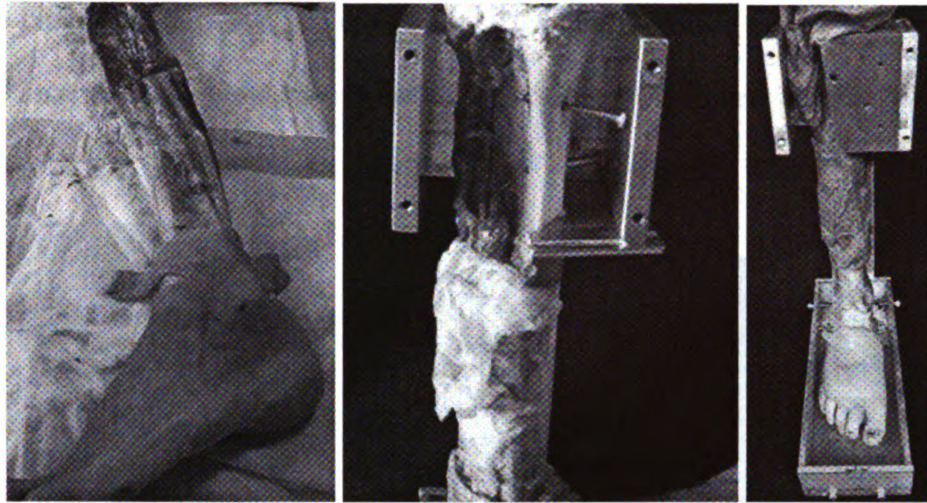
Figure C1: Procedure for potting the proximal end of the cadaver lower extremity.

Pour/push the potting mixture in through the medial and lateral sides and spread around the front and back. Jam it all the way down to the bottom and keep adding more until you are sure it is full (This is a messy process and you may have to move quickly to finish before it hardens). Remove the extra from the top edge when it is full and clean up all material that has spilled out the sides or onto other tissues. After it is partially set remove the duct tape and the front plate and clean up the edges so it can be taken in and out easily and will fit into the CT-stress device.

If potting the foot; remove the leg from the potting jig and oil down the foot bed. Insert medial and lateral set screws so they will stick about 1 inch into the potting (Figure C2). Mix a large batch of potting material (almost a full large cup) with plenty of activator for quick hardening. Pour it into the foot bed and reinsert the tibia into the upper fixture pressing the foot into the bed of potting at the same time so that the heel is centered directly below the tibia. Pour additional potting around the sides and back of the heel, but it is not necessary to cover the top of the foot as long as the fixation screws are fully covered. When the potting is partially set remove the medial and lateral set screws

137

and take the potted foot out of the foot bed. Clean up the edges of the potting so it can easily be inserted and removed from the lower fixture and CT-stress device.
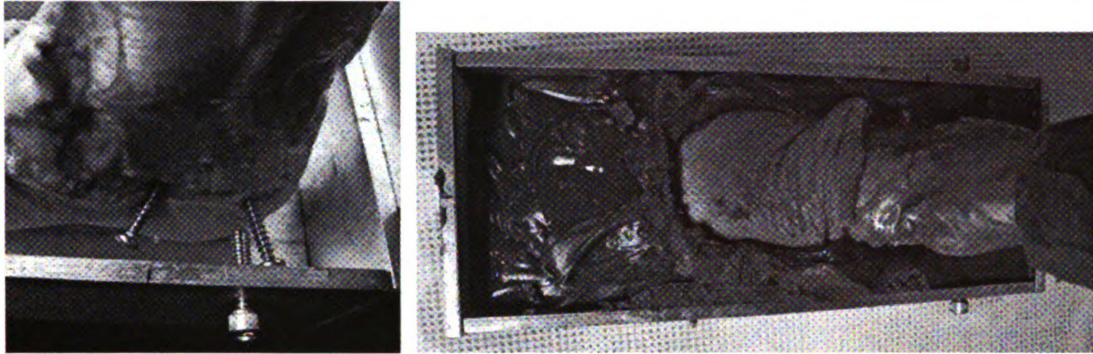

Figure C2: Potted foot constraint with fixation screws into the calcaneous.

If taping the foot; place the foot onto the polycarbonate plate. Prewrap is then placed around the foot and heel. Elasticon (Athletic Tape) is then used to constrain the foot to the plate (Figure C3). The tape should be stretched ~50%. Remember to apply tape around the heel for support.
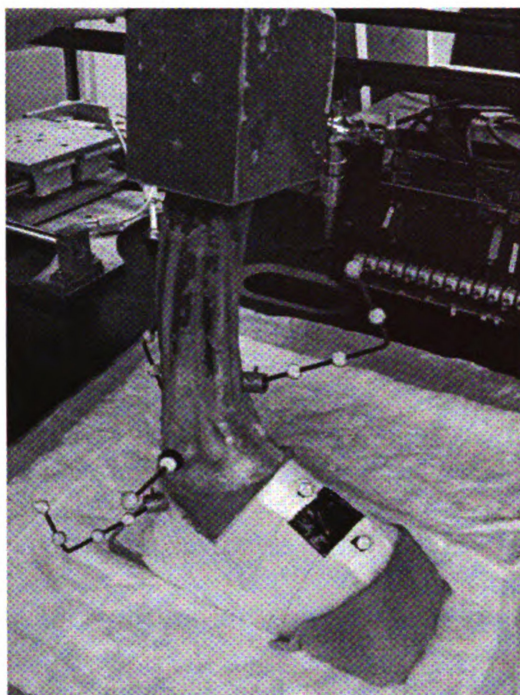
Figure C3: Specimen prepared for testing with taped foot constraint.

Install the bone markers on the fibula by cleaning a small circle of bone near the malleolus and drying it slightly with alcohol. Then use superglue to attach the marker to the bone. Arrays are also inserted into the Tibia, Talus, and Calcaneous. If the foot is maximally dorsiflexed it may be impossible to insert the talus array anteriorly, then it should be placed posteriorly. Exercise caution when attaching these arrays. The tibia array is attached medially to the ATiFL insertion site. When attaching the calcaneous array, ensure that it will not interfere with the footbed fixture.

Stressed CT Procedure

Before testing and after failure the ankle should be taken over to Radiology and CT scanned in the unstressed and stressed conditions with the markers and array fixtures attached. These arrangements can be made by calling 355-0120 ext 316 and speaking to

one of the x-ray technicians directly. Usual scanning must be done in the evenings after the technicians are finished with their patients (4-5pm). Place the leg in the stress device and keep it wrapped in PBS soaked paper towel before taking it out of Fee Hall. Adjust the position/rotate the turntable so the leg fits properly and the foot will be externally rotated. Tighten the anterior set screw so it holds the potting material against the edge of the rectangular hole. A large black garbage bag can be used to transport the device to Radiology and must only be partially opened to allow the weight hanger clearance during the CT scans (Figure C4). Place the device on the CT table and raise it so that it is near the top of the CT tube (to allow the most clearance for the weight hanger) with the foot end in the tube. Set the dial indicator near the knee to 0 degrees and do the first (unstressed) CT scan. Then add the weight hanger (with 12 lbs, for 5 Nm) and check how far the upper leg rotated on the dial indicator. Do the second (stressed) CT scan and have the tech burn them both onto a CD (without additional reconstructions). Bring the leg and CD back to Fee and remove from stress device for experimental testing.
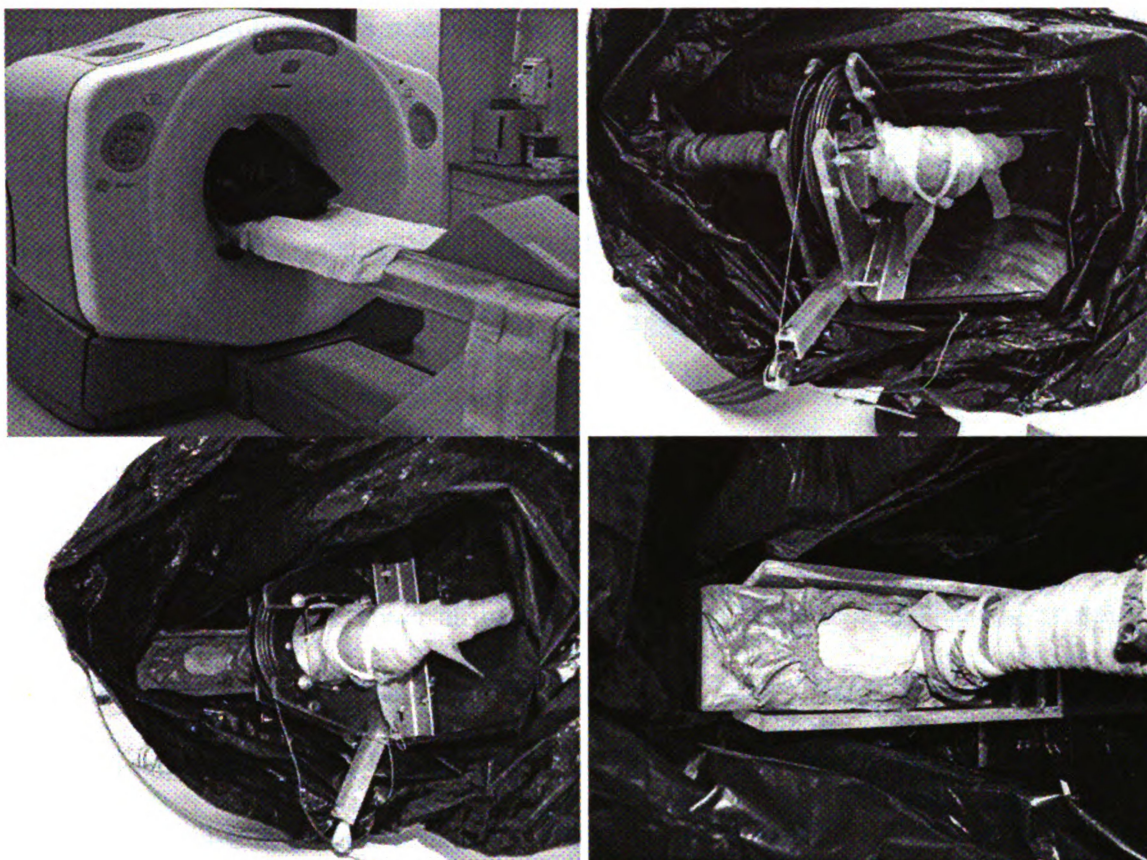
Figure C4: Computated tomography procedure for ankle specimen.

Motion Analysis Procedure

Check all camera and camera mounts to ensure stability. Make sure all knobs on the Manfrotto tripod units are secure, as well as checking the connection between the cameras and mounts. The cameras should be oriented as to include the range of motion for the foot/ankle complex as it rotates. Varying the heights of the tripods, and positioning two cameras behind the MTS and three cameras in fromt of the MTS has worked optimally in the past. Ensure that the tripods are not placed on the cabinet housing the pump. The vibration from the pump could cause error in the camera units.

Turn on the designated Vicon system computer. Start the Vicon Nexus program. While the Nexus program is running, turn on the Vicon MX Control unit. This starts the system. Ensure that all cameras are running correctly and are acquiring data. This can be done on the "Communications" panel of the Nexus software. If the "Communications" panel is not currently open, go to "Window" and click on the "Communications" option. For the NFL Ankle Testing, the settings for trigger signals, camera options, and other important data is saved underneath the Official NFL Ankle Testing header.

For NFL Ankle Testing, the MX Cameras box will show the number of working cameras. The DV Camcorder box will read 1 next to the play button. To begin calibration of the system, cover all marker points that the cameras are seeing except for the points on the Vicon calibration wand. Check the Nexus software to be sure that you are in the real time mode. If the "Live" is active, it will be shown in a darker blue color. When calibrating, the Nexus software needs to be in live mode. Next, place the dedicated Vicon calibration wand onto the lower unit of the MTS. Make sure that the plates are correctly arranged on the guide marks on the MTS and that both levels are reading as being level on the calibration wand. The wand should be placed so that the x and y axis correspond to the anterior/posterior and medial/lateral directions of the foot when it is initially placed into the MTS.

Select the Camera Calibration Icon. Highlighting the cameras, make sure that they can all see all five markers of the calibration wand. When this is done, click the "Start" button under the Aim Cameras heading. The cameras should snap into place. When satisfied, click the "Stop" button under the same heading. Now, take the calibration wand out of viewing range of the cameras. Click the "Start Calibration"

142

button under the Camera Calibration heading. Move the wand into the desired capture space. Do not block any camera while this is taking place. While moving the wand throughout the desired volume, you will notice an orange LED glowing on each camera. It will blink at an increasing speed, indicating that it is picking up all five markers on the calibration wand. When the calibration is complete, the camera will have a solid green LED lit. Looking at the Nexus software, make sure that the camera calibration values are all green after the computer has run its calculations. Verify that the error is less than 0.2 for each camera. Error greater than this can still be accurate, but it is common for the errors to be smaller than 0.2 according to the calibrations that have been done previously on the same apparatus. You will notice that in the real time panel of Nexus, one camera has been placed at an origin. When calibration of the capture volume has completed, place the Vicon calibration wand on the same spot that it occupied during the "Aim MX Cameras" step. Make sure that all three cameras can see all five points of the calibration wand. Click the "Set Volume Origin" button on the screen. Rotate the Nexus real time frame to view the calibration wand and verify that there are white line segments between the markers on the frame. After verifying the accuracy of the line segments, click the "Set Origin" button. The Nexus real time frame should snap the cameras to the correct view. The next calibration that must be done is of the DV Camera. Make sure that the DV Camera can see all five points. Click the "Calibrate DV Cameras" button. A large real time view of what the camera is seeing will fill the Nexus panel. Click on the center of each of the 5 markers on the calibration wand. When finished, click the "Set Calibration" button. This will snap the DV camera calibration to the correct size and shape similar to the Vicon MX3+ cameras. The calibration of the system is complete.

DO NOT BUMP ANY OF THE CAMERAS. If you accidentally bump or intentionally move any of the cameras, you must perform a full calibration of the system all over again. While it is possible to load calibrations, this is not recommended because of the ease of calibrating the system.

To capture a trial, click the "Capture" heading that is on the upper-right hand side of the Nexus panel. This will bring you into more options for the capturing settings. First, go to the Data Management icon in the upper left hand portion of the screen. In the Data Management screen, highlight the NFL Ankle heading. This is done by double clicking on the heading. When this is properly highlighted, select the circular yellow icon with a stick figure in it. This gives you a new subject. Name the new subject with the identification number and indicate whether the leg is a left or right leg. For example, if the identification number is 12345 and it is a right leg, name the subject 12345R. After naming the subject, click the icon directly to the right of the new subject icon. This is the new session icon. When the new session is highlighted, it is the active session. Click the Data Management button once again in the Nexus panel to hide the Data Management screen. In the capture panel, you now have options on several items. In the naming area, make sure that "Overwriting files with the same name" is not a checked option. The name of the trial should include the same string of characters that you used to name the subject as well as the rotation being applied to the system. For example, a 5 degree rotation trial should have the name 12345R 5degree. If there is a need for a second trial at the same load, it should be called 12345R 5degree02. Also needed for the system to run properly is the correct options selected under the capture options heading. The Digital Data option should be checked, while the Analog Data option should be left

unchecked. Also, the Start/Stop data acquisition on remote signal option should be checked and the recording time should be 4 seconds (longer if the speed of rotation is below 0.5 Hz). In order to capture data, the Arm button must be enabled. This can be verified by checking the color of the button. If the Arm button is enabled, the button will turn a darker blue than if it is not enabled. After every trial, the data is automatically saved. To review the data, go into the Data Management system again and double click on the trial that was just run. A blank window will come up. Go to the Pipeline option. The NFL Ankle pipeline should be selected. Currently, this pipeline will reconstruct the analysis that you have selected. Press the "Play" button to evaluate the data. When finished, click the save button next to the data management button. Your data is now reconstructed and saved. You can move on to the next trial by pressing the "Live" button again, changing the filename to the correct loading conditions, and arming the system.

Torsion Procedure

Depending on which leg is being tested it is will change the sign of the applied torque. Check that the serial control wire and A2D interface are connected to the back of the computer. Check that all 4 data channels are connected to the A2D interface.

- Channel 0 - Vertical Displacement

- Channel 1 - Vertical Load (from Biaxial Load Cell)

- Channel 2 - Angular Displacement (Strain output from 442)

- Channel 3 – Torque (from Biaxial Load Cell)

Check the pump oil level on the sight gauge on right side of pump located under the cabinet to the right of the MTS system. Make sure that the vertical actuator & crosshead are located so that movement of the actuator will not damage any fixtures or specimens mounted on the MTS table.

Turn on the MTS controllers (458 and 442 boxes) and computers and when it is warm, press the Enter key on the 458 Microconsole control panel located below the "Hit Enter" Display and to the left of the number keypad. The console will say "Sel. Disp. Module". Press the Display button at the top of the Stroke Control Module. This is the module immediately to the right of the console control panel.

Verify that the Percent Full Scale LED located to the right of the Display is lit. If not press the "Scale Select" button located directly below it until it is lit. Before turning on the Hydraulics, press Up or Down "Display Select" on the console control panel until the "DC Error" L.E.D. is lit. Adjust the "Set Point" dial on the Stroke control module until the DC error reads 0.0 ±0.1. This will stop the actuator from making a sudden movement as soon as the hydraulics are turned on.

Press the Interlock Reset button at the bottom right of the console control panel. You will have to press this button to clear the errors anytime there is a system error. Press the rotary position button on the 442 Controller so that it lights up. Turn the Meter switch to DC Error and read this value on the sliding bar meter directly above, set to 0.0 with the "Set Point" knob in the lower, left corner of the panel.

Turn on the Hydraulics by pressing the Low and then the High buttons to the right of the large red emergency stop button on the 458 console control panel. The MTS pump should start and the pressure should gradually rise to approx 3000 psi. Run a warm up of the hydraulics by using Program # 11 in the Microprofiler which should generate a +-30% 1 Hz sin wave with 50 repeats in both the vertical and rotary actuators. See more detailed programming instructions to verify. Move the vertical actuator to the center of its stroke by turning the "Set Point" knob of the Stroke Control box, then do the same for the rotary actuator. Check the Span knobs on both controllers and if you would like to gradually increase the warmup displacement you can start them at 0 and work your way up to 10. Run the program by pushing the "Funct Select" button until the "Run Enable" light is on then press enter to load the program and "Go" to start it.

Load MTSACLTorsion.vi programs and check that the load (channel 1) and torque (channel 3) are zero. Check that 4 channels of data will be recorded and that the sample rates and times are the same for both computers. Calibration factors should be 10, -900, 13.5 and 11, respectively for the A2D computer and 1000 and 24000 for the encoder computer. Run a practice test in displacement control with the motion system synced to check that data is recording properly and the rotation is in the proper direction.

Move the actuator up nearly to the top by turning the "Set Point" knob of the Stroke Control box, then lower the crosshead close to its position by unlocking and turning the down valve on the front of the MTS, move the clamp into place and turn off the hydraulics. Zero the torsion load cell by opening the 442 panel and twisting the knob until the computer screen readout is 0. Load the foot into the lower fixture and tighten the set screws. Zero the compression load cell by twisting the zero knob on the 458. Lower the upper fixture until there is a slight compressive preload then tighten the set screws into the potting material and lock the upper fixture in place. If necessary switch the 458 to load control as well, by first checking that the DC error is 0 then press the "Control Transfer Enable" and "Control" button in the Load Control Box simultaneously. Exercise exterme caution when operating the MTS in load control.

SAFETY GLASSES SHOULD BE WORN DURING THE IMPACTING PROCEDURE. DO NOT PLACE HANDS/BODY PARTS UNDER ACTUATOR DURING TESTING.

Make sure the loads are still near zero for both directions. Check program #15 in the Microprofiler which should have 4 segments; a ramp segment to level -50 at a rate of 50 %/sec, an endmark segment, a pause segment, and a final return to zero segment with the same rate. The compressive load is controlled by adjusting the span knob on the load controller of the 458 (1 xBW=0.18 span, 2 xBW=0.38 span, 3 xBW=0.57 span). The applied rotation is triggered by the endmark signal after the compressive load has been applied. The amount of rotation can be adjusted by changing the span knob on the 442 (5 deg=0.037 span, 10 deg=0.074 span, 15 deg=0.111 span, 20 deg=0.148 span, 55 deg=0.185 span, 30 deg=0.222 span, 35 deg=0.259 span, 40 deg=0.296 span, 45

deg=0.333 span, 50 deg=0.37 span). The 410 controller controls the shape (haversine) by pressing that button and rate by setting the frequency value (.5 Hz = 1 sec to peak rotation) into the left-most dial. The direction of external rotation must be changed for right versus left (use the invert button). Also verify that the 410 is in remote trigger mode and the "stop at zero" button is pressed. Switch to "Run Enable" on the 458 and load the program then switch to "Remote" control by pressing the "Mode Select" button. Press the "Run" button and the test will wait for a trigger signal to be sent from the A2D computer to the start the test.

Apply a 1 Nm torque preload and a 200 N compressive preload by adjusting the set point knobs. Press play on the .vi program. Press start on the Motion computer and press "Start" on the A2D computer to begin the test and data collection, when ready. Save all data files in .csv format then open that file and copy the data manually to a template file and resaving with a new name as a .xls file.

Check for damage and repeat testing as needed, stopping when a catastrophic failure is noticed. Between each test, change the span knob on the 442 to increase the rotation. Then press play and start on the computers to begin a new test (you do not need to repress run on the 458 unless you change the level in the program itself).

Programming

1. Tests are designed using the 458.91 Microprofiler, which is the doublewide module on the far right side of the Microcontroller. Programs should be checked and tested before any specimen is mounted on the system.

2. To change any of the microprofiler settings (select a test, edit a test, view a test) you must first make sure you have the "Output at Zero" LED lit by pressing the "Ret. to 0" button at the bottom right corner of the Microprofiler. This immediately ends the current test and returns the actuator to its starting position if pressed during a test.

3. To select a test, or edit a test, or view a test, switch to "Programmed" mode by pressing the "Mode Select" button at the top left of the Microprofiler until the programmed LED is lit. Then, press the "Functn Select" button at the top right of the microprofiler until the "Ed. Prog" LED is lit.

4. Select the test to be run, edited, or viewed by entering the test number using the number keypad on the microprofiler and then pressing the "Enter/Yes" button to the left of the keypad on the microprofiler.

5. To view the current program settings of the selected program, first press the "Seg" button to switch to displaying segments of the test. Then press the up or down arrow buttons under "Display Sel" to step through the segment of the currently selected test.

6. Use program number 11 to warm-up the hydraulics with 50 cycles of a .33 Hz sine waveform at 30% of displacement in both actuators. Before running this program you must switch the 448 to displacement control by setting the Xdcr #3 DC error to zero before turning the hydraulics on. Then move both actuators to the middle of the stroke with the set point knob = 5.0.

7. Use program 12 to clear out the servo-valves with 20 cycles of a 1 Hz square waveform at 1% of displacement in both actuators.

150

8. After verifying the test program press the "Functn Select" button on the microprofiler until the "Run Enable" LED is lit. Make sure the desired program is still showing in the "Program /Block" display. Press the "Enter/Yes" button to load the Program (this preprocesses the commands and places the waveform into the run buffer of the micoprofiler). The microprofiler will say "busy" for a second and then display the words "memory left" and a number in the repeats display. This means the microprofiler has finished its preprocessing and is ready to run the test.

9. Press the green "Run" button at the bottom left corner to start the program.

Appendix E: Standard operating procedure for ankle motion analysis

Label Markers

Create segments by adding a new subject and typing the names into the labeling template builder box. The order of segments should follow Table E1 and the corresponding markers must be selected in order, before you go on to the next segment. After all segments are created go to the marker drop down menu and change the names as shown in the properties box at the bottom-left of the screen.

It is important to stay consistent with your naming structure and order so that your exported excel files are similar. Array numbering should always start at the marker closest to the specimen and continue out. Do the fibula first, then tibia, talus, calcaneous, and finally the foot.

Table E1: Segment order and marker labels for a test subject in Vicon.

Label Order	Segment	Marker
1	Fibula	Fib1
2		Fib2
3	Tibia	Tib1
4		Tib2
5		Tib3
6		Tib4
7	Talus	Tal1
8		Tal2
9		Tal3
10		Tal4
11	Calcaneous	Cal1
12		Cal2
13		Cal3
14		Cal4
15	Foot	Foot1
16		Foot2

After the marker labels are created you will be able to reuse them for other files as long as you do not close Nexus, but you cannot save the specimen because it is not a complete model. To label other files go to the Label/Edit tab in the right-hand box, click on the first label and choose the corresponding marker, then continue choosing markers until they are all done.

Next you need to make sure that the markers are labeled for the entire time period of interest. Youmay want to crop the timebar to start at the beginning of compression and end at the peak rotation. Then under Pipeline operations run "delete unlabeled trajectories" and "fill gaps". Go back to Label/Edit and try to fill any other gaps with the spline fill function at the bottom-left box (you can adjust the spline by selecting the arrows near the marker you are trying to fill). Remember, you only need three markers to define a segment. Performing the boybuilder analyses includes a substitute macro in which it analyses the position of each four marker array and substitutes for missing or erratic data. Finally, go back to Pipeline and export data to ASCII file. Now you can open the motion data in Excel and it will be organized as x, y, and z coordinates for each marker (in order) and time.

Bodybuilder Analyses

The relative translations and rotations of the fibula during an external rotation experiment of the foot/ankle complex can be calculated using the Bodybuilder software. Since the fibula is rotating and translating, it is important that the geometric center of the bone structure be used as reference for the translation. Using an acquired CT with the markers attached, the relative displacement can be calculated from the marker to the

geometric center. These displacements can then be used in conjunction with Ankle_Centers.mod to determine the Vicon coordinates for the geometric bone centers. The output of this analysis can then be entered into Ankle.mod to determine the rotations and translations. Both codes include comments to detail the analyses. The marker file Ankle.mkr is used with both .mod files. The marker file may need to be edited depending on the specific marker setup used in the experiment.

Ankle.mkr

[Markers]

Fib1

Fib2

Tib1

Tib2

Tib3

Tib4

Tal1

Tal2

Tal3

Tal4

Cal1

Cal2

Cal3

Cal4

Foot1

Foot2

Tibia = Tib1,Tib2,Tib3,Tib4

Fibula = Fib1,Fib2

Talus = Tal1,Tal2,Tal3,Tal4

Calcaneous = Cal1,Cal2,Cal3,Cal4

Foot = Foot1,Foot2

[Segments]

Fibula

Tibia

Talus

Calcaneous

Foot

[Angles]

FibA

TibA

TalA

CalA

FootA

Ankle.mod

{*Tibia/Fibula Translations and Rotations*}

{*Ankle.mod*}

{*Use with BodyBuilder*}

{*Use with Ankle.mkr file*}

{*Use with Ankle.mp*}

GOrigin = {0,0,0}

Global = [Gorigin,{1,0,0},{0,0,1},xyz]

xaxis = {100,0,0}

yaxis = {0,100,0}

zaxis = {0,0,100}

{*Start of macro section*}

{*This macro is executed on a 4 marker segment and is designed to eliminate marker

error due to erratic movement of one marker.*}

{*======================*}

macro Substitute4(p1,p2,p3,p4)

s234 = [p3,p2-p3,p3-p4]

p1V = Average(p1/s234)*s234

s341 = [p4,p3-p4,p4-p1]

p2V = Average(p2/s341)*s341

s412 = [p1,p4-p1,p1-p2]

p3V = Average(p3/s412)*s412

s123 = [p2,p1-p2,p2-p3]

p4V = Average(p4/s123)*s123

p1 = (p1+p1V)/2 ? p1 ? p1V

p2 = (p2+p2V)/2 ? p2 ? p2V

p3 = (p3+p3V)/2 ? p3 ? p3V

p4 = (p4+p4V)/2 ? p4 ? p4V

endmacro

{*Create segments*}

Fibula = [Fib1,(Fib2-Fib1),(zaxis-GOrigin),1]

Foot = [Foot1,(Foot2-Foot1),(zaxis-GOrigin),1]

Substitute4(Tal1,Tal2,Tal3,Tal4)

Talus = [Tal1,(Tal2-Tal1),(Tal4-Tal3),1]

Output(Tal1,Tal2,Tal3,Tal4)

Substitute4(Tib1,Tib2,Tib3,Tib4)

Tibia = [Tib1,Tib2-Tib1,Tib4-Tib3,1]

Output(Tib1,Tib2,Tib3,Tib4)

Substitute4(Cal1,Cal2,Cal3,Cal4)

Calcaneous = [Cal1,(Cal2-Cal1),(Cal4-Cal3),1]

Output(Cal1,Cal2,Cal3,Cal4)

{*Define Fib1 and Tib1 markers in local coordinates*}

%Fib1 = Fib1/Fibula

%Tib1 = Tib1/Tibia

{*Define fibula and tibia geometric center using output %CORfib & %CORtib from

Ankle_Center.mod. The shaded numbers are edited for each specimen*}

%Centerfib = {%Fib1(1)-■■■,%Fib1(2)-■■,%Fib1(3)-■■}

%Centertib = {%Tib1(1)-■■■,%Tib1(2)+■■,%Tib1(3)+■■}

{*Convert local tib/fib centers to global coordinates*}

Centerfib = %Centerfib*Fibula

Centertib = %Centertib*Tibia

Output(Centerfib,Centertib)

{*Calculate global segment angles*}

TibA = <Tibia,Global,xyz>

FibA = <Fibula,Global,xyz>

FootA = <Foot,Global,xyz>

TalA = <Talus,Global,xyz>

CalA = <Calcaneous,Global,xyz>

Output(TibA,FibA,FootA,TalA,CalA)

159

{*The translation of the fibula will be Centerfib and the translation of the tibia will be Centertib. The rotations of them will be TibA and FibA. Correct calibration and orientation of the Vicon system is important when determining medial-lateral, anterior-posterior translation as well as directions of rotation *}

Ankle_Center.mod

{*Determine Tibia/Fibula Geometric Centers Using CT Displacements*}

{*Ankle_Center.mod*}

{*Use with BodyBuilder*}

{*Use with Ankle.mkr file*}

{*Use with Ankle.mp*}

GOrigin = {0,0,0}

Global = [Gorigin,{1,0,0},{0,0,1},xyz]

xaxis = {100,0,0}

yaxis = {0,100,0}

zaxis = {0,0,100}

{*Start of macro section*}

{*===================*}

macro Substitute4(p1,p2,p3,p4)

s234 = [p3,p2-p3,p3-p4]

p1V = Average(p1/s234)*s234

s341 = [p4,p3-p4,p4-p1]

p2V = Average(p2/s341)*s341

s412 = [p1,p4-p1,p1-p2]

p3V = Average(p3/s412)*s412

161

s123 = [p2,p1-p2,p2-p3]

p4V = Average(p4/s123)*s123

p1 = (p1+p1V)/2 ? p1 ? p1V

p2 = (p2+p2V)/2 ? p2 ? p2V

p3 = (p3+p3V)/2 ? p3 ? p3V

p4 = (p4+p4V)/2 ? p4 ? p4V

endmacro

{*Create segments*}

Fibula = [Fib1,(Fib2-Fib1),(zaxis-GOrigin),1]

Foot = [Foot1,(Foot2-Foot1),(zaxis-GOrigin),1]

Substitute4(Tal1,Tal2,Tal3,Tal4)

Talus = [Tal1,(Tal2-Tal1),(Tal4-Tal3),1]

Output(Tal1,Tal2,Tal3,Tal4)

Substitute4(Tib1,Tib2,Tib3,Tib4)

Tibia = [Tib1,Tib2-Tib1,Tib4-Tib3,1]

Output(Tib1,Tib2,Tib3,Tib4)

Substitute4(Cal1,Cal2,Cal3,Cal4)

Calcaneous = [Cal1,(Cal2-Cal1),(Cal4-Cal3),1]

Output(Cal1,Cal2,Cal3,Cal4)

{*Define Fib1 and Tib1 markers in local coords*}

%Fib1 = Fib1/Fibula

%Tib1 = Tib1/Tibia

{*Define tibia array fixture location using known fixed distance displacement from

Tib1*}

%FixT = {%Tib1(1)-32,%Tib1(2)+0,%Tib1(3)+0}

FixT = %FixT*Tibia

{*Define fibula and tibia center of rotation using global displacements from CT scan*}

{*Go to the transverse slice in the CT that includes the array fixture for the Tibia or the

Fib1 marker for the fibula. Then calculate the anterior/posterior and medial/lateral

displacement from the fixture/marker to the geometric center of the bone structure. This

point will serve as the reference point for tibia/fibula translations. The displacements will

be entered into the shaded boxes below.*}

CORfib = {Fib1(1)+█▌,Fib1(2)-█▌,Fib1(3)+0}

CORtib = {FixT(1)-█▌,FixT(2)-█▌,FixT(3)+0}

%CORfib = CORfib/Fibula

%CORtib = CORtib/Tibia

{*Output COR for fib and tib wrt to segments. The initial coords can be input as

displacements in Motions_Rotations.mod*}

Output(%CORfib,%CORtib,CORfib,CORtib,FixT)